

RT magnet design, fabrication and testing

Attilio Milanese



CAS course on Normal- and Superconducting Magnets

19 Nov. – 2 Dec. 2023

St. Pölten, Austria

If you want to know more...

1. D. Tommasini, Practical Definitions & Formulae for Normal Conducting Magnets
2. Special CAS on magnets, Bruges, Jun. 2009
3. Lectures about magnets in JUAS (Joint Universities Accelerator School)
4. Lectures about magnets in previous general CAS
5. N. Marks, Magnets for Accelerators, JAI (John Adams Institute) course, Jan. 2015
6. J. Tanabe, Iron Dominated Electromagnets
7. And many many more!!

Thanks in particular to [Davide Tommasini](#), [Thomas Zickler](#) and the colleagues of the [TE-MS-C-NCM \(MNC\)](#) section at CERN!

2

1. [edms.cern.ch/document/1162401](https://cds.cern.ch/document/1162401)
2. cdsweb.cern.ch/record/1158462
3. indico.cern.ch/event/683638 for the 2018 edition, as an example – however this seems protected now
4. cas.web.cern.ch/previous-schools
5. indico.cern.ch/event/357378/session/2/#all
6. ISBN 9789812563811

Introduction

We have many normal conducting magnets at CERN, many of them can be considered "references"...



The CERN Normal Conducting Magnets database

The portal with information about the magnets, their components and activities linked to their operation and maintenance.

<https://norma-db.web.cern.ch>

(link available within CERN)

NORMA DATABASE				
MAGNET ADVANCED SEARCH				
Found 4551 results. Page 58 of 304.				
Previous 50 51 52 53 54 55 56 57 58 59 60 61 62 63 64 65 Next				
Magnet	Status	Condition	Location	
PXMBHEDWWP-E2000001 Type W-01	Installed	Not Checked	AD , stor DI.BHZ6064	
PXMBHEDWWP-E2000002 Type W-02	Installed	Not Checked	AD , stor DI.BHZ6065	
PXMBHEDWWP-E2000003 Type W-03	Installed	Certified Good (2020-01-08)	AD , stor DI.BHZ6045	
PXMBHEDWWP-E2000004 Type W-04	Installed	Certified Good (2020-01-08)	AD , stor DI.BHZ6044	

4551 installed
315 design codes

The CERN Normal Conducting Magnets database is also a key tool for quality management, tracking for example nonconformities per magnet type or per machine, and providing at once all the key information for each magnet or magnet design code.

PS main unit magnets: operated (with several consolidation campaigns) since 1959



MPS/Int. DL 63-13
31.5.1963

[EDMS 1262033](#)
268 pages

CERN, Genève. Division du synchrotron à
protons.

THE CERN PROTON SYNCHROTRON MAGNET

5

Picture CERN-PHOTO-5612555: Margherita – *The first combined-function magnet, named after particle-physicist Margherita Cavallaro (pictured here), was completed in 1956, and is still in use today.*

Considering the various consolidation campaigns, in particular for the coils, the PS main units are a bit like the ship of Theseus... although the yokes are still the original ones.

The cited report is a very detailed and interesting document about the design and the construction of the PS magnets, for one of the first alternating gradient synchrotrons ever built.

The PS main units are resistive magnets, with main coils in aluminum, cooled by a forced flow of demineralized water, plus a number of auxiliary windings. They provide a dipolar + quadrupolar field, in fact the quadrupole gradient changes polarity within each unit: over half the length, the pole profile is a focusing quadrupole, over the other half, it is a defocusing one. The central field goes up to 1.27 T at top energy.

There are 100 such units in the CERN PS.

SPS main bending magnets



2.0 T, 5.8 kA
vertical gap 39 mm (MBA) or 52 mm (MBB)

6

The SPS main dipoles are resistive magnets, with coils in copper. Demineralized water flows in the conductor to remove the Joule heating.

At the peak current of 5.8 kA, they provide a dipole field of 2.0 T in a rectangular aperture. Two types of magnets with a smaller (39 mm, MBA) and larger (52 mm, MBB) vertical gap are used.

Each dipole bends the beam by $360 / 744 = 0.48$ deg.

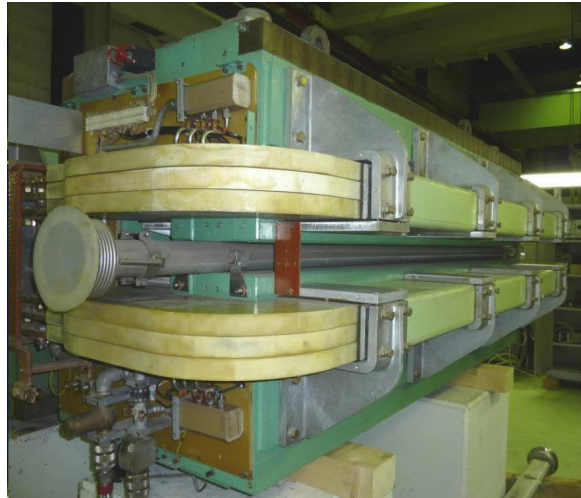
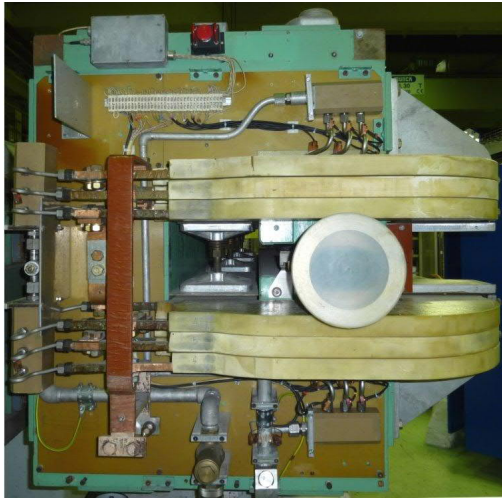
They now work in cycled mode and they can be ramped in a few seconds.

In the 1970s, also a superconducting option was studied (but then abandoned) for the SPS.

The main SPS power converters can give a peak power of around 100 MW. The average (rms) power depends on the duty cycle, though it is usually around 30 MW.

The photo was taken in 1974.

MCB (HB2) dipoles, East Area and North Area



1.74 T, 880 A
vertical gap 80 mm

7

This is an example of classical resistive dipoles, again from the old days. They were originally designed and procured for the ISR beam transfer lines, see this document for a very detailed specification:

Specification for the bending magnets for the ISR beam transfer system

[edms.cern.ch/document/1100428](https://cds.cern.ch/record/1100428)

Nov. 1967

One interesting feature is that two versions of the same magnet exist – a low current and a high current one – see later in this course.

SPS main quadrupoles



22 T/m, 2.1 kA
aperture diameter 88 mm

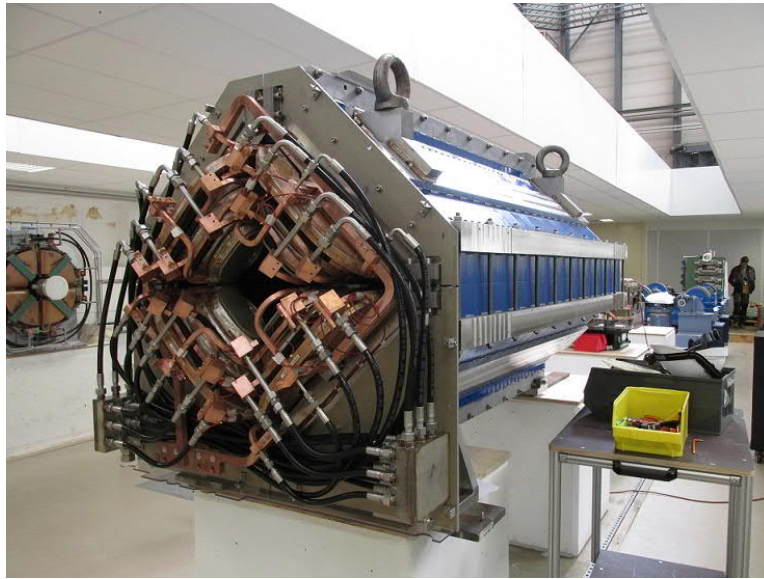
8

The SPS main quadrupoles are resistive magnets, with coils in copper.

Demineralized water flows in the conductor to remove the Joule heating, as for the SPS dipoles.

At the peak current of 2.1 kA, the gradient is 22 T/m in an 88 mm diameter circular aperture. The pole tip field is then 1.0 T ($= 22 \times 0.044$).

Q200 L quadrupoles, East Area



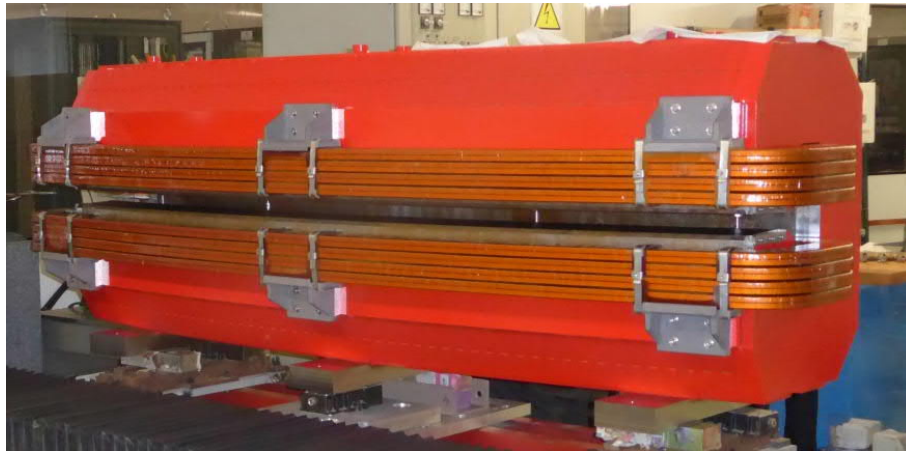
11.85 T/m, 800 A
aperture diameter 200 mm

9

The Q200 L magnets are large aperture quadrupoles which have been designed and procured for the East Area upgrade at CERN – these magnets are relatively recent, as they have been delivered around 2020. They replace old units with similar aperture and gradient (the Q200), which were not laminated and thus could not be pulsed.

One of the challenges was the coil construction and cooling, with many hydraulic circuits in parallel. Also the coil shimming required special care, to avoid movements.

SESAME combined function main bending



1.46 T, -2.79 T/m, 494 A
vertical gap 40 mm

10

These combined function bending magnets were followed up by CERN for the SESAME light source. Magnetic measurements were performed via Hall probe mapping at ALBA.

A few references are reported below for the interested reader:

Design Report of the SESAME Storage Ring Combined Function Dipole Magnets
edms.cern.ch/document/1279692, Apr. 2013

A. Milanese, E. Huttel, M. Shehab
Design of the Main Magnets of the SESAME Storage Ring
IPAC2014, accelconf.web.cern.ch/IPAC2014/papers/tupro105.pdf

J. Marcos, V. Massana, J. Campmany, A. Milanese, C. Petrone, L. Walckiers
Magnetic Measurements of the SESAME Storage Ring Dipoles at ALBA
IPAC2016, accelconf.web.cern.ch/ipac2016/papers/tupmb018.pdf

MQW twin quadrupoles for LHC

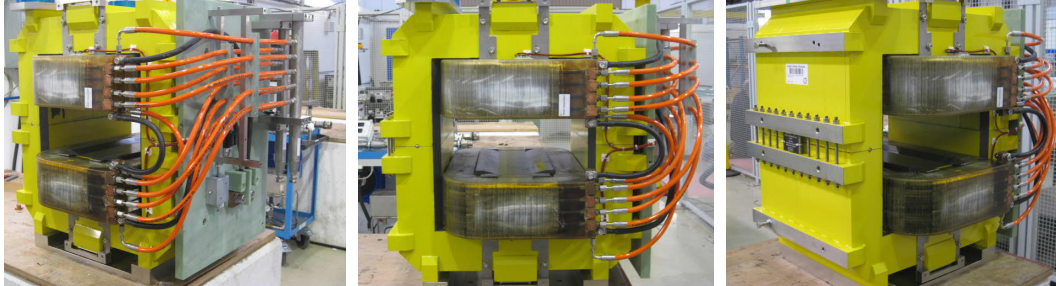


35 T/m, 710 A
aperture diameter 46 mm

11

Resistive quadrupoles are installed also in the LHC, in some of the insertion regions. The peculiarity of these magnets is a twin aperture design. They are operated in two modes, that is, either with the same polarity in the two apertures, or with opposite polarities – in both cases, with the same strengths, as the coils are all in series.

MDX L 150 correctors, East Area

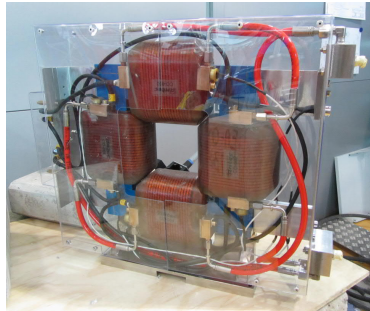


0.70 T, 240 A
vertical gap 150 mm

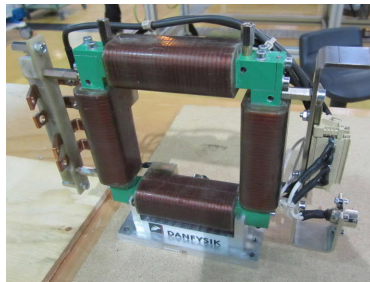
12

These correctors, like the Q200 L quadrupoles shown before, are also part of the East Area upgrade. In this case, new laminated yokes were designed and procured and all coils (from the MDX original magnets) were used.

H+V correctors: HIE Isolde and AWAKE electron line



9.1 mT·m, 48 A
gap 92 × 92 mm



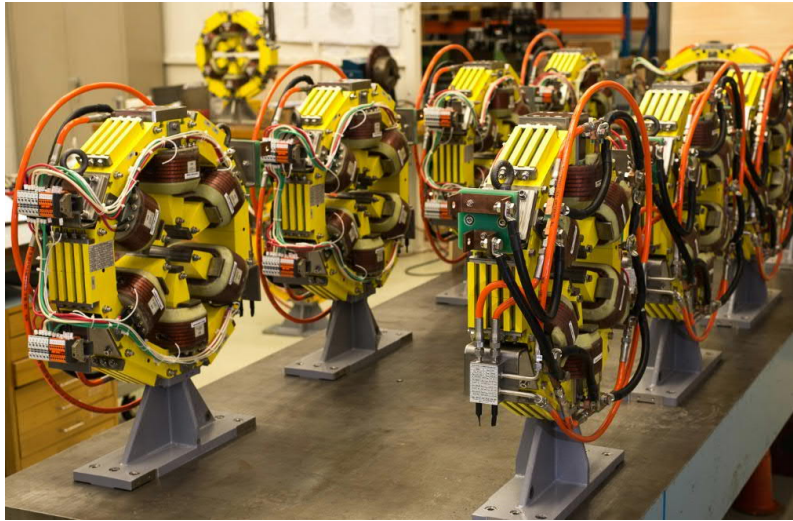
0.414 mT·m, 5 A
gap 100 × 100 mm

13

These are two examples of dual plane correctors. In these cases, the magnets are intrinsically 3D and we often prefer to give the integrated dipole strength instead of the 2D field.

The two designs share a similar geometry for the yoke. The coils in one case are water cooled, in the other they are not.

SESAME sextupoles (with embedded correctors)



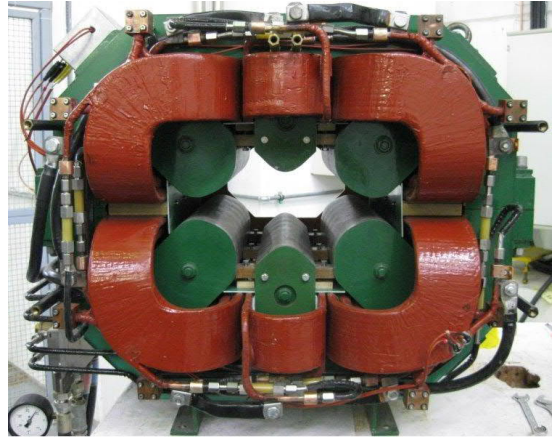
220 T/m², 223 A
aperture diameter 75 mm

14

This is an example of a common design found in synchrotron light sources, where the (short) sextupoles have additional windings so that they can be used also as corrector magnets.

In this case, the embedded correctors are a horizontal / vertical dipole – providing up to 0.5 mrad kick at 2.5 GeV – and a skew quadrupole.

Type 610 sextupoles, PS

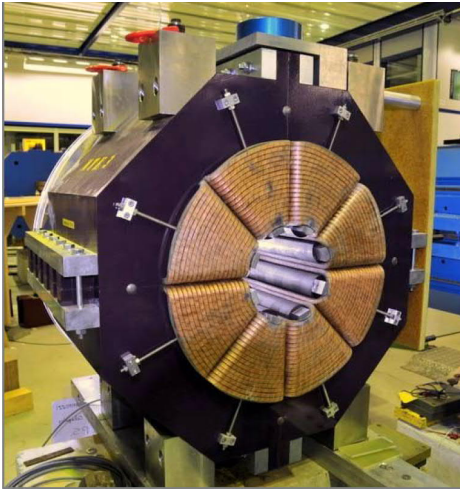


150 A
non-circular aperture, 350 mm × 112 mm

15

Sextupoles do generally have six poles, but they do not have to be arranged all at the same distance from the center – this is an example from the CERN PS, where the central poles are closer, so to take advantage of the elliptical shape of the vacuum chamber. The Ampere-turns are then scaled considering the distance to the center at the third power, since it is a sextupole. This will be covered later in the course.

MTE octupoles, PS (Multi-Turn Extraction)



14360 T/m³, 700 A
aperture diameter 140 mm

16

We do also have a few resistive octupoles at CERN. This is an example of an iron dominated octupole which is very compact in the longitudinal direction – notice in particular the design of the coil heads and their electrical / hydraulic connections.

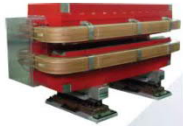


SR facilities : storage ring dipoles

	ELETTRA	ALS	ESRF	ANKA	ASP	ALBA	SOLEIL	SPRING-8	SLS	DIAMOND
Bending radius [m]	5.5	∞	23.37	5.56	∞	7.05	5.36	39.27	5.73	7.16
N. of magnets	24	36	64	16	28	32	32	88	36	48
Dipole field [T]	1.21	1.35	0.86	1.5	1.3	1.42	1.71	0.68	1.4	1.4
Gradient [T/m]	2.86	5.19	0	0	3.35	5.65	0	0	0	0
Gap [mm]	70	50	54	41	42	36	37	64	41	46.6
Current [A]	1420	924	700 ?	660	695	530	538	1090	557	1337



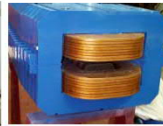
ANKA



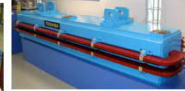
ALBA



ELETTRA



SLS



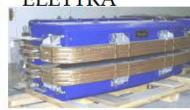
SPRING-8



SOLEIL

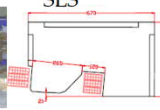


DIAMOND



CLS

Gap=45 mm B= 1.35 T G= 3.8T/m



ASP



SPEAR3

Gap = 50 mm B= 1.4 T G= 3.6 T/m

Introduction to accelerator physics

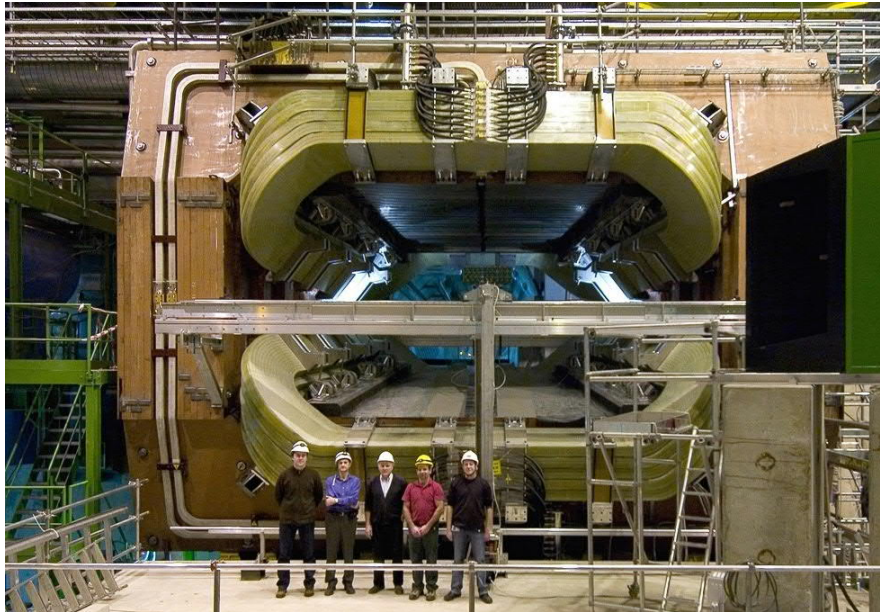
Varna, 19 September, 1 October 2010

Davide Tommasini : Magnets (warm)

[Courtesy of D. Tommasini]

We recall this slide of 2010, with a few examples of main bending magnets for synchrotron facilities. Since then, several others have been built, some with innovative features for the magnets, such as MAX IV in Sweden (yokes of several magnets machined from the same iron block), ESRF-EBS in France (extensive use of permanent magnets).

Experimental magnets: LHCb dipole



18

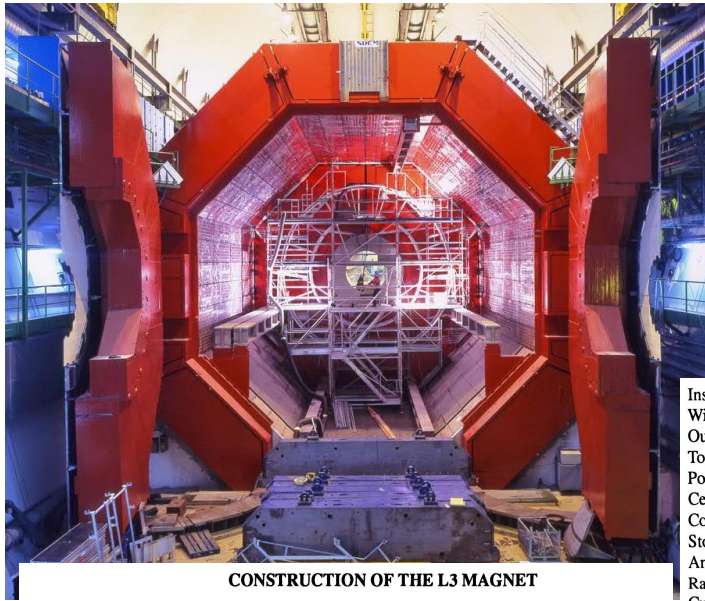
At CERN there are also large resistive experimental magnets – this is the one installed for LHCb in the LHC.

Details can be found in several references, including:

<http://lhcb-magnet.web.cern.ch/>

The coils are wound in aluminum and the power consumption is 4.2 MW. The aperture is wedged and the integrated dipole field is 4 Tm.

Experimental magnets: L3 / ALICE solenoid – the largest resistive magnet?



CONSTRUCTION OF THE L3 MAGNET

Inside radius	5930 mm
Width of the coil	890 mm
Outside radius	7900 mm
Total length	14000 mm
Power at the taps	4.2 MW
Central field	0.5 T
Coil contribution	0.36 T
Stored energy	150 MJ
Amper turns	5 MA _t
Rated current	30 kA
Current density	55.5 A/cm ²
Cooling water	150 m ³ /h
Coil weight (Al)	1100 t
Shielding weight	6700 t

F. Wittgenstein¹, A. Hervé¹, M. Feldmann¹, D. Luckey² and I. Vetlitsky³

- 1 CERN, European Organization for Nuclear Research, CH-1211 Geneva 23, Switzerland
- 2 Massachusetts Institute of Technology (MIT), Boston, MA 02115, USA
- 3 Institute of Theoretical and Experimental Physics (ITEP), Moscow 117259, USSR

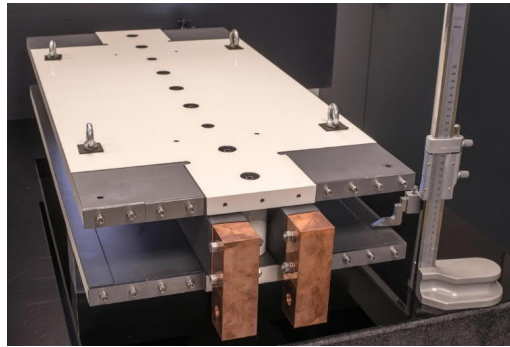
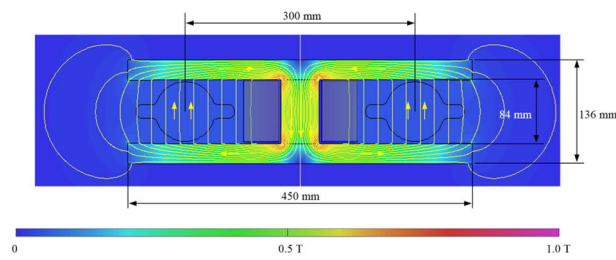
19

The largest of them all – for resistive accelerator magnets – is probably the L3 solenoid, which was first used in LEP and it is now installed for the ALICE experiment in the LHC.

Among the many interesting features, we recall the magnetic hinged doors (to close the solenoid field longitudinally), the material used for the coil (an aluminum alloy instead of pure aluminum) and the collaboration across several countries (including USA and USSR).

The original magnet dates from the mid 1980s.

Twin dipole short model for FCC-ee



54.3 mT, 3.65 kA
vertical gap 84 mm

20

To close this parade of resistive magnets, we show short models proposed for FCC-ee, starting with a twin aperture bending magnet.

Details can be found for ex. in the following paper, and references therein.

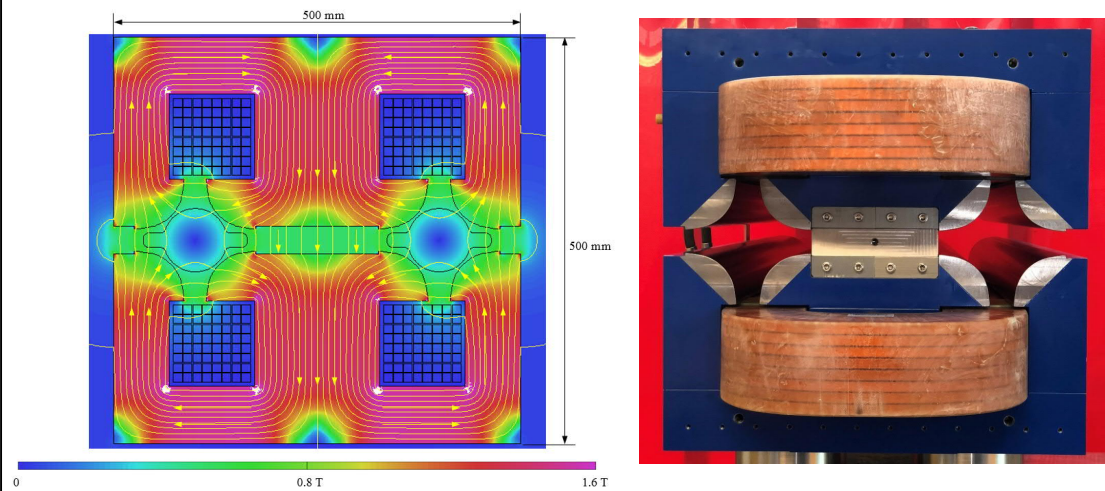
A. Milanese, J. Bauche, C. Petrone

Magnetic measurements of the first short models of twin aperture magnets for FCC-ee

IEEE Trans. Appl. Supercon., v. 30, n. 4, Jun. 2020

For the dipole, the twin concept allows to reduce the Ampere-turns (and the power consumption) by 50% with respect to separate units.

Twin quadrupole short model for FCC-ee



10 T/m, 222 A
aperture diameter 84 mm

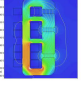
21

For the quadrupole as well, the twin concept comes with a 50% reduction of the Ampere-turns and power consumption. Moreover, this concept allows to have a twin quadrupole configuration, thus 8 magnetic poles, with only 2 coils.

More details can be found for example in the reference given in the previous slide.

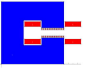

And so much more is out there... see also the bonus slides

Weird



MAGNETS

that I have known

Neil Marks; ASTeC, STFC;
University of Liverpool.

Science & Technology
Facilities Council

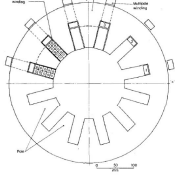
Solution – first concept (*)

A 12 pole magnet with:

- sextupole coils hard wound around 6 poles;
- 12 multipole coils on the back-leg, individually powered;
- backleg currents vary as $\cos n\theta$ for 'upright' components – $\sin n\theta$ for skew.

This would provide (simultaneously):

- H and V dipole correction;
- Upright and skew quad;
- Sextupole for full chromaticity correction.



NOTE- It is essential that:
 $\sum \text{back-leg currents} = 0$

(*) N.Marks; Proc of 8th Magnet Tech Conf, Frascati, 1975.

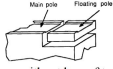
Neil Marks; ASTeC, STFC. 'Weird Magnets that I have known' PAR, April 2013

Science & Technology
Facilities Council

Solution (*)

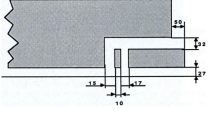
A short end section with double the gap.

Initial pole face concept:



But to provide the necessary longitudinal gap without loss of transverse field quality at the beam, an intermediate section was necessary.

As engineered:




(*) N.Marks and M.Lieuvin, Proc. MT 10, Boston, 87; IEEE Trans on Magnetics, Vol 24, No 2, 1988.

Neil Marks; ASTeC, STFC. 'Weird Magnets that I have known' PAR, April 2013

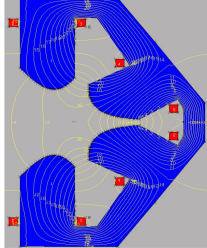
Science & Technology
Facilities Council

Losing poles!



"To lose one pole is unfortunate – to lose two, smacks of carelessness." (*)

The **4 pole sextupole** and other bizarre magnets in 'Pumplet' – a non-linear, non-scaling FFAG lattice design by Grahame Rees.



(*) Lady Bracknell; 'Importance of Being Earnest'; Oscar Wilde, Penguin Popular Classics, £2.00 at Amazon.

Neil Marks; ASTeC, STFC. 'Weird Magnets that I have known' PAR, April 2013

Courtesy of N. Marks, www.ukri.org/wp-content/uploads/2013/04/STFC-Weird-magnets-presentation.pdf

Conclusions (introduction)

There is a long tradition and experience with room temperature magnets in accelerators

We did not look at cyclotrons, FFAGs, synchrocyclotrons, etc.

There are many types of resistive magnets: dipoles, quadrupoles, combined function, sextupoles, octupoles, solenoids, experimental magnets, wigglers, undulators, etc.

We focus on dipoles and quadrupoles

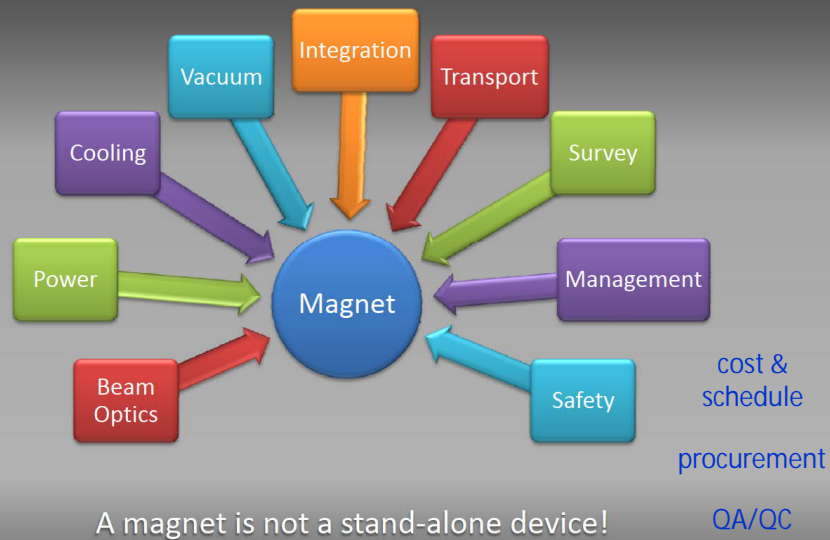
Most of them are iron dominated, with coils wound from copper (or aluminum) conductor

There are coil dominated RT magnets, but they are more of a niche

Requirements



Input parameters



CERN Accelerator School – Specialized Course on Magnets
Bruges, Belgium, 16 – 25 June 2009

Basic Magnet Design
© Th. Zickler, CERN

[Courtesy of T. Zickler]



General requirements

Magnet type and purpose

- Dipole: bending, steering, extraction
- Quadrupole, sextupole, octupole
- Combined function, solenoid, special magnet

Installation

- Storage ring, synchrotron light source, collider
- Accelerator
- Beam transport lines

Quantity

- Installed units
- Spare units (~10 %) [spare magnets / coils](#)

[Courtesy of T. Zickler]



Performance requirements

Beam parameters

- Type of beam, energy range and deflection angle (k-value)
- Integrated field (gradient)
- Local field (gradient) and magnetic length

Sometimes there might be ambiguity in the communication between beam physicists and magnet engineers: typical examples are the strength of a sextupole (factor of 2 difference) or field quality (like field homogeneity vs. gradient homogeneity in a quadrupole).

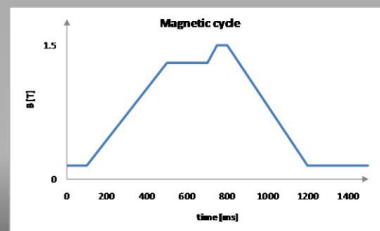
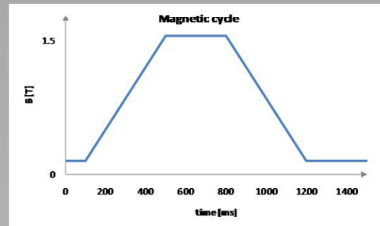
[Courtesy of T. Zickler]



Performance requirements

Operation mode

- Continuous
- Pulsed-to pulse modulation (ppm)
- Ramped – ramp rate (T/s)
- Fast pulsed



CERN Accelerator School – Specialized Course on Magnets
Bruges, Belgium, 16 – 25 June 2009

Basic Magnet Design
© Th. Zickler, CERN

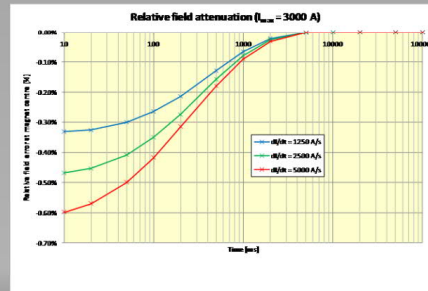
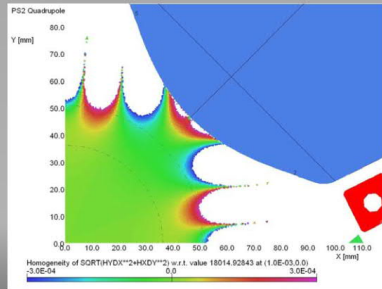
[Courtesy of T. Zickler]



Performance requirements

Field quality

- Homogeneity (uniformity)
- Allowed harmonic content
- Stability & reproducibility
- Settling time (time constant)



[Courtesy of T. Zickler]



Physical requirements

Geometric boundaries

- Available space
- Transport limitations
- Weight limitations

Accessibility

- Crane
- Connections (electrical, hydraulic)
- Alignment targets

Aperture

- Physical aperture
- 'Good field region'

[Courtesy of T. Zickler]



Interfaces

Equipment linked to the magnet is defining the boundaries and constraints

Power converter

- Max. current
- Max. voltage
- Pulsed/dc

Cooling

- Max. flow rate and pressure drop
- Water quality (aluminium/copper circuit)
- Inlet temperature
- Available cooling power

Vacuum

- Size of vacuum chamber
- Space for pumping ports, bake out
- Captive vacuum chamber

[Courtesy of T. Zickler]



Environmental aspects

Other aspects, which can have an influence on the magnet design

Environment temperature

- Risk of condensation
- Heat dissipation into the tunnel

Ionizing radiation

- High radiation levels require radiation hard materials
- Special design to allow fast repair/ replacement

Electro-magnetic compatibility

- Magnetic fringe fields disturbing other equipment (beam diagnostics)
- Surrounding equipment perturbing field quality

Safety

- Electrical safety [earthing, protection covers](#)
- Interlocks

[Courtesy of T. Zickler]

Conclusions (specifications)

Make sure you know which magnet you have to design, build, test, install

Ideally before starting the design... though some iterations in the early phases are normal

Make sure this is validated by all colleagues

A specification and a preliminary design document can help, this depends also on the size of the project

Yoke design

2D

The design of the yoke usually starts in 2D, considering several aspects

Pole tip

Back or return legs

Space for coils

Integration: overall dimensions, weight

Construction and assembly considerations

Confinement of stray field

Field trimming after magnetic measurements

- integrated strength (main component)

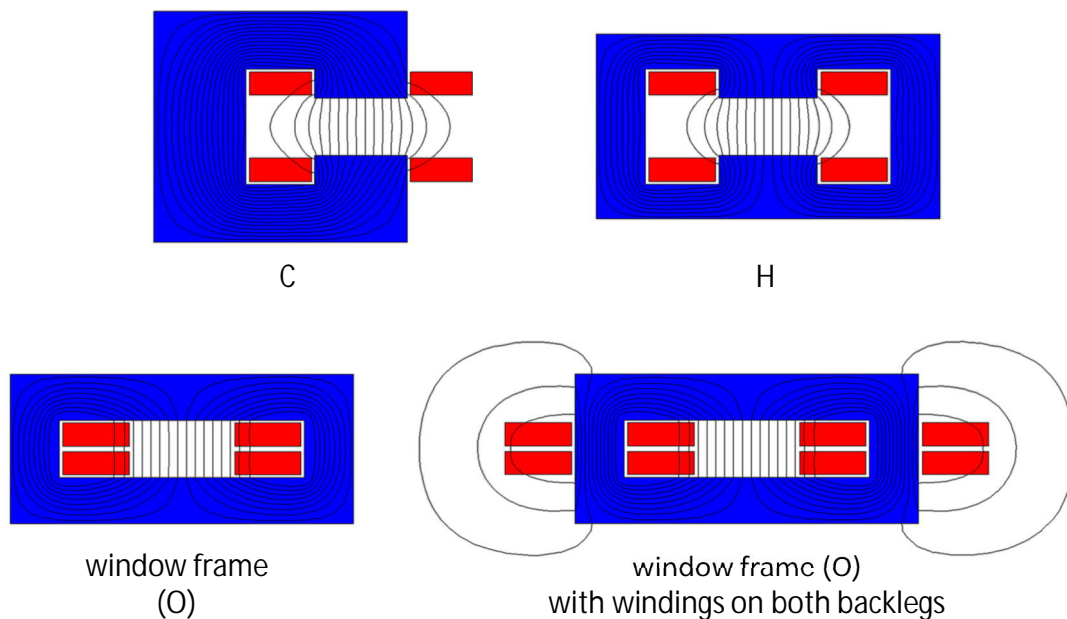
- integrated field quality

Different ferromagnetic materials

- solid vs. laminated

- iron based, usually electrical steel, but also ARMCO® and cobalt-iron alloys (in very specific cases)

These are the most common types of resistive dipoles
(cartoon representation)



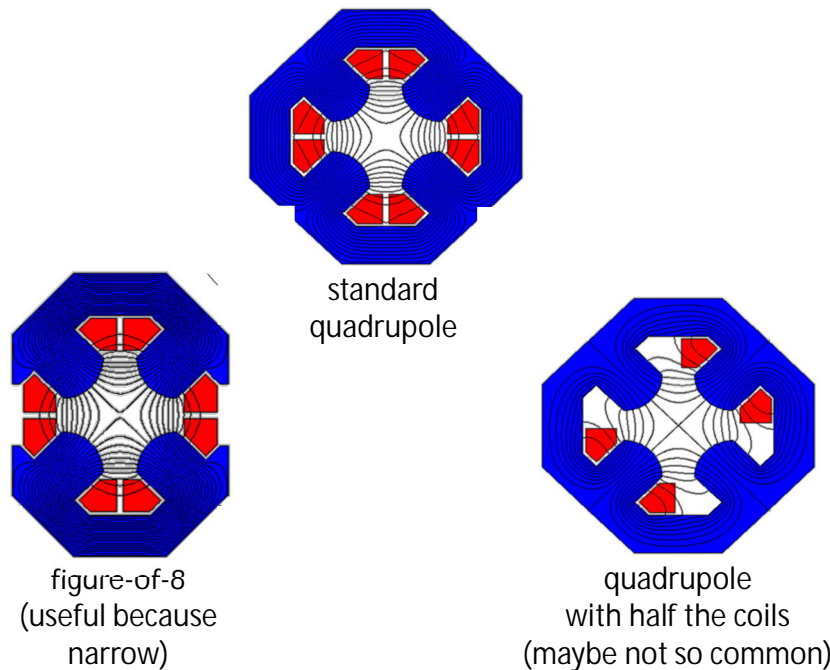
36

The C-shape provides easy access to the gap for the vacuum chamber – for this it is often found in light sources – at the cost of a (slight) asymmetry, which introduces the even terms in the allowed multipoles, in particular the quadrupole (gradient).

The H-shape is symmetric, at the cost of some access problems to the gap. For the same field, this is more compact and mechanically stable than a C. The coils can extend till the midplane – like in the SPS case, which is then a hybrid between an H and a window frame – though then they need to be bent up in the ends to clear the gap region. If the coil gets close to the aperture, then its position can have an impact on field quality, especially at higher fields.

The window frame geometry provides the best field quality, thanks to the wide pole; it has the same access problems of the H, plus there has to be enough room to dimension the coil properly. As for the other cases, the position of the windings can impact the field quality if the coil gets very close to the gap. This type is often used for correctors, where the field is low, with the coils wound on the return legs (figure on the bottom right). In this latter configuration, it is somehow inefficient in 2D – the outer conductors are useless to create field in the gap. In practice, this layout is still convenient for short magnets. The return current on the outside adds flux in the side legs of the magnets, so more material is needed if the working point becomes close to saturation – which is not an issue if the magnet works at low field, like a corrector.

These are the most common types of resistive quadrupoles (cartoon representation)



37

Resistive quadrupoles are most often of the standard type shown in the central top figure, with four symmetrical quadrants.

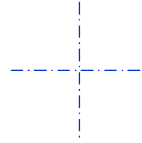
Sometimes figure-of-8 (referred to also as Collins) quadrupoles are used, with the magnetic circuit split in two halves. In this way, the magnets can be quite compact transversally, which might be needed in very crowded regions. For example, some quadrupoles in light sources are of this kind, to make room for outgoing photon beam lines. We also have a few of these at CERN, as first quadrupoles in an extraction line or after a switch dipole. This layout breaks the symmetry, somehow like the C-shape does in dipoles.

A quadrupole with only half the coils also works just fine for weak strengths, though it is seldom used as far as I know.

Note: in the simulations, the same current density is applied to the various configurations, corresponding to a pole tip field (for the standard quadrupole in the top) of 0.8 T. This value starts to be on the high side for quadrupoles, as extra flux is then collected in the yoke from the pole sides. As a term of comparison, the SPS quadrupoles – which are quite “pushed” – have 1.0 T on the pole tip.

Reminder: the allowed / not-allowed harmonics refer to some terms that shall / shall not cancel out thanks to design symmetries

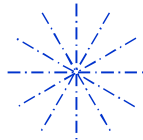
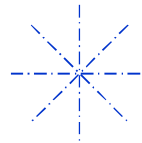
fully symmetric dipoles (ex. H)
allowed: B_1, b_3, b_5, b_7, b_9 , etc.



half symmetric dipoles (ex. C)
allowed: B_1, b_2, b_3, b_4, b_5 , etc.



fully symmetric quadrupoles
allowed: $B_2, b_6, b_{10}, b_{14}, b_{18}$, etc.



fully symmetric sextupoles
allowed: B_3, b_9, b_{15}, b_{21} , etc.

38

As a reminder, we like to divide the multipole errors in two families: allowed and not-allowed (or random).

The not-allowed (or random) terms are the ones that should not be there, thanks to symmetries in the design. They arise due to asymmetries introduced during the fabrication.

The allowed multipoles are the ones that are allowed by the symmetries, that is, that are expected by design. Part of the magnetic design focuses on optimizing the geometry to cancel out these terms.

The SPS (a hybrid between an H-shape and a window frame) main dipoles are fully symmetric dipoles.

Half symmetric dipoles are resistive magnets with a C-shape yoke, for ex. the ones of various light sources (ANKA, DIAMOND) or the LEP dipoles.

Out of curiosity, the table lists the allowed multipoles for the different layouts of the dipole (cartoon) examples

	C-shape	H-shape	O-shape
b_2	1.4	0	0
b_3	-88.2	-87.0	0.2
b_4	0.7	0	0
b_5	-31.6	-31.4	-0.1
b_6	0.1	0	0
b_7	-3.8	-3.8	-0.1
b_8	0.0	0	0
b_9	0.0	0.0	0.0

b_n multipoles in units of 10^{-4} at $R = 17$ mm

$NI = 20$ kA, $h = 50$ mm, $w_{\text{pole}} = 80$ mm

39

The allowed harmonics for the C and H designs contains rather large sextupoles b_3 and decapoles b_5 . Solutions to improve field quality involve adding side shims (discussed later) or widening the pole. Still, the differences between the asymmetric C and the symmetric H layouts are rather small.

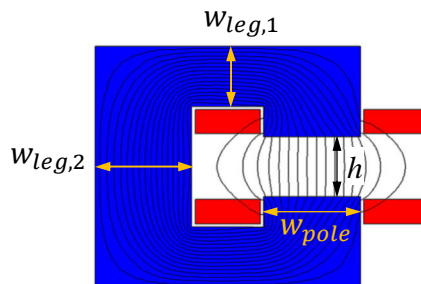
The window frame – as expected – is better, as the pole is much wider.

Note 1: in these examples, w_{pole} does not follow the rule $w_{\text{pole}} \approx w_{\text{GFR}} + 2.5h$, as here it is rather $w_{\text{pole}} \approx w_{\text{GFR}} + h$; this is why the field quality is in the 10^{-2} region.

Note 2: entries with a “0” correspond to not-allowed harmonics

Note 3: it is possible to take the center of the C (for the beam) not in the middle of the pole, but where the good field region is wider, though the improvement is minor.

The magnetic circuit is dimensioned so that the pole is wide enough for field quality, and there is enough room for the flux in the return legs



$$w_{pole} \cong w_{GFR} + 2.5h$$

$$B_{leg} \cong B_{gap} \frac{w_{pole} + 1.2h}{w_{leg}}$$

40

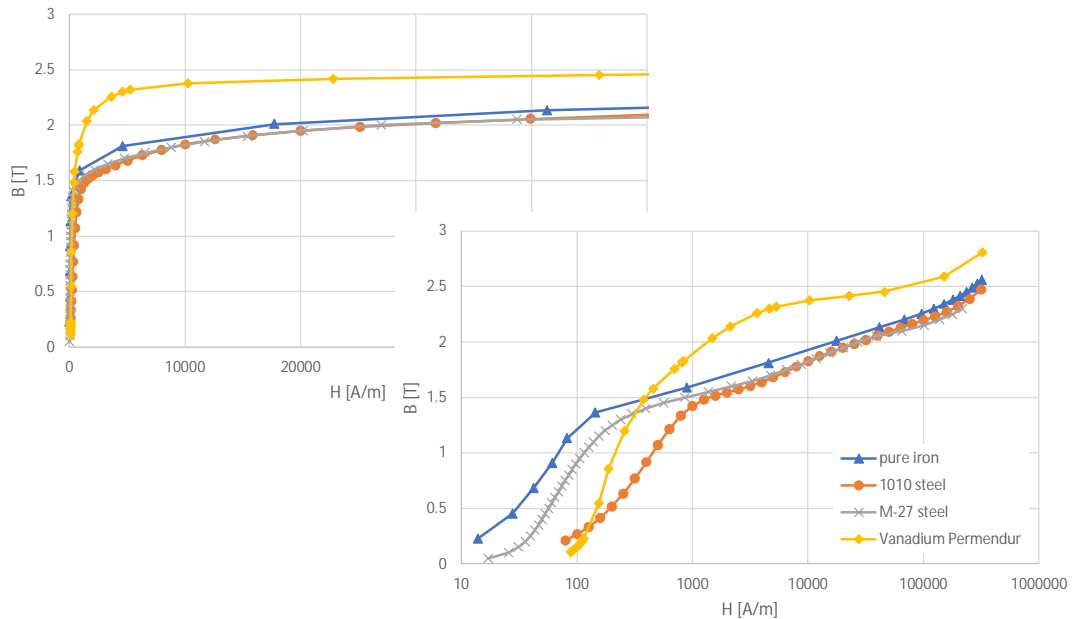
The magnetic circuit is designed in 2D as follows:

- * the pole is wide enough to provide the required field homogeneity in the good field region; its actual width depends on pole shims, on iron saturation, on field uniformity (10^{-2} , 10^{-3} or 10^{-4} level), etc., though the above formula provides a good first guess in many cases;

- * to dimension the return legs, we consider that the flux in the yoke includes the flux in the gap, but also some stray flux. The stray flux extends about one gap width on either side of the aperture. The width of the legs is chosen to limit B in the yoke, usually below saturation, so to work in the high permeability regime of the material.

Note: the density of the flux lines in the figure is – well – the flux density, that is, the B field (Faraday); in this example, B is higher in the top / bottom legs than in the back one.

The BH response of the yoke material in an important parameter



41

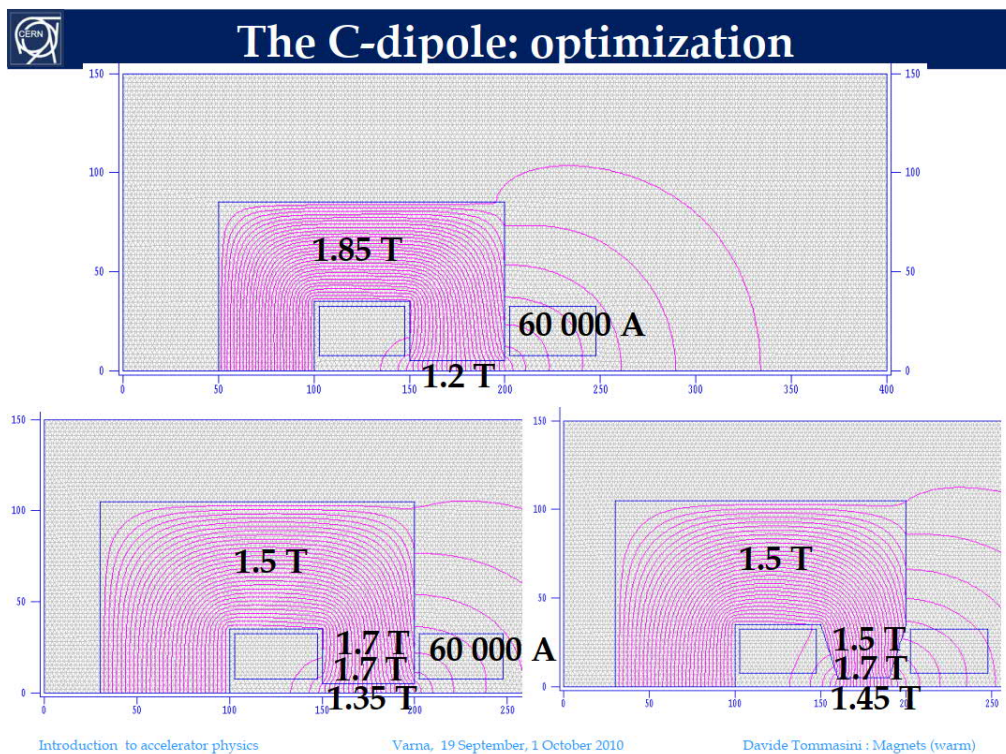
These representative curves are taken from the library of materials available in FEMM, the simulation code that will be used for the exercises.

In these plots, the B field obtained for a given H excitation is given. This nonlinear behavior is the BH characteristics of the material. Hysteresis effects are not considered here as the virgin magnetization curve is used in general for these simulations. Alternative plots involve the relative magnetic permeability.

The four curves correspond to the following materials:

- pure iron: typical ARMCO®, see www.aksteel.eu/products/armco-pure-iron
- 1010 steel: plain carbon steel with 0.10% carbon content, used for example in large solid yokes
- M-27 steel: typical electrical steel, like M330-50A, where Si is added to decrease resistivity and hysteresis
- Vanadium Permendur: a Co-Fe alloy, high saturation material, very rarely used for accelerator magnets (also for its cost), sometimes it is considered for the pole insert, for high field

Below a didactic example of yoke optimization for a dipole



[Courtesy of D. Tommasini]

The high field target is 2.0 T, at the limit but doable (standard iron, reasonable Ampere-turns, reasonable size of yoke, field quality at various currents)

SPS @ 450 GeV

bending

$$B = 2.0 \text{ T}$$

quadrupole

$$B_{\text{pole}} = 21.7 * 0.044 = 0.95 \text{ T}$$

TI2 / TI8 (transfer lines SPS to LHC, @ 450 GeV)

bending

$$B = 1.8 \text{ T}$$

quadrupole

$$B_{\text{pole}} = 53.5 * 0.016 = 0.86 \text{ T}$$

PS @ 26 GeV

combined function bending $B \approx 1.5 \text{ T}$

43

The range of B fields covered by resistive magnets is wide. Just to have some terms of comparison, here we look at the top fields in the gap of dipoles and pole tip fields of quadrupoles for the largest CERN (resistive) synchrotrons and transfer lines.

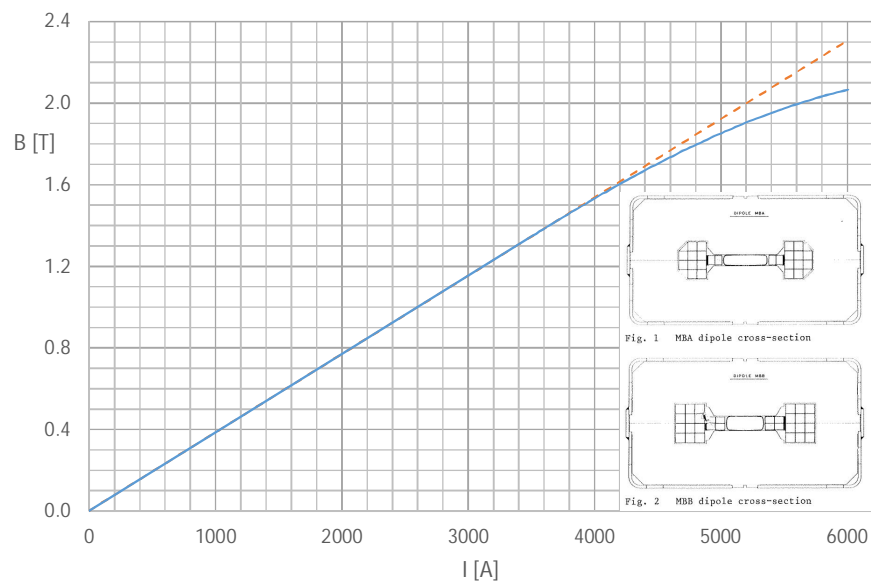
The PS – CERN's oldest running machine – has combined function bending magnets with a central gap field of about 1.5 T. These magnets are C-shaped.

The SPS – CERN's largest resistive synchrotron – has bending magnets which run up to 2.0 T and quadrupoles with pole tip fields up to about 1.0 T. Pushing the central field above that in a large resistive machine is not realistic, because of the large electric consumption and the size of the magnet.

For the long transfer lines from the SPS to the LHC (combined length of 5.6 km), the dipoles run at 1.8 T while the quadrupoles are designed for 0.9 T at the pole tip.

Note: the pole tip field of quadrupoles (and sextupoles, etc.) is lower than what can be achieved in a dipole, as this kind of magnets "collect flux lines in the yoke", that is, there is more field in the iron that you do not have in the useful (good field region) part of the air gap.

This is the (average) transfer function field B vs. current I for the SPS main dipoles



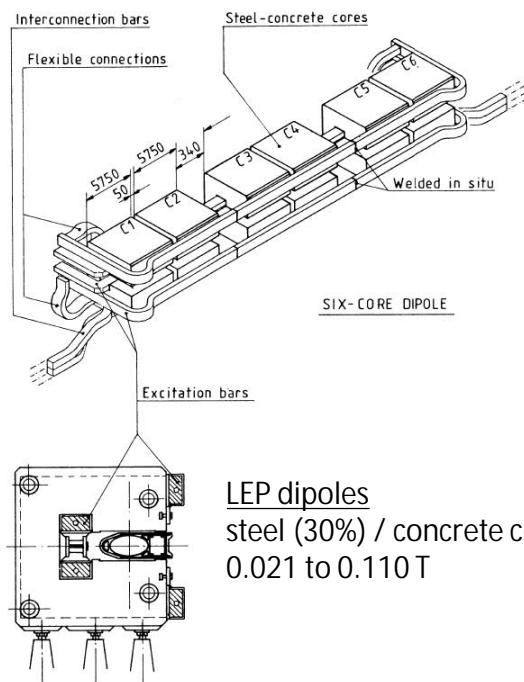
44

As an example of magnets working into saturation, we show the transfer function of the SPS main dipoles at CERN.

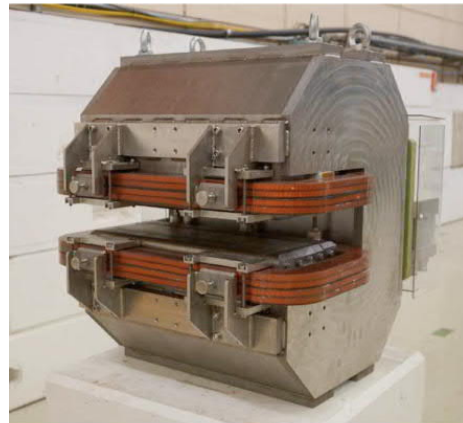
The plot is the actual calibration curve used by operation at CERN, which is the average of $384 + 360 = 744$ bending magnets, powered in series. The dashed line is an extrapolation of the initial linear part, that is, it represents the field if there were no saturation. At 6 kA the efficiency (the ratio of the two curves) is 89%.

When injecting beams into the LHC, the SPS works up to 450 GeV, with a field of 2.02 T.

What about low field? This is another challenge, typically a few tens of mT



LEP dipoles
steel (30%) / concrete cores
0.021 to 0.110 T



ELENA dipoles
prototypes with diluted
/ not diluted cores
0.36 to 0.05 T

45

The challenges of working with low fields are typically the impact of the remanent field and the variability of magnetic characteristics of the iron at low excitation – in fact, sometimes pure coil dominated, ironless magnets are used, to avoid these issues.

As examples of synchrotron bending magnets operating at relatively low field we report LEP and ELENA.

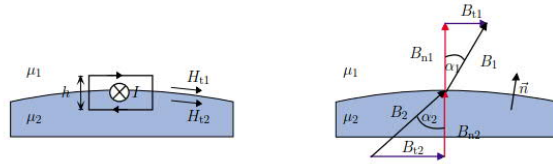
For details, a good paper is the following:

D. Schoerling

Case study of a magnetic system for low-energy machines

Phys. Rev. Accel. Beams 19 (2016), 1-17

The ideal poles are curves of constant scalar potential



If we apply Ampère's law in the integral form

$$\oint \vec{H} \cdot d\vec{s} = \int_A \vec{J} \cdot d\vec{A}, \quad (30)$$

to the loop displayed in fig. 4 (left), and let $h \rightarrow 0$, then the enclosed current is zero, as in an infinitesimal small rectangle there cannot be a current flow. Therefore

$$H_{t1} = H_{t2}, \quad (31)$$

i.e.,

$$\vec{n} \times (\vec{H}_1 - \vec{H}_2) = 0. \quad (32)$$

Because of $\oint \vec{B} \cdot d\vec{A} = 0$ we get at the interface

$$B_{n1} = B_{n2}, \quad (33)$$

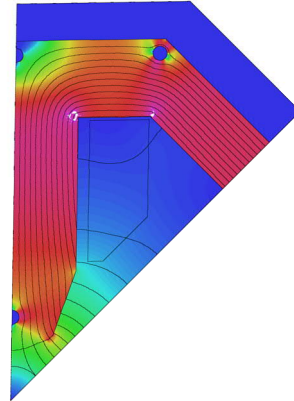
i.e.,

$$\vec{n} \cdot (\vec{B}_1 - \vec{B}_2) = 0. \quad (34)$$

Now

$$\frac{\tan \alpha_1}{\tan \alpha_2} = \frac{\frac{B_{t1}}{B_{n1}}}{\frac{B_{t2}}{B_{n2}}} = \frac{\mu_1 H_{t1}}{\mu_2 H_{t2}} = \frac{\mu_1}{\mu_2}. \quad (35)$$

For $\mu_2 \gg \mu_1$ it follows that $\tan \alpha_1 \gg \tan \alpha_2$. Therefore for all angles $\pi/2 > \alpha_2 > 0$ we get $\tan \alpha_1 \approx 0$, see also fig. 4 (right). The field exits vertically from a highly permeable medium into a medium with low permeability. We will come back to this point when we discuss ideal pole shapes of conventional magnets.



[Courtesy of S. Russenschuck]

Unless the iron is heavily saturated – in that case the relative permeability decreases significantly – field lines come out perpendicularly with respect to the iron. The example on the right is the simulation of a sector of a typical quadrupole (SESAME, in this case).

The ideal poles for a dipole, a quadrupole, a sextupole, etc. are curves of constant scalar potential, of infinite length

dipole

$$\rho \sin(\theta) = \pm h/2 \quad y = \pm h/2 \quad \text{straight line}$$

quadrupole

$$\rho^2 \sin(2\theta) = \pm r^2 \quad 2xy = \pm r^2 \quad \text{hyperbola}$$

sextupole

$$\rho^3 \sin(3\theta) = \pm r^3 \quad 3x^2y - y^3 = \pm r^3$$

combined function dipole + quadrupole: translated hyperbola (that is, a pure quadrupole with a horizontal offset)

47

It can be shown that the ideal pole profiles are curves of constant scalar potential. This follows from the definition of the scalar potential itself and from the fact that the flux lines are perpendicular to the iron pole, if the iron permeability is infinite.

The expressions are quite neat in polar coordinates, though they become cumbersome – already for a sextupole – in Cartesian coordinates.

The ideal pole profile for a dipole is a straight line.

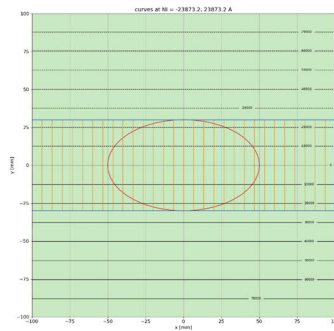
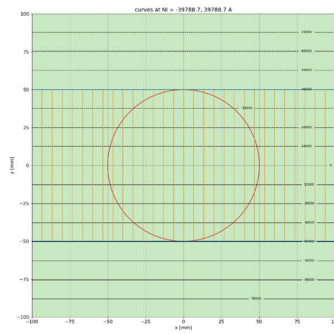
The ideal pole profile for a quadrupole is a hyperbola.

My personal preference is for simple profiles – i.e., profiles that can be described with line segments and circular arcs. This is often possible without any detrimental effect on field quality, especially when the pole is not very wide.

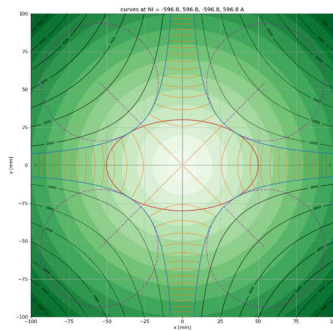
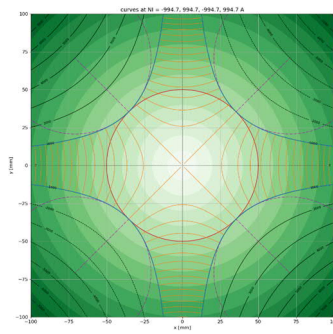
All these profiles can be derived also using conformal mapping and a bit of elegant complex mathematics.

h [m] full vertical gap (for dipole)
r [m] aperture radius (for quadrupole and sextupole)

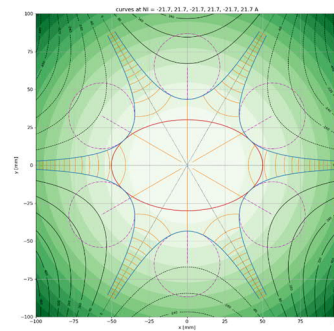
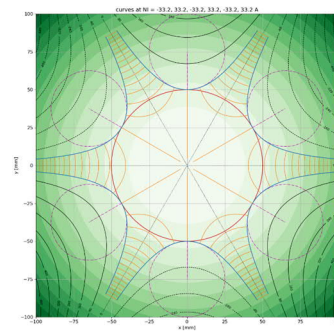
dipole



quadrupole



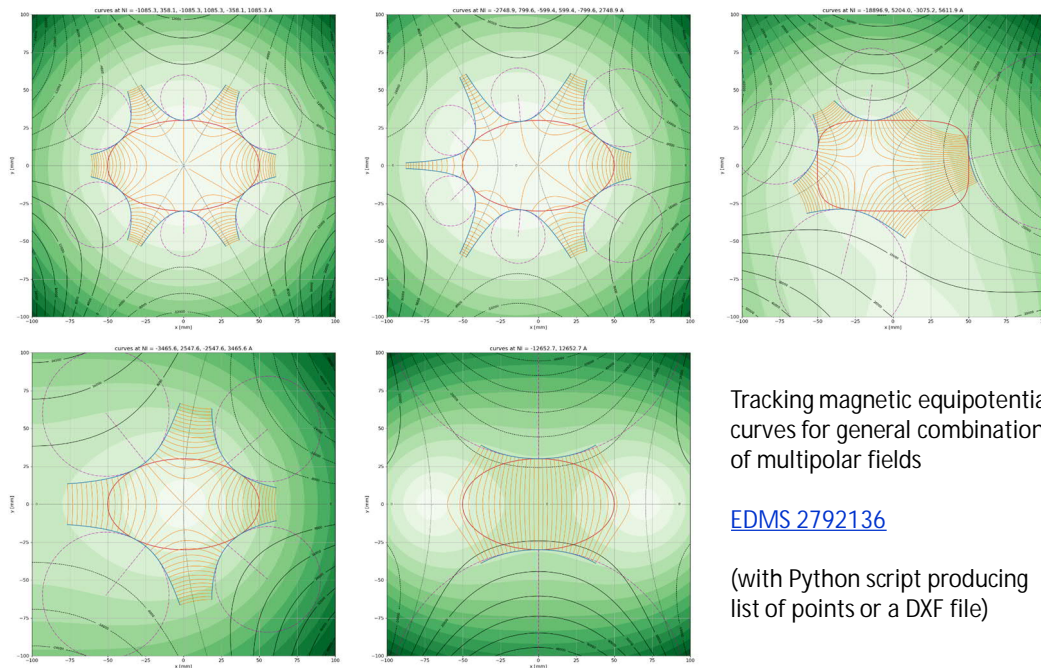
sextupole



As examples, contour plots of scalar potentials are shown for the cases of pure dipole, quadrupole and sextupole fields. The ideal pole profiles tangent to a circle or an ellipse are given in the top and bottom row, respectively. In the case of the sextupole around an ellipse, the middle poles could be pushed closer to the center, varying the Ampere-turns (see the ex. of the 610 sextupole in the PS). The colormap relates to the strength of the field.

The software used for these plots is the same of the next page.

Ideal poles can be found for any linear combination of multipole terms (also tangent to non-circular apertures)



Tracking magnetic equipotential curves for general combinations of multipolar fields

[EDMS 2792136](#)

(with Python script producing list of points or a DXF file)

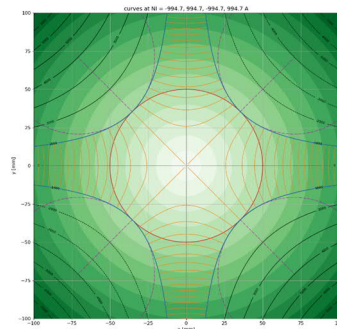
49

Less common field configurations are also possible, when mixing several multipole terms or when considering poles with a difference distance from the center (see the reference in the slide for details).

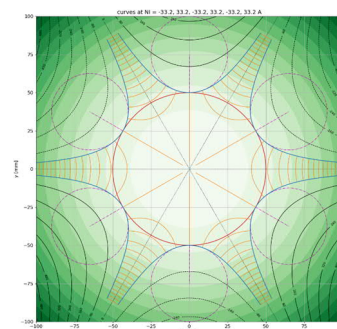
Combining multiple terms with a fixed ratio among them seems not so common nowadays, with the exception of combined dipole and quadrupole units. There are examples of combined quadrupole and sextupole magnets, or also dipoles with quadrupolar and sextupolar components (ALBA booster ring, ISR main bending).

The examples shown in this slide are arbitrary, just to show what is possible, and include a sextupole with all poles tangent to a central ellipse, a combined quadrupole and sextupole, a dipole with a sextupole, and so on.

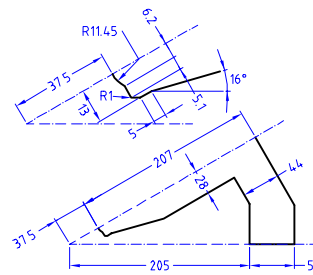
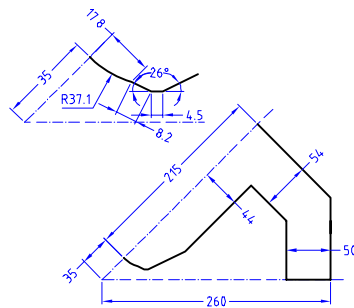
The osculating circle at the pole tip can also be a starting point



quadrupole: $R_{\text{fit}} = r$



sextupole: $R_{\text{fit}} = r/2$



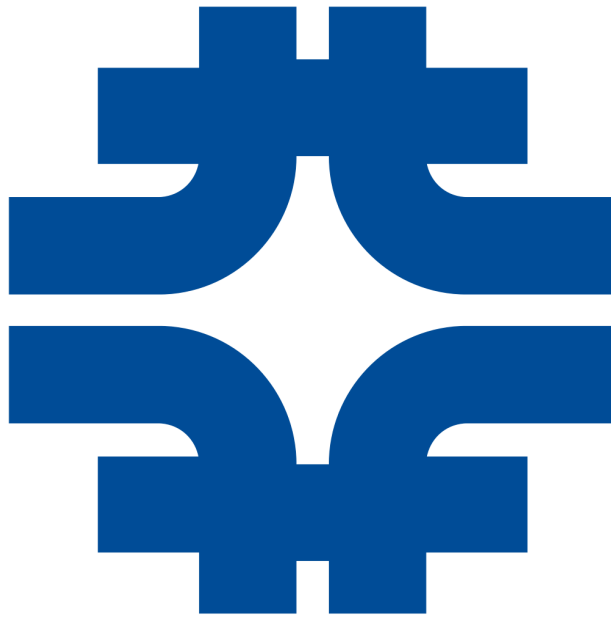
For a dipole, the osculating circle degenerates into a line.

For a quadrupole, it can be shown that the osculating circle at the tip of the hyperbola is equal to the aperture radius itself.

For a sextupole, this fitting circle is half the aperture radius.

Just as examples, the sketches on the bottom refer to the SESAME quadrupoles and sextupoles.

Pole profiles are even used for logos of large laboratories...



51

Fermilab logo, courtesy from www.fnal.gov/faw/designstandards/logo.html

Ideal poles are a (useful) starting point to design the pole tip, nowadays we have 2D (and 3D) simulation tools



CERN-PS/JPB 7
April 2, 1954.

SHAPING OF MAGNET POLES FOR GENERATION OF UNIFORM GRADIENTS

J.P. Blewett

In the design of magnet poles for alternating-gradient synchrotrons it is usually assumed that the pole shape will be a section of a rectangular hyperbola. Although this makes a good first approximation it is in error for four reasons :

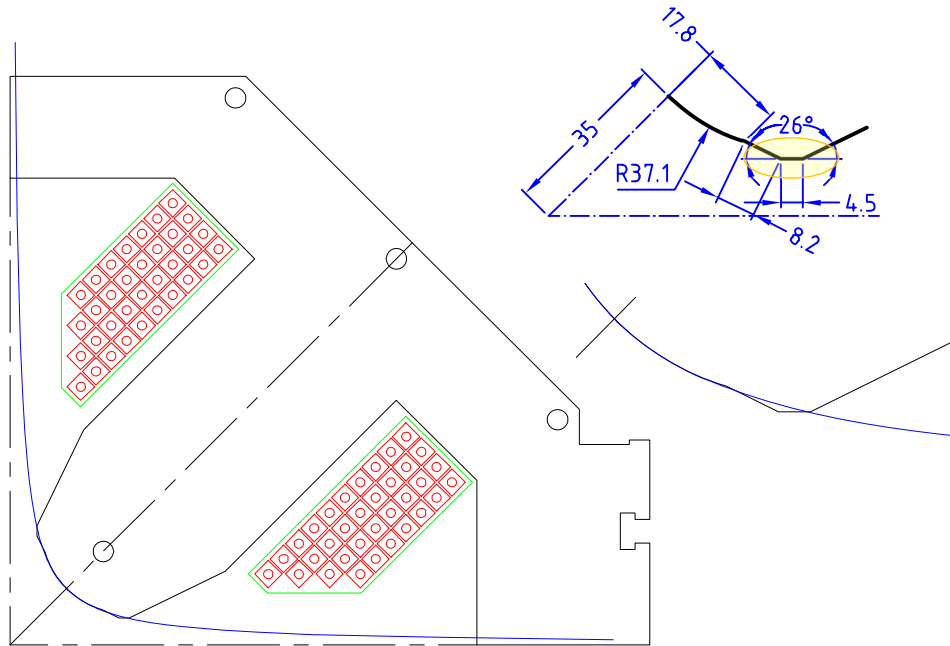
- i) No present designs include the neutral pole which is an essential unit of the hyperbolic configuration.
- ii) The hyperbolic contour is not continued to infinity but is cut off at boundaries close to the operating field region.
- iii) The magnetising coil in all practical designs is sufficiently close to the useful field that it introduces perturbations of the field pattern.
- iv) Effects of finite magnet permeability are not included.

52

The limitations of using such curves – of constant scalar potential – to design pole tips are known since the early days of accelerator magnet design: the paper shown above refers to a study for the PS main units, in the mid 1950s.

One of the main difference with respect to that era is that now we have powerful simulations codes, both in 2D and 3D – modeling the nonlinear BH characteristics of the iron and even including transient effects.

Every magnet designer has his / her preference: below the pole tip of the SESAME quadrupoles vs. the hyperbola



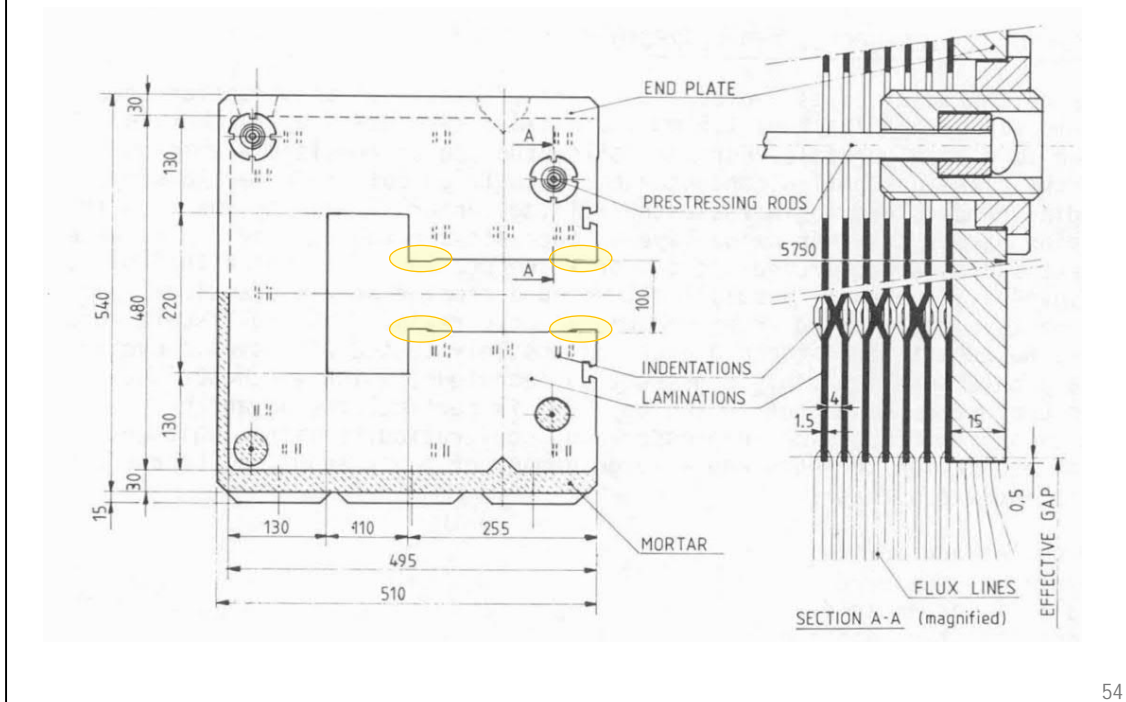
53

As an example of theoretical vs. real pole tip profile, we consider the quadrupoles for the SESAME light source.

The hyperbola extends till infinity, without space for the coils: this is not practical. The real pole shape is not far from the theoretical one, and then it is terminated with shims, which are used at the design stage to minimize the allowed harmonics, that is, to improve field quality. In a way, those shims bring in extra material, which is in a way substituting the one going all the way to infinity in the theoretical profiles.

In this specific case, the central part of the pole tip is not a hyperbola and the profile is described with lines and circular arcs – with no compromise on field quality. When designing the pole tip in 2D (with OPERA), the starting point for the radius of the central part of the pole was the curvature radius of the theoretical hyperbola – which turns out for a quadrupole to be simply equal to the aperture radius itself, 35 mm in this case.

Below the example of the LEP main bending magnets, also with side pole shims



54

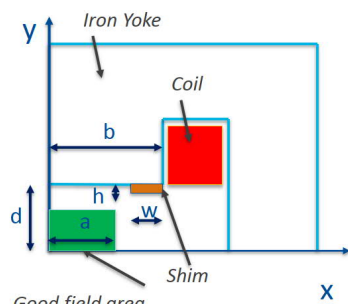
The ideal poles for a dipole are two infinite parallel lines. Wide poles indeed help for field quality – though they need to be terminated somewhere. At the extremes, shims are then introduced. For long magnets, their size and shape can be simulated in 2D to optimize the field quality. The real field quality will depend also on the mechanical tolerances and the possible asymmetry in the magnetic properties of the material.

Here the lamination for the LEP magnets is shown, where about $\frac{1}{4}$ of the pole width is used for shims.

These magnets were rather particular – see the right picture. The top field was only 110 mT, which allowed the yoke to be made in steel / concrete, with the steel being 30% in volume. This is referred to as dilution. We say that the stacking factor is 0.30. In the great majority of cases, the stacking factor is above 97%; the few % unoccupied by iron is taken up by insulation in between laminations and voids.

Some authors give guidelines: ex. for dipoles

Dipole Magnet Field Quality



Good field area
 $B = B_y = \text{const}$ in the ideal dipole

Shim area: $S = 0.021 \cdot d^2$

This relation is good for w/d
 in the range of 0.2 – 0.6.

Field in the magnet midplane:

$$B = B_0(1 + b_1 \cdot x + b_2 \cdot x^2 + \dots)$$

Without shims the good field area width is:

- for 1% field homogeneity $a = (b - d)$;
- for 0.1% field homogeneity $a = (b - 2d)$.

The good field area could be extended by adding shims:

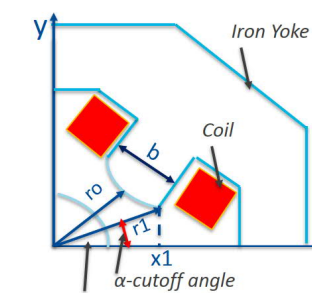
- for 1% field homogeneity $a = (b - d/2)$;
- for 0.1% field homogeneity $a = (b - d)$.

For gap fields above 0.8 T used
 more smooth shims to reduce iron
 saturation effects in pole edges
 and shim areas.

[Courtesy of V. Kashikhin]

Some authors give guidelines: ex. for quadrupoles

Quadrupole Magnets



Good field area

At $\alpha = 18^\circ$ the first undesired multipole b_5 vanishes.

$r_1 = 1.122 \cdot r_0$, $x_1 = 1.077 \cdot r_0$

Field gradient at $\mu = \infty$:

$G = dBy/dx = b_1 = \text{const}$

$By = G \cdot x$, $G = 2\mu_0 \cdot lw / r_0^2$

Field in the magnet midplane:

$B = B_0(1 + b_1 \cdot x + b_2 \cdot x^2 + \dots)$

For the quadrupole $B_0 = 0$,

The ideal quadrupole field : $B = b_1 \cdot x$
generated by a hyperbolic pole
profile: $x \cdot y = r_0^2 / 2$

The quadrupole half gap ampere-
turns: $(H_p + H_o) / 2 \cdot r_0 = lw$, or at $H_o = 0$;

Quadrupole coil ampere-turns:

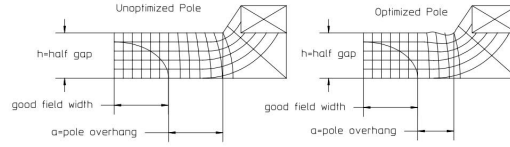
$H_p \cdot r_0 / 2 + H_{fe} \cdot L_{fe} = lw$,

$B_p \cdot r_0 / 2\mu_0 + B_{fe} / \mu \cdot L_{fe} = lw$.

H_{fe} , B_{fe} – defined as for dipoles, but
because of field gradient the flux
through the yoke two times lower.

[Courtesy of V. Kashikhin]

Some authors give guidelines: whole chapter (40 pages) in J. Tanabe's book



Optimized Pole

The expressions for the potential field quality and the pole overhang required to achieve a specified field quality for an optimized pole are given in eqs. (3.2) and (3.3).

$$\left(\frac{\Delta B}{B}\right)_{\text{optimized}} = \frac{1}{100} \exp[-7.17(x - 0.39)] \quad (3.2)$$

$$x_{\text{optimized}} = \frac{a}{h} = -0.14 \ln \frac{\Delta B}{B} - 0.25 \quad (3.3)$$

Unptimized Pole

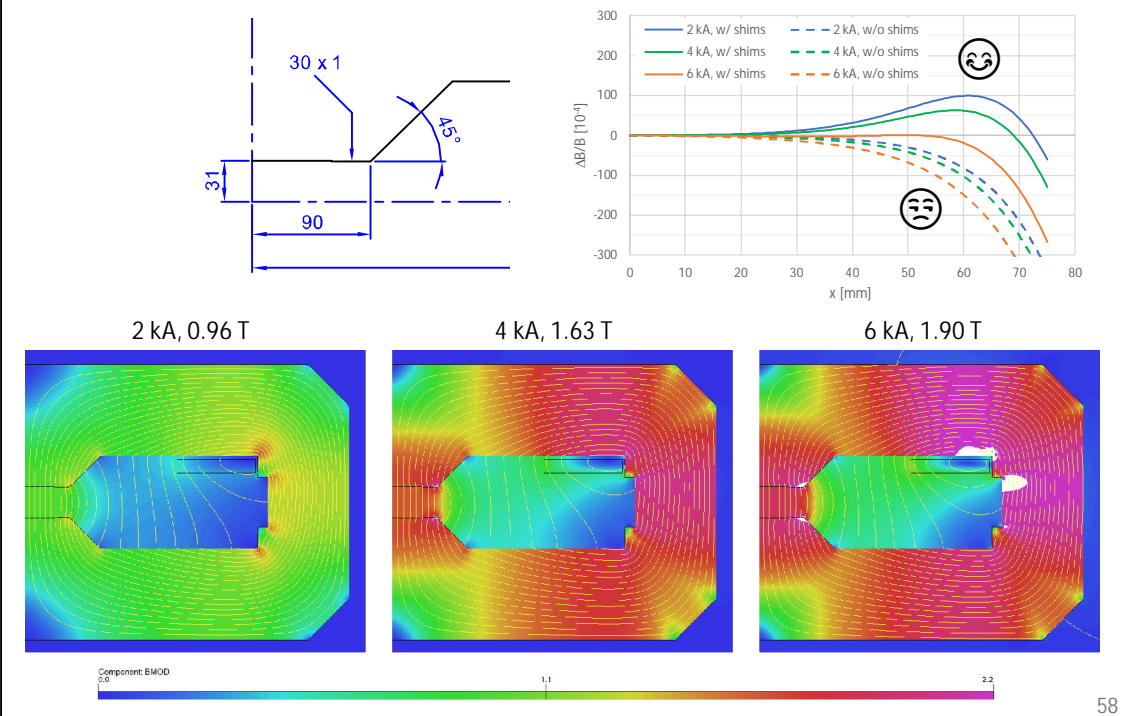
The expressions for the potential field quality and the pole overhang required to achieve a specified field quality for an unoptimized pole are given in eqs. (3.4) and (3.5).

$$\left(\frac{\Delta B}{B}\right)_{\text{unoptimized}} = \frac{1}{100} \exp[-2.77(x - 0.75)] \quad (3.4)$$

$$x_{\text{unoptimized}} = \frac{a}{h} = -0.36 \ln \frac{\Delta B}{B} - 0.90 \quad (3.5)$$

[Courtesy of J. Tanabe]

The size of these side shims can depend on the field level and on the BH characteristics of the material



This example is taken from a superferric magnet – in this case, the coil is quite far from the aperture, so the variation in field quality is only due to iron saturation.

The field homogeneity is given as a $\Delta B/B$ plot, which is typical for a resistive dipole where the aperture has an elongated aperture rather than a circular one. In such a plot, we move along the midplane and we look at the field difference with respect to the field in the center, normalized again by the field in the center. Without side shims, the field has a tendency of decreasing when moving towards the extremity of the pole. Side shims provides a field increase to compensate this effect, though at higher current they are less effective, due to saturation. This is a typical behavior, with a “happy” $\Delta B/B$ which then turns to “sad”.

Good practice at the design phase is to check the impact of different BH curves as well as the integrated field homogeneity in 3D.

Conclusions (yoke design 2D)

The yoke shall be dimensioned considering various aspects

- There is not a unique solution

- Several magnet layouts are possible

- Pole width, pole tip profile, side shims: the starting point is often given by the curves of constant scalar potential

The material of the yoke is ferromagnetic with $\mu_r \gg 1$

- In most cases, electrical steel

The maximum (reasonable) field for a dipole is 2.0 T

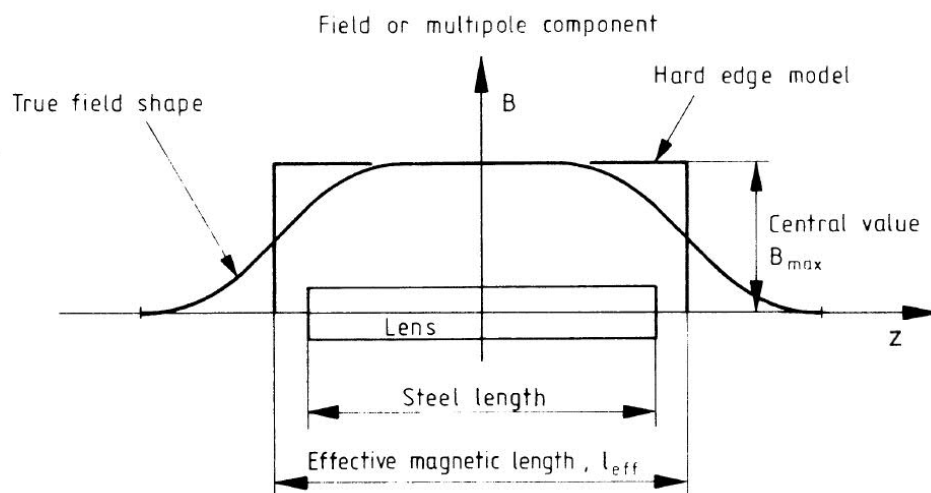
- In most cases, we prefer to stay below, in the 1.5 T region

Forces in the iron are (usually) not a main concern

Yoke design

3D

In 3D, the longitudinal dimension of the magnet is described by a magnetic length



$$l_m B_0 = \int_{-\infty}^{\infty} B(z) dz$$

61

Looking along the longitudinal (z) direction, B is maximum at the center ($z = 0$) of the magnet, it is more or less constant till reaching the ends, where it rolls off to reach a 0 value outside. The magnetic length l_m is defined as that length which – multiplied by the central field value B_0 – provides the same integrated field.

The same holds substituting the field B with the gradient G , or with any multipole B_n , A_n . In this case, the integrals are carried out on the not-normalized (upper case) coefficients, and the normalized terms (lower case) are then obtained by dividing by the integral of the fundamental harmonic.

For long magnets – where the longitudinal dimension is much larger than the gap – the behavior is dominated by the (long) central part, so taking the values of 2D simulations and multiplying by a length yields good results. For short magnets, the behavior is intrinsically 3D.

The magnetic length can be estimated at first order with simple formulae

$$l_m > l_{Fe}$$

dipole

$$l_m \cong l_{Fe} + h \quad h$$

quadrupole

$$l_m \cong l_{Fe} + 2/3r \quad r \quad \text{aperture radius}$$

sextupole

$$l_m \cong l_{Fe} + r/2 \quad r \quad \text{aperture radius}$$

62

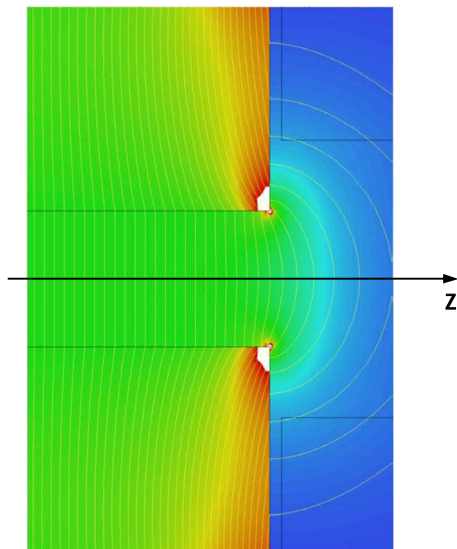
The magnetic length is larger than the iron length: there is some stray flux, that is, there is still some field left after the iron yoke terminates, since B rolls off in a continuous way.

The actual value of l_m depends mainly on the geometry of the pole ends – abrupt, with shims, with chamfers, with some rounded (Rogowski-like) profile – and on the iron saturation. The same magnet can actually have slightly different magnetic lengths when the excitation current – hence, the field level – is different. All these effects can be assessed precisely only by 3D simulations and measurements.

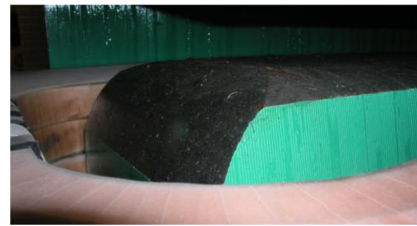
In most cases, though, it is possible to estimate at first order the length with the given simple formulae. In general, the higher the order of a magnet (quadrupole, sextupole, octupole, etc.), the less stray field is found on the axis at the ends, and the closer are the values of l_m and l_{Fe} .

Note: since in lattice codes l_m is used, crowded regions – with many nearby magnets – might have to be looked at in detail, to make sure there is enough physical space for the magnets and their coil ends. Moreover, there might be also some magnetic coupling between magnets which are installed very close to each other.

There are many different options to terminate the poles in 3D, depending on the type of magnet, its field level, personal preferences, etc.



abrupt



rounded (DIAMOND dipole)



shims (SPS MB)

63

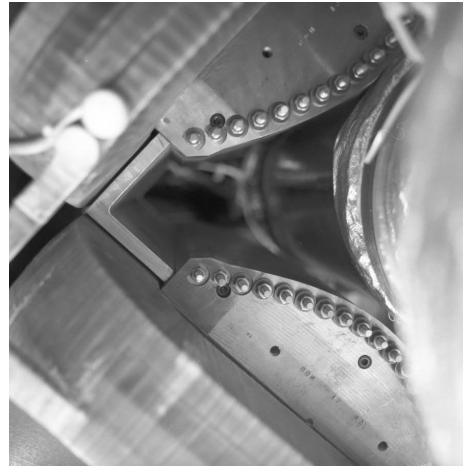
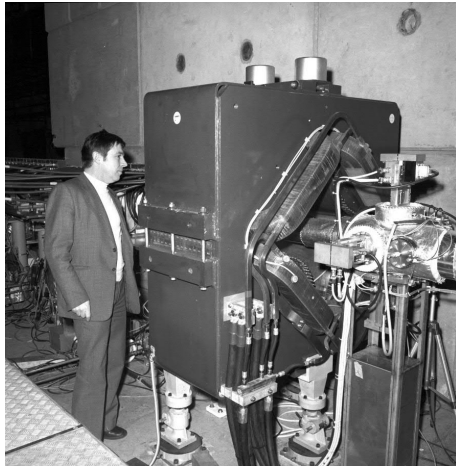
One option is to have square ends – the pole profile is simply extruded in 3D and then terminated abruptly (left figure). This introduces some field amplification in the end of the iron, that has to carry also the stray field that extends past I_{Fe} . This might lead to saturation and possibly non-linear behavior at different excitation currents.

Another possibility is to have end shims. These are also used to trim the iron length so to have a closer magnet-to-magnet reproducibility of the field integrals. The bottom right figure shows the design used for the SPS main dipoles, with shims at the extremities which are adjusted following magnetic measurements, to tune the integrated field vs. the reference magnet.

In some cases, a rounded Rogowski-like profile is used, to avoid flux concentration in the ends, like for the DIAMOND dipole shown in the top right figure.

In all cases, there is an impact on the magnetic length and on the integrated field quality; optimizing the termination of the poles is a main reason to set up 3D magnetic simulations.

Shims and washers on quadrupole ends for the AA quads

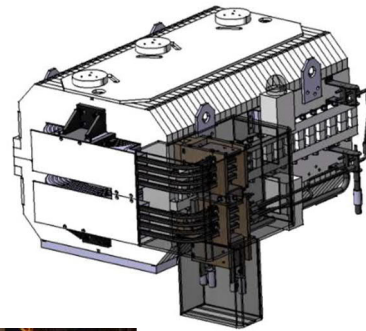
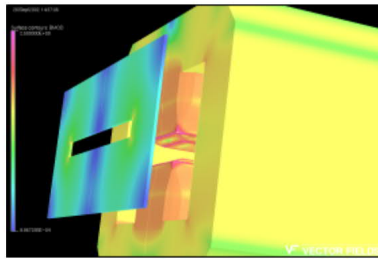


64

<https://cds.cern.ch/record/1820347>

Due to the fact that much of the field of the quadrupoles was outside the iron (in particular with the wide quadrupoles) and that thus the fields of quadrupoles and bending magnets interacted, the lattice properties of the AA could not be predicted with the required accuracy. After a first running period in 1980, during which detailed measurements were made with proton test beams, corrections to the quadrupoles were made in 1981, in the form of laminated shims at the ends of the poles, and with steel washers. With the latter ones, further refinements were made in an iterative procedure with measurements on the circulating beam. Here we see the shims and washers on a narrow quadrupole (QFN, QDN).

In some cases, a ferromagnetic plate delimits the field in the longitudinal direction: ex. SOLEIL dipole



[Courtesy of A. Dael and B. Launé]

Some machines are very crowded, also in the longitudinal direction: see latest light sources, ex. ESRF-EBS

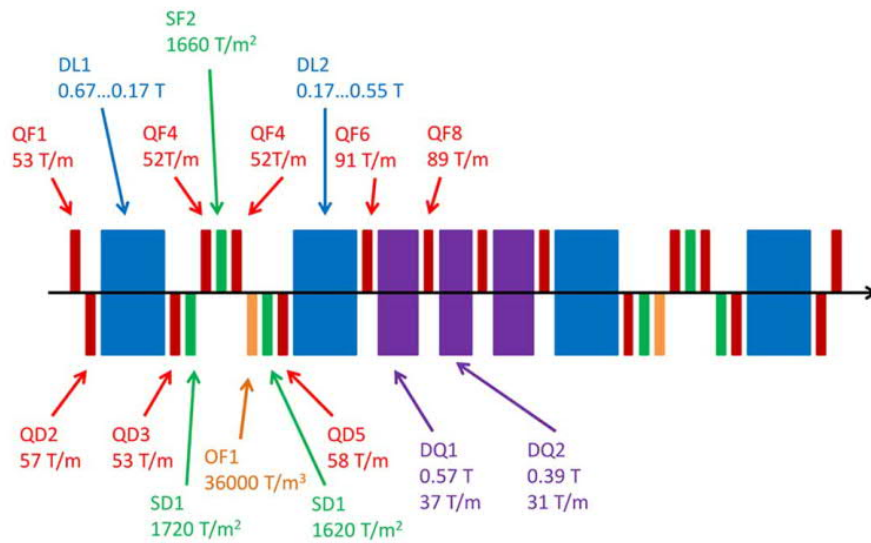


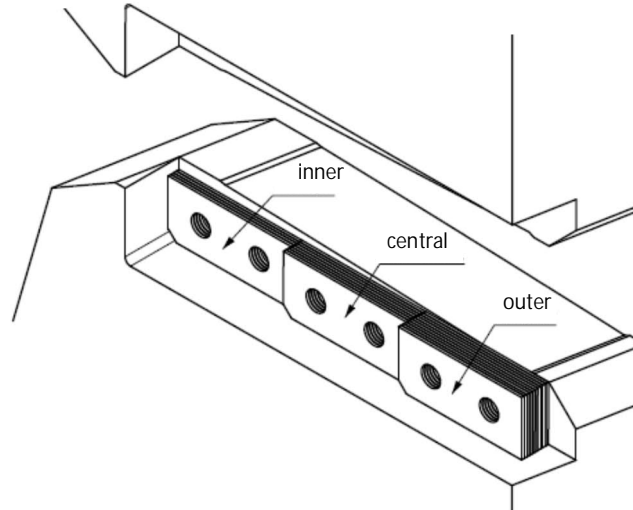
Fig. 1. Schematic view of the magnets of one cell: dipoles with longitudinal gradient (DL), quadrupoles (QF, QD), combined dipole–quadrupoles (DQ), sextupoles (S), and octupoles (O). Corrector magnets are not shown.

66

[G. Le Bec *et al.*, Magnets for the ESRF Diffraction-Limited Light Source Project, IEEE Trans. Appl. Supercon., v. 26, n. 4, Jun. 2016]

This situation is not uncommon in other light sources and elsewhere. There can be also areas crowded transversally, which call for narrow designs for the magnets.

SESAME main bending: three degrees of freedom to correct integrated field, quadrupole and sextupole (if needed), after magnetic measurements

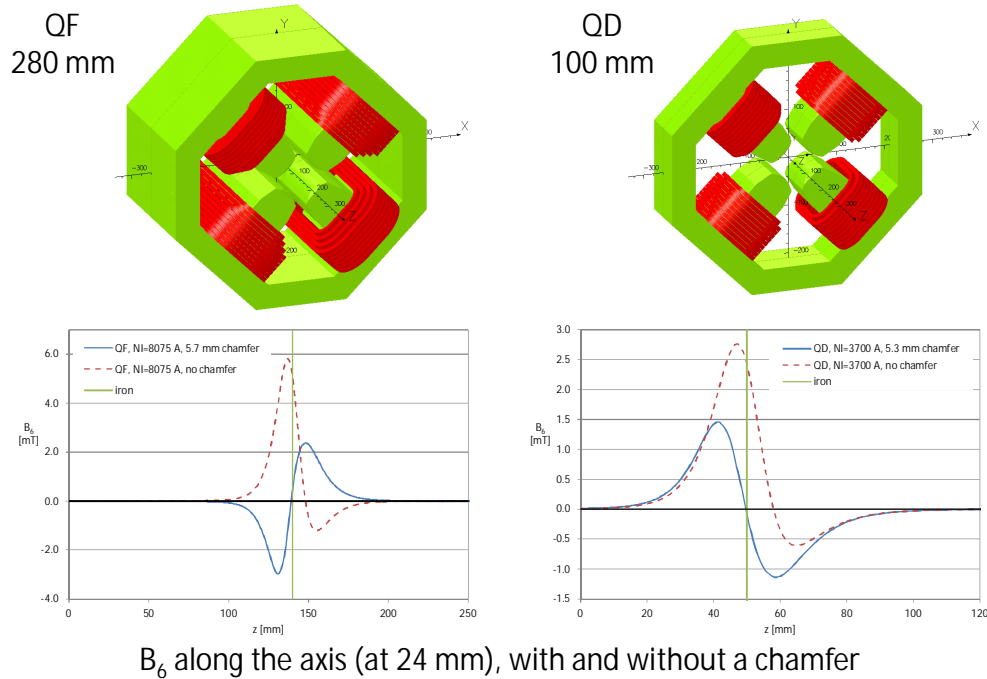


67

The SESAME combined function bending magnets had three separate stacks of end pole shims to tune integrated dipole, quadrupole and sextupole components separately (if needed), following magnetic measurements. For this specific case, at the end only the integrated gradient was adjusted, acting on the inner and outer shims, in about half the series production (total of 17 magnets). Considering the combined function nature of the field, the integrated dipole was adjusted by a radial displacement. The vertical position and roll angle were also used to cancel the integrated skew dipole and skew quadrupole, respectively.

More details can be found in the bonus slides.

SESAME quadrupoles: same cross-section, different end chamfers (45°) to cancel the first allowed harmonic



68

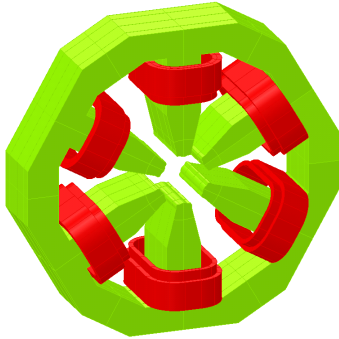
Chamfers are also a popular option, for example 45 deg chamfers are often used for quadrupoles and sextupoles.

As an example, we report the case of the SESAME quadrupoles. The cross-section is the same for both the focusing and defocusing magnets, however the field strength and length are different. This called for a slightly different chamfer to cancel out the first integrated harmonic.

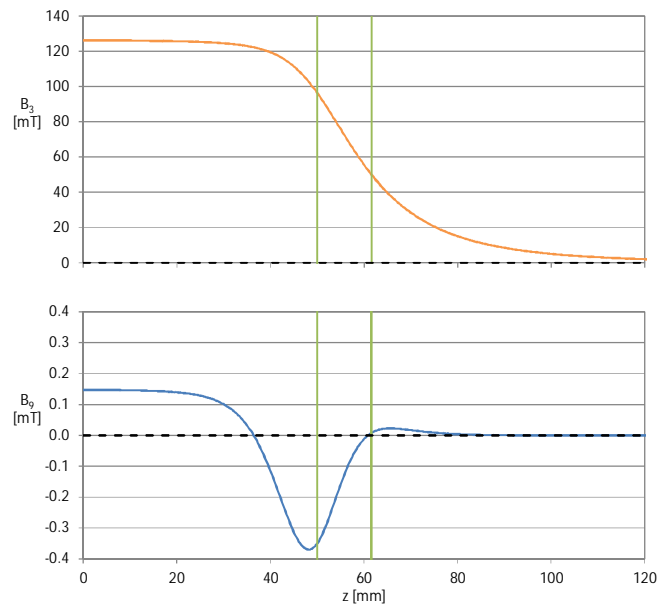
Often the pre-series magnets come with end pole inserts, where different geometries are tried before freezing the design for the series. For this specific example, we did on the other hand relied on 3D magnetic simulations, waiting anyway for a confirmation from pre-series units of each type before going on with the series production.

More details can be found in the bonus slides.

SESAME sextupoles: no end chamfer, first integrated allowed harmonic compensated with an offset in 2D



In 2D, $b_9 = 12.8 \cdot 10^{-4}$



B_3 and B_9 along the axis (at 24 mm), no end chamfer

69

Also for sextupoles end chamfers are often used. This is not mandatory, as the above example of the SESAME sextupole shows.

In this case, the poles are not chamfered – still, the first allowed harmonic cancels out by introducing in 2D an offset which is then compensated in 3D in the ends.

This approach can be used also for different orders, however it is less interesting when a magnet works both in a non-saturated and saturated design, as typically the ends saturate even before the cross-section.

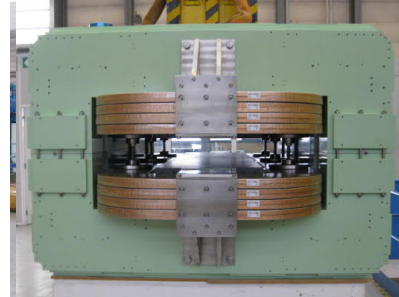
More details can be found in the bonus slides.

Solid vs. laminated iron? Simplifying at the extreme, solid ---> dc application, laminated ---> can be pulsed

M200



M200 L



70

This example refers to the East Area renovation at CERN, which was already introduced when considering the Q200 L magnets.

For more details, see for example the following reference:

R. Lopez and J. Renedo Anglada, The New Magnet System for the East Area at CERN, IEEE Trans. Appl. Supercon., v. 30, n. 4, Jun. 2020

Stacking factor: see below for a formal treatment

In case of anisotropic magnetic material the permeability has the form of a diagonal rank 2 tensor, so that $\mathbf{B} = [\mu] \mathbf{H}$ with

$$[\mu] = \begin{pmatrix} \mu_x & 0 & 0 \\ 0 & \mu_y & 0 \\ 0 & 0 & \mu_z \end{pmatrix}. \quad (60)$$

In many materials, such as in rolled metal sheets, the fabrication process produces some regularity in the crystal structure and consequently a dependence of the magnetic properties on the direction. The most well known (and strongest) anisotropy in magnetic materials can be achieved by laminating the iron yokes. Between each of the ferromagnetic laminations of thickness l_{Fe} (magnetically isotropic to first order) there is a non-magnetic ($\mu = \mu_0$) layer of thickness l_0 , as shown schematically in Fig. 7.

Consider a lamination in z -direction and the field components B_i in the xy -plane. Because of the continuity condition $\mathbf{H}_i^I = \mathbf{H}_i^{II} = \bar{\mathbf{H}}_i$ we get for the effective macroscopic tangential flux density

$$\bar{\mathbf{B}}_i = \frac{1}{l_{Fe} + l_0} (l_{Fe} \mu \bar{\mathbf{H}}_i + l_0 \mu_0 \bar{\mathbf{H}}_i). \quad (61)$$

In most cases 0.97-0.98
and in practice no major
impact on results

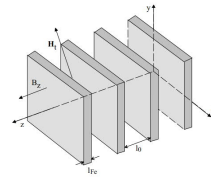


Fig. 7: On the calculation of the μ tensor for laminated materials. The transversal dimensions are large with respect to l_0 and l_{Fe} .

As the normal component of the magnetic flux density is continuous, i.e., $B_z^I = B_z^{II} = \bar{B}_z$, the average magnetic field intensity can be calculated from

$$\bar{H}_z = \frac{1}{l_{Fe} + l_0} \left(l_{Fe} \frac{\bar{B}_z}{\mu} + l_0 \frac{\bar{B}_z}{\mu_0} \right). \quad (62)$$

With the packing factor

$$\lambda = \frac{l_{Fe}}{l_{Fe} + l_0} \quad (63)$$

which is 0.985 for the LHC yokes, we get for the average permeability in the plane of the lamination

$$\bar{\mu}_i = \lambda \mu + (1 - \lambda) \mu_0 \quad (64)$$

and normal to the plane of the lamination

$$\bar{\mu}_z = \left(\frac{\lambda}{\mu} + \frac{1 - \lambda}{\mu_0} \right)^{-1}. \quad (65)$$

We have obtained a simple equation for the packing factor scaling of the material characteristic. For laminations in the x and y direction, i.e. with the plane of the laminations normal to the 2D cross-section, the laminations have a strong directional effect and the packing factor scaling is no longer appropriate. A macroscopic model for these circumstances is developed in [5].

[Courtesy of S. Russenschuck]

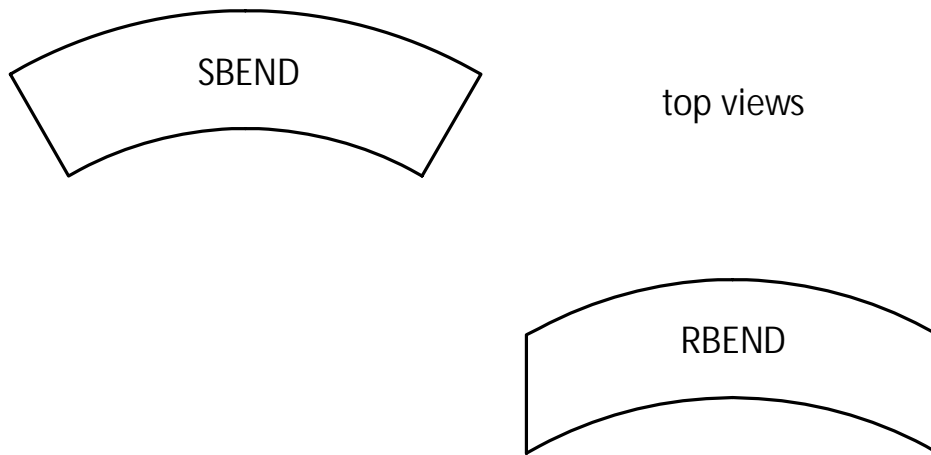
The stacking factor is usually quite close to 1 – a notable exception was the core of the LEP bending magnets.

For laminated magnets, the stacking factor depends on the lamination thickness, its surface treatment and possibly the fabrication process – in some cases, ranges are given in the specification documents.

For solid magnets, the stacking factor is 1.

In my opinion, there is not a large impact on the field in the gap. Still, modern codes allow to consider it, also in 2D, so it can be interesting to check.

Usually two dipole elements are found in lattice codes: the sector dipole (SBEND) and the parallel faces dipole (RBEND)



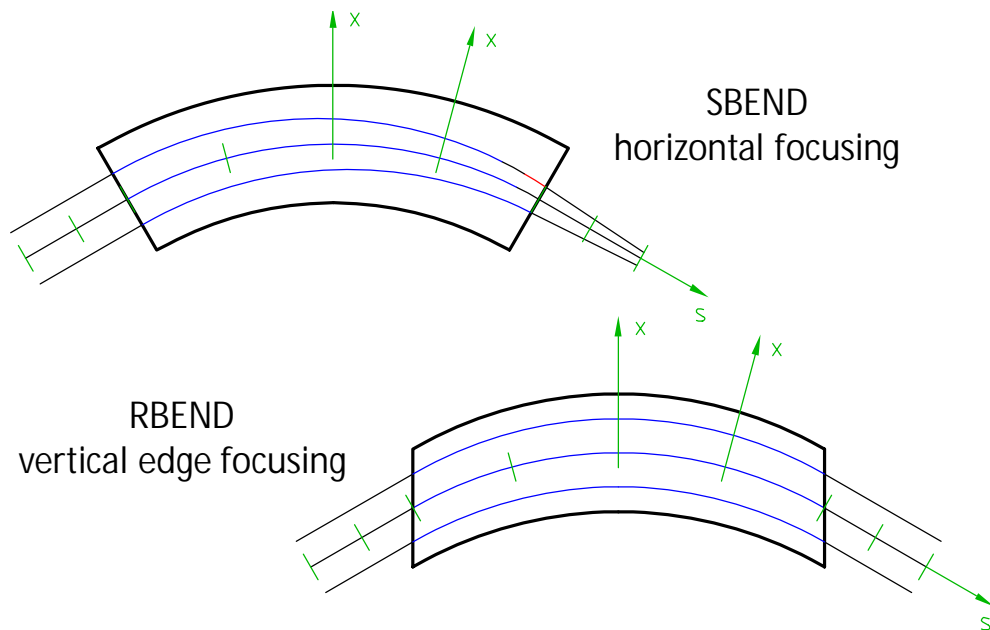
72

A sector dipole and a parallel faces (or rectangular) one both provide a region of space with constant field, though they have different focusing effects on the beam.

Other cases are possible, if the dipole ends are shaped with another angle with respect to the incoming / outgoing beam, or even curves.

Note: the curvature has no effect, it is just for saving material, otherwise the pole would have to be wider. In jargon, people talk about the *sagitta* of the beam going through a dipole and then evaluate whether to curve the magnet or not. In most light sources – where the bending radii are a few meters – the main dipoles are curved.

The two types of dipoles are slightly different in terms of focusing, for a geometric effect



and anything in between, playing with the edges, also curved

73

In a dipole, since the field is constant, particles are bent according to the same bending radius – given by the field and the beam rigidity.

In a sector dipole, there is a difference in how much space is travelled within the uniform field depending on the transverse position: a sector dipole focuses horizontally.

This effect is not there in parallel ended dipoles. However, these have an edge effect. In fact, the edges are defocusing, but the overall magnet has zero focusing horizontally. Still, it remains some vertical focusing at the edges. Most often, if the bending angle is not so high (at least up to 45 deg) parallel ended dipoles are more convenient to manufacture, as the yoke is built stacking up sheets of laminations (like a deck of cards) and the pole width is reduced because the sagitta of the beam does not need to be added.

These effects are handled differently in the various lattice codes, according to some assumptions on the field roll-off in the ends, that somehow gradually goes from a constant value (inside the dipole) to zero (outside). Some details about what MAD-X does are given in its documentation, in the section *Bending Magnet*.

Conclusions (yoke design 3D)

The concept of magnetic length is important

Special attention is needed in crowded lines

As in 2D, several options are possible for the termination of the poles in 3D

Again, there is not a unique solution

3D simulations are powerful tools to check field integrals

Either solid or laminated yokes are used

The default preference at CERN now is to go for laminated yokes, possibly machined (that is, not stamped)

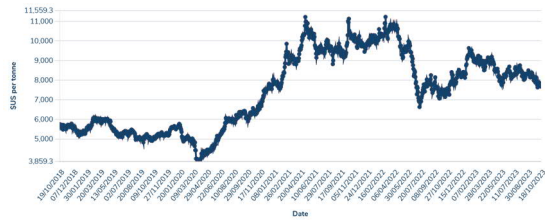
Coil design

The conductor is either copper (in most cases) or aluminum

Copper

$$1.72 \cdot [1 + 0.0039 \cdot (T - 20)] \cdot 10^{-8} \, \Omega/\text{m}$$

$$8.9 \, \text{kg}/\text{dm}^3$$



Aluminium

$$2.65 \cdot [1 + 0.0040 \cdot (T - 20)] \cdot 10^{-8} \, \Omega/\text{m}$$

$$2.7 \, \text{kg}/\text{dm}^3$$



76

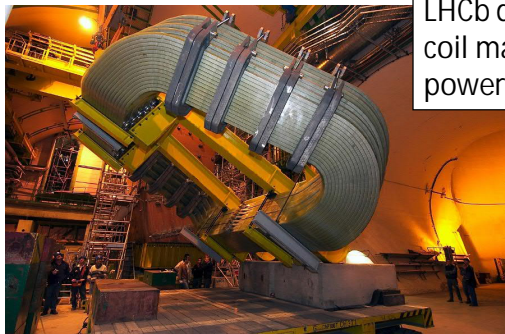
Copper is the most common choice nowadays for accelerator magnets, as it offers a lower resistivity. The SPS magnets at CERN have coils in copper. This was also the choice for all new resistive magnets at CERN in the last years.

Sometimes aluminum becomes interesting because it is lightweight and less expensive, also when additional material is added to keep the resistance (and power) of the coil low: examples are given in the following slide.

Both Cu and Al become more resistive as the temperature increases, with about a 4‰ increase per degree.

The raw metal prices evolve continuously, the plots are taken from the London Metal Exchange website: <https://www.lme.com>.

Some examples of coils with aluminum conductor



LHCb detector dipole
coil mass 2×25 t
power 2×2.1 MW



LEP dipole
busbars



PS main
units

77

The PS main units at CERN are in aluminum, which was chosen for economical reasons.

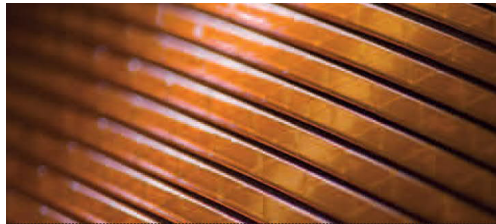
The LEP main bending magnets were powered with aluminum busbars. [Picture courtesy of ASG]

The LHCb dipole, as other large experimental magnets, also uses aluminum as conductor.

When demineralized water is needed for direct cooling of aluminum coils, the hydraulic circuit shall be separate from that connected to copper coils.

Aluminum is used routinely in electrical power transmission lines.

Focusing on copper, both hollow conductors (long length, mostly non-insulated) and solid conductors (also insulated) are commercially available



Nowadays long lengths of hollow copper conductor are commercially available. They are most often produced on demand. Often suppliers have a catalogue of sizes for which the tooling is already available – other geometries can be purchased, with the additional cost of a custom made tooling. Also non-circular cooling holes are an options (in this case, for cooling calculations, the hydraulic diameter is used).

For solid conductors, many geometries are available off the shelf, including insulated (ex. enameled) products.

[Picture of hollow conductors courtesy of Luvata]

[Picture of solid conductors courtesy of VonRoll]



Standard coil types

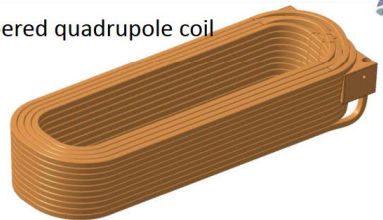
Bedstead or saddle coil



Racetrack coil



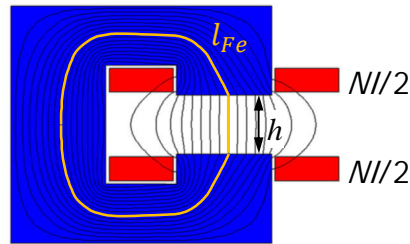
Tapered quadrupole coil



minimum bending radius (in particular for hollow conductor) typically 5x side / 10x the hole diameter – to avoid cooling restrictions and wedging

[Courtesy of T. Zickler]

For a dipole, the Ampere-turns are a linear function of the gap and of the field (at least up to saturation)



$$NI = \oint \vec{H} \cdot d\vec{l} = \frac{B_{Fe}}{\mu_0 \mu_r} \cdot l_{Fe} + \frac{B_{gap}}{\mu_0} \cdot h \cong \frac{B_{gap} h}{\mu_0}$$

$$NI = \frac{Bh}{\eta \mu_0} \quad \eta = \frac{1}{1 + \frac{1}{\mu_r} \frac{l_{Fe}}{h}}$$

80

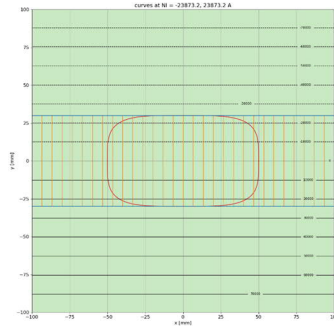
The basic formula to compute the Ampere-turns needed for a given field and vertical gap can be derived from the circulation of H around a flux line (Ampere's law).

The term with B_{Fe} , l_{Fe} and μ_r is difficult to expand exactly – those can actually be interpreted as averages along the integral – however it does not matter. In fact, B_{Fe} is similar to B_{gap} , while μ_r has a high value (thousands, unless the iron is heavily saturated) which makes that contribution small.

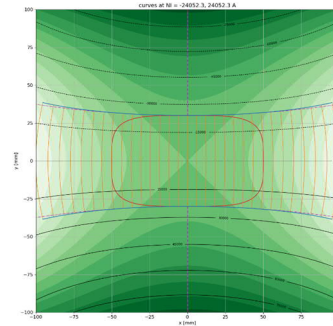
The concept of magnetic efficiency η can also be introduced. Typical values are above 95%.

This formula is very useful, but it also assumes a pure dipole field: see below for ex. when adding a sextupole error

$$\frac{NI}{2} = \frac{B_1}{\mu_0} \frac{h}{2} - \frac{B_3}{3\mu_0 R^2} \left(\frac{h}{2}\right)^3$$



$B_1 = 1 \text{ T}$
 $B_3 = 0 \text{ T}$ at $R = 20 \text{ mm}$
 $h = 60 \text{ mm}$
 $NI = 2 \times 23873.24 \text{ A}$



$B_1 = 1 \text{ T}$
 $B_3 = -0.01 \text{ T}$ at $R = 20 \text{ mm}$
 $h = 60 \text{ mm}$
 $NI = 2 \times 24052.29 \text{ A}$

81

A somehow tacit assumption when deriving the formula in the previous slide was that the field is perfect, in this case a pure dipole. In reality, even without considering manufacturing tolerances, allowed harmonics are always there.

As an example, we show above the formula for a dipole when also a sextupole component is present – this is in fact the first allowed harmonic for a symmetric dipole. This is quite academic: since the design is such that the allowed harmonics are rather small compared to the fundamental component, the correction in the formula is very minor. In the example, considering a large sextupole error – 1%, or $100 \cdot 10^{-4}$ at a reference radius of $2/3$ the aperture – the correction amounts to 0.75%.

The same computation can be tackled using magnetic reluctances and Hopkinson's law, which is a parallel of Ohm's law

$$\mathcal{R} = \frac{NI}{\Phi}$$

$$R = \frac{V}{I}$$

$$\mathcal{R} = \frac{l}{\mu_0 \mu_r A}$$

$$R = \frac{l}{\sigma S}$$

$$\eta = \frac{1}{1 + \frac{\mathcal{R}_{Fe}}{\mathcal{R}_{gap}}}$$

82

There is a simple parallel between magnetic and electrical circuits:

- * voltage drop ---> magnetomotive force
- * resistance ---> reluctance
- * current ---> flux
- * Ohm's law ---> Hopkinson's law

NI – the Ampere-turns – is the magnetomotive force.

A and l are the cross-section of the magnetic circuit and its length. In 2D, the area A is the width of the magnetic circuit * 1 m.

The B field (flux density) is then the flux Φ divided by the section A .

The Ampere-turns spent in the yoke are like the voltage drop spent in connection wires in an electric circuit.

In most cases, there are two main magnetic reluctances in series: the one for the air gap (usually predominant) and the one for the iron.

The Ampere-turns grow with the order of the magnet, so there is an interest in keeping the aperture small

Dipole

$$NI \cong \frac{Bh}{\mu_0}$$

$$B \cong \frac{\mu_0 NI}{h}$$

Quadrupole

$$NI \cong \frac{2B'r^2}{\mu_0}$$

$$B' \cong \frac{\mu_0 NI}{2r^2}$$

Sextupole

$$NI \cong \frac{B''r^3}{\mu_0}$$

$$B'' \cong \frac{\mu_0 NI}{r^3}$$

83

Similar formulae can be derived for quadrupoles, sextupoles and other magnets: a few are reported here for convenience.

μ_0 [H/m] vacuum permeability, $4\pi \cdot 10^{-7}$ H/m

NI [A] total (not per pole) Ampere-turns

Dipole

B [T] field in the aperture

h [m] full vertical gap

Quadrupole and sextupole

B' [T/m] field gradient, i.e. first derivative of B in the origin

B'' [T/m²] second derivative of B in the origin

r [m] aperture radius

These formulae are very useful and they show the power law dependence of the field strength with respect to the aperture size.

As a reminder, they are (very good) approximations as they do not consider:

- the Ampere-turns spent in the iron
- 3D effects
- field errors (i.e., not pure fields, see ex. before of dipole with sextupole term)

These are the same formulae – including the more general one – using the fundamental harmonic rather than B , B' , B''

<u>Dipole</u>	$B = B_1$	$B_1 \cong \frac{\mu_0 NI}{2r}$	$NI \cong \frac{2B_1 r}{\mu_0}$
<u>Quadrupole</u>	$B' = \frac{B_2}{R}$	$B_2 \cong \frac{\mu_0 NIR}{2r^2}$	$NI \cong \frac{2B_2 r^2}{R\mu_0}$
<u>Sextupole</u>	$B'' = \frac{2B_3}{R^2}$	$B_3 \cong \frac{\mu_0 NIR^2}{2r^3}$	$NI \cong \frac{2B_3 r^3}{\mu_0 R^2}$
<u>General</u>		$B_n \cong \frac{\mu_0 NIR^{n-1}}{2r^n}$	$NI \cong \frac{2B_n r^n}{\mu_0 R^{n-1}}$

84

The symbols are the same as in the previous slide, for consistency we consider an aperture radius also for the dipole:

μ_0 [H/m] vacuum permeability, $4\pi \cdot 10^{-7}$ H/m

NI [A] total (not per pole) Ampere-turns

B_n [T] harmonic of order n

r [m] aperture radius

R [m] reference radius (for the harmonics)

B' [T/m] field gradient, for a quadrupole

B'' [T/m²] second derivative of B in the origin, for a sextupole

Note: notice the factor 2, in the definition of the sextupole strength – for sextupoles and higher order, in my opinion the clearer definition of strength is the field (or the integrated field in 3D) at the reference radius, rather than derivatives

Geometric errors in the pole have a larger impact on the magnetic field in the gap, as the order increases

$$\text{Dipole} \quad \frac{\Delta B}{B} = \frac{B(h + \Delta h) - B(h)}{B(h)} \cong -\frac{\Delta h}{h}$$

$$\text{Quadrupole} \quad \frac{\Delta B'}{B'} = \frac{B'(r + \Delta r) - B'(r)}{B'(r)} \cong -2\frac{\Delta r}{r}$$

$$\text{Sextupole} \quad \frac{\Delta B''}{B''} = \frac{B''(r + \Delta r) - B''(r)}{B''(r)} \cong -3\frac{\Delta r}{r}$$

85

The formulae in the previous slide can be used to check the impact on the main field component when the aperture differs from the nominal size – the power law dependency translates into a linear one here (considering small dimensional changes), with a increasing factor: 1 for a dipole, 2 for a quadrupole and 3 for a sextupole.

Dipole

h [m] full vertical gap
 Δh [m] change in full vertical gap

Quadrupole and sextupole

r [m] aperture radius
 Δr [m] change in aperture radius

A similar analysis can be done for the allowed harmonics, showing that the higher the order of the magnet, the most sensitive the field to changes of the geometry of the pole.

Example of computation of Ampere-turns and current

central field $B = 1.3 \text{ T}$

total gap 80 mm

$$NI = \frac{Bh}{\eta\mu_0}$$

$\eta \cong 0.90$

$$NI = (1.3 \cdot 0.080) / (0.90 \cdot 4 \cdot \pi \cdot 10^{-7}) = 91956 \text{ A total}$$

low inductance option

64 turns, $I \cong 91956/64 = 1437 \text{ A}$

$L = 62.9 \text{ mH}$, $R = 15.9 \text{ m}\Omega$

low current option

204 turns, $I \cong 91956/204 = 451 \text{ A}$

$L = 639 \text{ mH}$, $R = 172 \text{ m}\Omega$

86

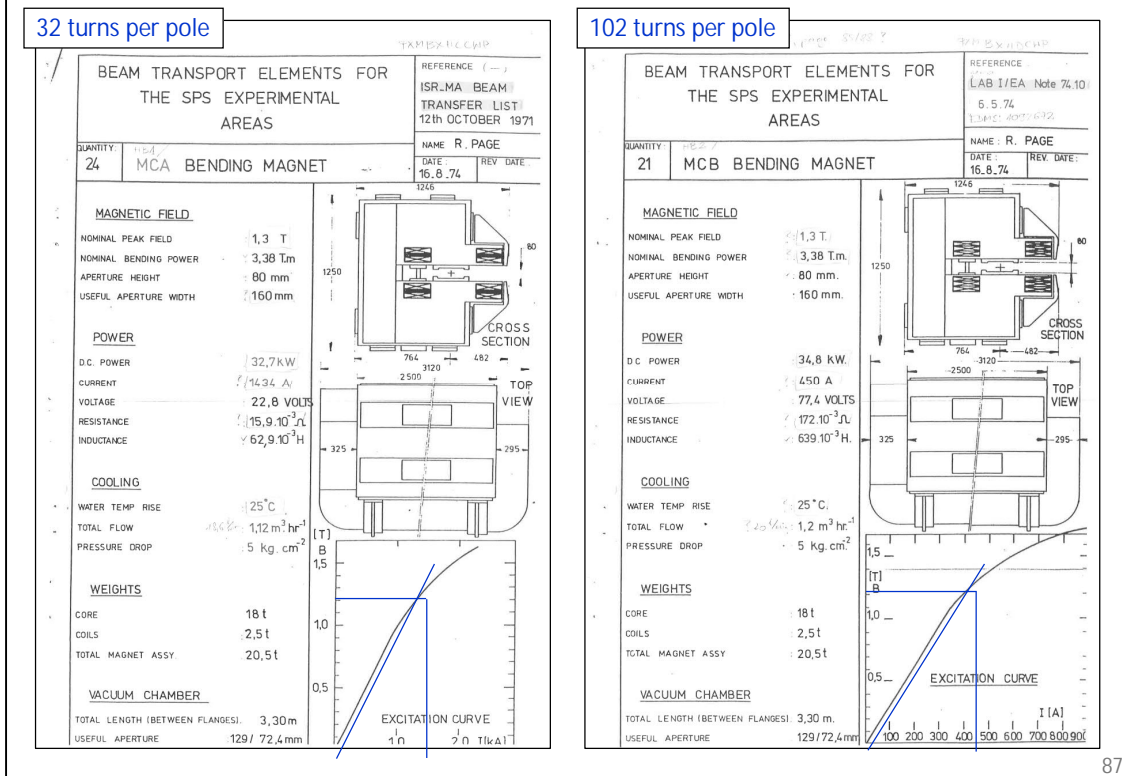
These values are taken from existing magnets, designed in the late 1960s at CERN: the so-called MCAs and MCBs (see also next slide).

Having a small number of turns carrying a large current brings down the inductance. This can be convenient if the machine is ramped or pulsed, as the inductive voltage $L \cdot di/dt$ can be significant. On the other hand, high current means larger cables and connections.

The same Ampere-turns can be obtained with a higher number of turns carrying a smaller current each. In this case the inductance is high, which is not an issue if the magnet is almost dc. The size of the cables and of the connections is smaller if the current is smaller.

Best practice calls for a design of the coil considering also the power converters, possibly with several iterations.

MCA/MCB dipole: same yoke, different coils



87

This is the example of the previous slide.

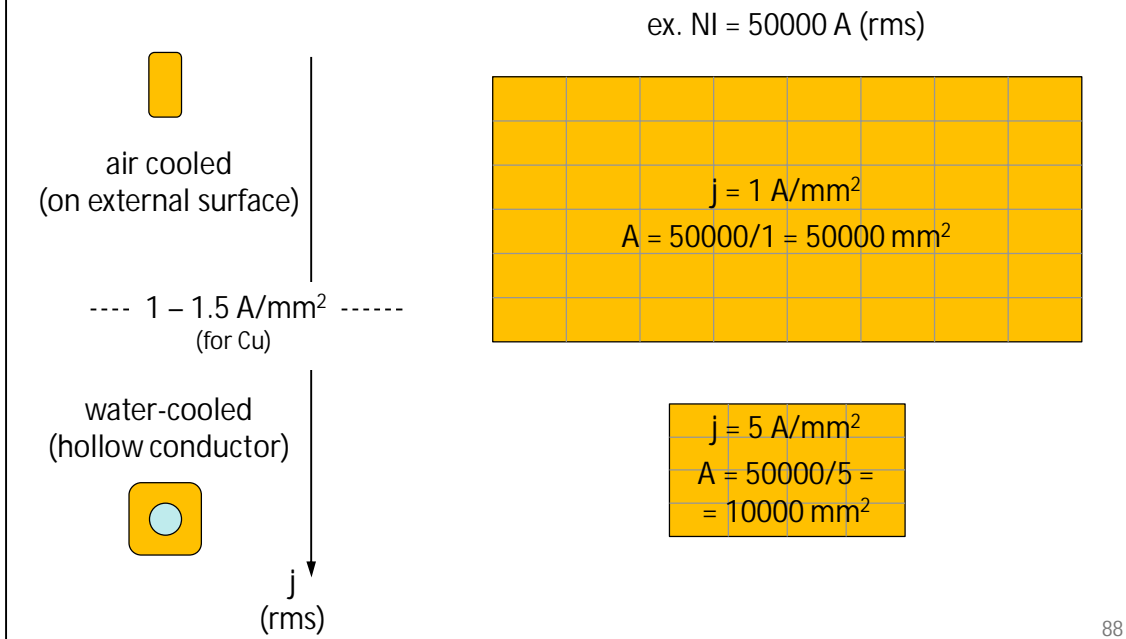
The yoke is identical in the two cases, just the coils are different, with a high current / low inductance and a low current / high inductance designs. The iron length is 2.5 m. As the magnetic energy ($\frac{1}{2} \cdot L \cdot I^2$) is basically the same, the inductance scales with (number of turns)².

The above ID cards are extracted from:

Beam transport elements for the SPS Experimental Areas

<https://edms.cern.ch/document/1714754>

Besides the number of turns, the overall size of the coil depends on the current density, which drives the resistive power consumption (linearly)



88

Given the Ampere-turns – which depend on the field strength, the gap and (to a lesser degree) the saturation level of the iron – the size of the coil depends on the current density j .

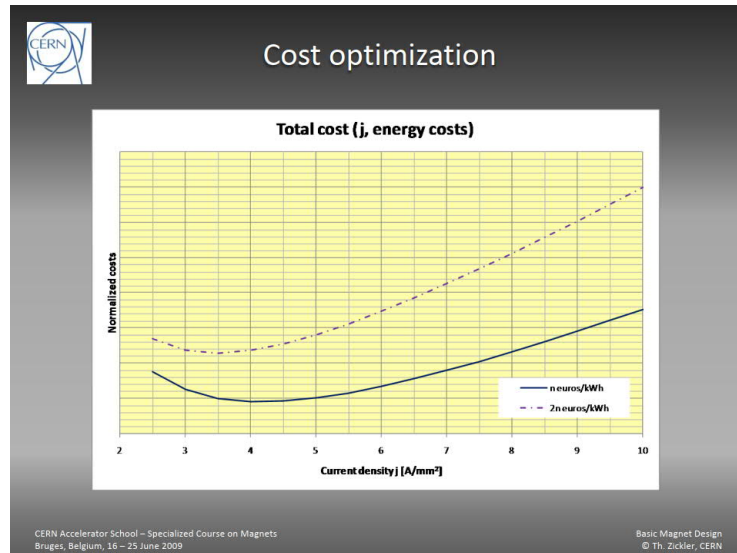
The dc resistive power dissipated in the windings scales linearly with j – at fixed field (that is, for the same Ampere-turns).

Below $1 - 1.5 \text{ A/mm}^2$ (rms) the coils are usually not directly cooled, that is, they are “air cooled” on the exterior by natural air convection. Above those current densities, direct water-cooling (with demineralized water circulating inside the conductor) is used. A typical value is now around 5 A/mm^2 (rms) for dipoles, usually higher for quadrupoles. For both air and water-cooled cases, for dc or slow magnets, what needs to be removed is the resistive electrical power, that is $R \cdot I^2$. For very fast magnets, there are also eddy currents inside the conductor, which are not treated here.

The choice of j depends on several factors. For large machines, we look for a balance between an overall optimum of capital + running cost: large coils = large capital cost = low running (electricity) cost, and vice versa.

In other cases and for single or few magnets that need to be very compact, the current density can be much higher, like tens of A/mm^2 .

The size of the coil (for large magnets or many in series) is optimized considering capital and running costs (including infrastructure like power converters, cooling, cables, etc.)



[Courtesy of T. Zickler]

These are common formulae for the main electric parameters of a resistive dipole (1/2)

$$\text{Ampere-turns (total)} \quad NI = \frac{Bh}{\eta\mu_0}$$

$$\text{current} \quad I = \frac{(NI)}{N}$$

$$\text{resistance (total)} \quad R = \frac{\rho N L_{turn}}{A_{cond}}$$

$$\text{inductance} \quad L \cong \eta\mu_0 N^2 A / h$$

$$A \cong (w_{pole} + 1.2h)(l_{Fe} + h)$$

90

NI	[A]	total (not per pole) Ampere-turns
B	[T]	field in the aperture
h	[m]	full vertical gap
μ_0	[H/m]	vacuum permeability, $4\pi \cdot 10^{-7}$ H/m
η	[/]	magnetic efficiency, $\approx 0.95-0.98$ (depends on iron saturation)
I	[A]	current
N	[/]	total (not per pole) number of turns
R	[Ω]	resistance
L	[H]	inductance
ρ	[Ωm]	resistivity, $1.72 \cdot 10^{-8}$ Ωm for Cu, $2.65 \cdot 10^{-8}$ Ωm for Al, at 20 °C
L_{turn}	[m]	average length of a coil turn
A_{cond}	[m ²]	cross-section of a single conductor (counting only the metal)
l_{Fe}	[m]	iron length, in 3D (longitudinal direction)
w_{pole}	[m]	pole width

For the window frame layout with windings on both back legs, the Ampere-turns need to be doubled.

The resistance depends on the resistivity ρ of the conductor and its cross-section.

The inductance scales quadratically with the number of turns; then, for the same vertical gap, L is larger for a wider pole.

These are common formulae for the main electric parameters of a resistive dipole (2/2)

voltage $V = RI + L \frac{dI}{dt}$

resistive power (rms)
$$\begin{aligned} P_{rms} &= RI_{rms}^2 \\ &= \rho j_{rms}^2 V_{cond} \\ &= \frac{\rho L_{turn} B_{rms} h}{\eta \mu_0} j_{rms} \end{aligned}$$

magnetic stored energy $E_m = \int_0^I L di \cong \frac{1}{2} LI^2$

91

V	[V]	voltage
dI/dt	[A/s]	current ramp rate
P _{rms}	[W]	resistive power (rms)
j _{rms}	[A/m ²]	current density (rms)
V _{cond}	[m ³]	volume of conductor
E _m	[J]	magnetic stored energy

The voltage has a resistive and an inductive part. In cycled magnets, often the inductive voltage can be larger than the resistive one.

The resistive power is usually looked at in rms terms. The formula can be used also for the peak power, just with the peak current instead of the rms one. For a given coil size, the power scales linearly with the field B, the gap h and the current density j.

The magnetic stored energy can be computed also from the energy per unit volume (B²)/(2μ). Since the permeability is usually quite high in the yoke, the magnetic energy is basically all stored in the air volume.

In their more general form, these equations hold also for other magnets, not just dipoles.

These are useful formulae for standard resistive quadrupoles

pole tip field $B_{pole} = B'r$

Ampere-turns (total) $NI = \frac{2B'r^2}{\eta\mu_0}$

current $I = \frac{(NI)}{N}$

resistance (total) $R = \frac{\rho NL_{turn}}{A_{cond}}$

92

These formulae consider a standard quadrupole with 4 coils.

NI	[A]	total (not per pole) Ampere-turns
B'	[T/m]	field gradient in the aperture
r	[m]	aperture radius
μ_0	[H/m]	vacuum permeability, $4\pi \cdot 10^{-7}$ H/m
η	[/]	magnetic efficiency, ≈ 0.95 - 0.98 (depends on iron saturation)
I	[A]	current
N	[/]	total (not per pole) number of turns
R	[Ω]	total (not per coil) resistance
ρ	[Ω m]	resistivity, $1.72 \cdot 10^{-8}$ Ω m for Cu, $2.65 \cdot 10^{-8}$ Ω m for Al, at 20 °C
L_{turn}	[m]	average length of a coil turn
A_{cond}	[m ²]	cross-section of a single conductor (counting only the metal)

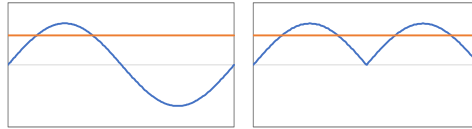
For the inductance, an approximate formula is reported for ex. by D. Tommasini.
For short magnets, 3D simulations or measurements are needed.

The resistive power can be computed from the current and the resistance, as for the dipoles.

If the magnet is not dc, then an rms power / current is taken, considering the duty cycle

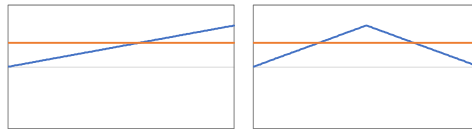
$$P_{rms} = RI_{rms}^2 = R \frac{1}{T} \int_0^T [I(t)]^2 dt$$

sine wave around 0



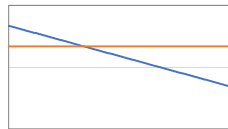
$$I_{rms}^2 = \frac{I_{peak}^2}{2}$$

linear ramp from 0



$$I_{rms}^2 = \frac{I_{peak}^2}{3}$$

linear ramp between I_1 and I_2



$$I_{rms}^2 = \frac{I_1^2 + I_1 I_2 + I_2^2}{3}$$

93

The subscript rms stands for root mean square. I_{rms} is the effective current, that is, the one which is equivalent w.r.t. the losses per Joule heating in a cycle. The same concept is used routinely in electrical systems working in ac.

If the magnet is operated in dc, then peak and rms values are the same thing.

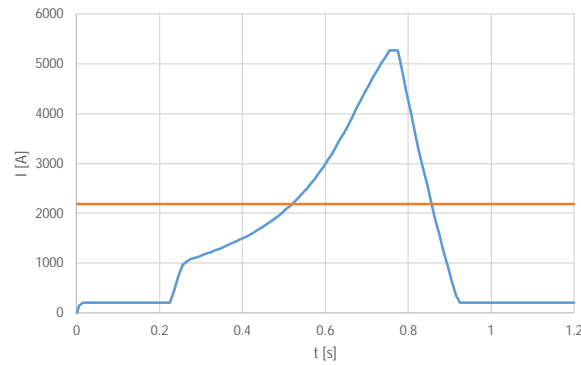
Duty cycles of synchrotrons often involves linear ramps up / down (possibly with some parabolic smoothing), and flat plateau for beam injection / extraction – rather than pure sinusoidal oscillations, like in electrical machines – so the corresponding rms values have to be computed on a case by case basis. For simple cycles made only of linear parts, this can be done using the formulae above. More details are given in the next slide.

The rms power can be computed piecewise, for example with a simple spreadsheet (considering a piecewise linear approximation for the current cycle)

$$I_{rms}^2 = \frac{I_{rms,1}^2 t_1 + I_{rms,2}^2 t_2 + I_{rms,3}^2 t_3 + \dots}{t_1 + t_2 + t_3 + \dots}$$

T	I rms	
[s]	[A]	
0	2184.1	
1.2	2184.1	

t	I	∫I ² *dt
[s]	[A]	[A ² *s]
0	0.0	-
0.005	137.9	32
0.015	200.0	289
0.225	200.0	8400
0.235	468.5	1177
0.245	729.6	3645
0.255	967.8	7250
0.265	1023.8	9919
0.275	1079.9	11067
0.285	1107.2	11959
0.295	1135.2	12571



94

The rms currents add up quadratically, with weights given by the time spent in each part, as in the given formula, which is the basis to compute the effective power using a piecewise approach.

As an example, the above spreadsheet is provided.

The cycle shown above is a typical one for the main dipoles of the PS Booster at CERN. The machine till a few years ago accelerated beams up to 1.4 GeV, though it was recently pushed with an upgrade to 2.0 GeV. The peak current is 5.3 kA, but the rms current is (only) 2.2 kA. The ramp up (with beam in) is much gentler than the ramp down (without beam).



Power requirements

Assuming the magnet cross-section and the yoke length are known, one can calculate the total dissipated power per magnet:

$$P_{dipole} = \rho \frac{Bh}{\eta\mu_0} j l_{avg} \quad (12^*)$$

$$P_{quadrupole} = 2\rho \frac{B' r^2}{\eta\mu_0} j l_{avg} \quad (13^*)$$

$$P_{sextupole} = \rho \frac{B'' r^3}{\eta\mu_0} j l_{avg} \quad (14^*)$$

- j : current density [A/m²]: $j = \frac{NI}{f_c A} = \frac{I}{a_{cond}}$ (15)
- ρ : resistivity [Ωm] (for copper: $1.86 \cdot 10^{-8}$ Ωm @ 40°C)
- l_{avg} : average turn length [m]; approximation: $2.5 l_{iron} < l_{avg} < 3 l_{iron}$ for racetrack coils
- a_{cond} : conductor cross section [m²]
- A : coil cross section [m²]
- f_c : filling factor = $\frac{\text{net conductor area}}{\text{coil cross section}}$ (geometric filling factor, insulation, cooling duct, edge rounding)

Note: for a constant geometry, the power loss P is proportional to the current density j.

[Courtesy of T. Zickler]



Air cooling

Air cooling by natural convection:

- Current density:
 - $j \leq 2 \text{ A/mm}^2$ for small, thin coils
 - $j \leq 1 \text{ A/mm}^2$ for large, captured coils
- Difficult to calculate analytically
- Numerical computations required to get reasonable results
- Round, rectangular or square conductor
 - Filling factor: 0.63 (round) to 0.8 (rectangular)
- Conductor pre-impregnated with varnish ($0.02 \leq t \leq 0.1 \text{ mm}$) or half-lapped polyimide (Kapton®) tape ($0.1 \leq t \leq 0.2 \text{ mm}$)
- Outer coil insulation: epoxy impregnated glass fibre tape



Cooling enhancement:

- Heat sink with enlarged radiation surface
- Forced air flow (cooling fan)

Only for magnets with limited strength (correctors, steering magnets....)

[Courtesy of T. Zickler]



Water cooling

Direct water cooling:

- Current density typically up to $j = 10 \text{ A/mm}^2$
- $j = 80 \text{ A/mm}^2$ have been realized, but difficult and risky (single turn cooling)
- Rectangular or square copper (or aluminium) conductor with central cooling duct for demineralised water
- Inter-turn and ground insulation: one or more layers of half-lapped epoxy impregnated glass fibre tape
- Inter-turn insulation thickness: $0.3 \leq t \leq 1.0 \text{ mm}$
- Ground insulation thickness: $0.5 \leq t \leq 3.0 \text{ mm}$

Indirect water cooling:

- Current density $j \leq 2 \text{ A/mm}^2$
- Tap water can be used



[Courtesy of T. Zickler]



Cooling water properties

Water properties:

- For the cooling of hollow conductor coils demineralised water is used (exception: indirect cooled coils)
- Water quality essential for the performance and the reliability of the coil (corrosion, erosion, short circuits)
- Resistivity $> 0.1 \times 10^6 \Omega\text{m}$
- pH between 6 and 6.5
- Dissolved oxygen below 0.1 ppm
- Filters to remove particles, loose deposits and grease to avoid cooling duct obstruction

[Courtesy of T. Zickler]



Cooling parameters

Recommendations and canonical values:

- Water cooling: $2 \text{ A/mm}^2 \leq j \leq 10 \text{ A/mm}^2$
- Pressure drop: $0.1 \leq \Delta p \leq 1.0 \text{ MPa}$ (possible up to 2.0 MPa) 1 to 10 bar
- Low pressure drop might lead to more complex and expensive coil design
- Flow velocity should be high enough so flow is turbulent
- Flow velocity $u_{av} \leq 5 \text{ m/s}$ to avoid erosion and vibrations < 3 m/s as a target
- Acceptable temperature rise: $\Delta T \leq 30^\circ\text{C}$ thermoswitch protection
- For advanced stability: $\Delta T \leq 15^\circ\text{C}$

Assuming:

- Long, straight and smooth pipes without perturbations
- Turbulent flow = high Reynolds number
- Good heat transfer from conductor to cooling medium
- Temperature of inner conductor surface equal to coolant temperature
- Isothermal conductor cross section

[Courtesy of T. Zickler]

Hydraulic parameters for cooling can be computed using different formulae

They assume all Joule heating is removed by the water
No contribution from air convection

Several sets of formulae are reported next

D. Tommasini --- more direct

T. Zickler, from J. Tanabe --- need iterative solution
both work in the turbulent regime

Friction Factors for Pipe Flow

By LEWIS F. MOODY,¹ PRINCETON, N. J.

The object of this paper is to furnish the engineer with a simple means of estimating the friction factors to be used in computing the loss of head in clean new pipes and in closed conduits running full with steady flow. The modern developments in the application of theoretical hydrodynamics to the fluid-friction problem are impressive and scattered through an extensive literature. This paper is not intended as a critical survey of this wide field. For a concise review, Professor Bakhmeteff's (1)² small book on the mechanics of fluid flow is an excellent reference. Prandtl and Tietjens (2) and Rouse (3) have also made notable contributions to the subject. The author does not claim to offer anything particularly new or original, his aim merely being to embody the now accepted conclusions in convenient form for engineering use.

IN the present pipe-flow study, the friction factor, denoted by f in the accompanying charts, is the coefficient in the Darcy formula

$$h_f = f \frac{L}{D} \frac{V^2}{2g}$$

with numerical constants for the case of perfectly smooth pipes or those in which the irregularities are small compared to the thickness of the laminar boundary layer, and for the case of rough pipes where the roughnesses protrude sufficiently to break up the laminar layer, and the flow becomes completely turbulent.

The analysis did not, however, cover the entire field but left a gap, namely, the transition zone between smooth and rough pipes, the region of incomplete turbulence. Attempts to fill this gap by the use of Nikuradse's results for artificial roughness produced by closely packed sand grains, were not adequate, since the results were clearly at variance from actual experience for ordinary surfaces encountered in practice. Nikuradse's curves showed a sharp drop followed by a peculiar reverse curve,³ not observed with commercial surfaces, and nowhere suggested by the Figs. 1 chart based on many tests.

Recently Colebrook (11), in collaboration with C. M. White, developed a function which gives a practical form of transition curve to bridge the gap. This function agrees with the two extremes of roughness and gives values in very satisfactory agreement with actual measurements on most forms of commercial piping and usual pipe surfaces. Rouse (12) has shown that it is a reasonable and practically adequate solution and has plotted a chart based upon it. In order to simplify the plotting, Rouse

Most of the equations are quite straightforward – see for ex. next slide – the tricky part is to get the flow rate as a function of the pressure difference. In fact, the difficulty is getting the friction coefficient.

A good reference is the paper of Moody (1944), shown above, where the friction coefficient is well explained and solutions are given in terms of plots – the famous Moody chart or Moody diagram.

The spreadsheet below is an example of cooling computations

INPUTS			CONSTANTS		
A_cable	[mm^2]	49	conductor dimensions (overall)		
d_hole	[mm]	3.7	cooling hole diameter		
r_fillet	[mm]	1	conductor round fillet		
L	[mm]	32860	length of the circuit		
T_inlet	[°C]	24	water inlet temperature		
		Cu	material (Cu or Al)		
I	[A]	235	current		
P	[kW]	0.851	power to be dissipated		
ε	[mm]	1.50E-03	surface roughness		
ΔT	[°C]	10	temperature rise		
COMPUTED QUANTITIES					
T_ave	[°C]	29	average temperature		
A_curr	[mm^2]	37.4	Cu area per conductor		
m_cable	[kg]	11.0	mass of the conductor		
ρ	[Ohm*m]	1.75E-08	resistivity		
R	[mOhm]	15.35	resistance		
P	[kW]	0.851	R*I^2		
j	[A/mm^2]	6.3	current density		
ρ	[km/m^3]	996	water mass density		
ν	[m^2/s]	8.21E-07	kinematic viscosity		
cp	[kJ/(kg*K)]	4.179	specific heat capacity		
OUTPUT (Colebrook)					
Δp	[bar]	5.24	pressure drop		
v	[m/s]	1.90	cooling water speed		
Re	[/]	8568	Reynolds number		
q	[L/min]	1.227	cooling water flow		
OUTPUT (Blasius)					
Δp	[bar]	5.26	pressure drop		
v	[m/s]	1.90	cooling water speed		
Re	[/]	8568	Reynolds number		
q	[L/min]	1.227	cooling water flow		
OUTPUT (Davide)					
Δp	[bar]	5.56	pressure drop		
v	[m/s]	1.89	cooling water speed		
Re	[/]	9771	Reynolds number		
q	[L/min]	1.217	cooling water flow		

Formulae for coil cooling computations

Notation

p	[Pa]	pressure drop	ν	[m^2/s]	kinematic viscosity
f	[/]	friction coefficient	ϵ	[m]	surface roughness
l	[m]	length	q	[m^3/s]	volume flow rate
d	[m]	hole diameter	ΔT	[°C]	temperature increase
ρ	[kg/m^3]	mass density	P	[W]	extracted power
v	[m/s]	velocity	c_p	[kJ/(kg K)]	specific heat capacity

Darcy equation

$$\Delta p = f \frac{l}{d} \frac{\rho v^2}{2}$$

Reynolds number

$$Re = \frac{vd}{\nu}$$

Colebrook formula

$$\frac{1}{\sqrt{f}} = -2 \log_{10} \left(\frac{\epsilon}{3.7d} + \frac{2.51}{Re \sqrt{f}} \right)$$

The first part is a Nikuradse term whereas the second one is of the Prandtl-v.Karman form.

$$\Delta p \Rightarrow k_v = \sqrt{\frac{2}{\rho} \Delta p} \Rightarrow f = \left[-2 \log_{10} \left(\frac{\epsilon}{3.7d} + \frac{2.51}{Re \sqrt{f}} \right) \right]^{-1/2} \Rightarrow v = \frac{k_v}{\sqrt{f}}$$

Blasius formula

$$f = \frac{0.3164}{Re^{1/4}}$$

$$\Delta p \Rightarrow v = \left[\frac{2 \rho \Delta p}{0.3164 Re^{1/4}} \right]^{1/1.75}$$

Volume flow rate

$$q = v \frac{\pi d^2}{4}$$

Temperature increase

$$\Delta T = \frac{P}{c_p \rho q}$$

The agreement among the different formulae is usually very good, at the % level for the main parameters, which is more than enough for all practical purposes. Some differences can be explained by the temperature dependence of some constants, which is neglected in case of simplified formulae.

In this spreadsheet, we compute the resistance – and thus the Joule heating to be dissipated – considering an average temperature, that is, the inlet temperature plus half the temperature increase, and the cooling parameters are estimated at this operating point. In particular, we compute the pressure difference required to generate a flow such to obtain the given temperature increase.

On the other hand, in other tabs of that spreadsheet, we vary the pressure difference and check which flow rate and temperature increase ΔT we obtain. In this case, there is an approximation, as we do not compute the resistance (and so the power) as a function of the different ΔT , which would require an iterative approach.

These are “Davide’s” formulae for the main cooling parameters of a water-cooled resistive magnet

cooling flow	$Q_{tot} \cong 14.3 \frac{P}{\Delta T}$	$Q_{tot} \cong N_{hydr} Q$	
water velocity	$v = \frac{1000}{15\pi d^2} Q$		
Reynolds number	$Re \cong 1400dv$		
pressure drop	$\Delta p = 60L_{hydr} \frac{Q^{1.75}}{d^{4.75}}$		derived from Blasius' formula for the friction coefficient

102

Technical units are used in these formulae, taken from D. Tommasini.

P	[kW]	power to be dissipated, that is, P_{rms} in most cases
ΔT	[°C]	water temperature increase between inlet and outlet typically up to 30 °C, in many cases lower
Q_{tot}	[l/min]	total (not per hydraulic circuit) flow rate
Q	[l/min]	flow rate per hydraulic circuit
N_{hydr}	[/]	number of hydraulic circuits in parallel
v	[m/s]	water velocity; for Cu conductor, typically < 3 m/s to avoid erosion problems, which could start already at 1.5 m/s
d	[mm]	(hydraulic) diameter of the cooling duct
Re	[/]	Reynolds number, typically $2000 < Re < 10^5$, to have moderately turbulent flow
Δp	[bar]	pressure drop, typically around 10 bar
L_{hydr}	[m]	length of each hydraulic circuit in parallel this can be different from NL_{turn} , as there could be a difference between electrical and hydraulic circuits, with for example sub-coils all electrically in series, but hydraulically in parallel

The expressions are valid for water at around 40 °C.

The hydraulic diameter, in case of non-circular holes, is $4 \cdot A/P$, where A is the area and P the wetted perimeter of the hole.



Cooling parameters

Pressure drop through a water circuit: $\Delta p = f \frac{l}{d} \frac{\delta u_{av}^2}{2}$ (16)

- p : pressure [Pa, N/m²]
- f : friction factor [.] Darcy equation
- l, d : cooling circuit length and diameter [m]
- δ : coolant mass density [kg/m³] (for water: 1000 kg/m³ = 1 kg/liter)
- u_{avg} : average coolant velocity [m/s]

Friction factor f depends on the Reynolds number Re $Re = \frac{u_{avg} d}{\nu}$ (17)

Laminar flow: $Re < 2000$ and $f = 64/Re$

- ν : kinematic viscosity of coolant is temperature depending, for simplification it is assumed to be constant ($9.85 \cdot 10^{-7}$ m²/s @ 21°C for water)

Turbulent flow: $Re > 4000$ and f is transcendental:

$$\frac{1}{\sqrt{f}} = -2 \log_{10} \left(\frac{\varepsilon}{3.7d} + \frac{2.51}{Re \sqrt{f}} \right) \quad \text{Colebrook formula (18)}$$

- ε : roughness of cooling channels ($\sim 1.5 \cdot 10^{-3}$ mm)

(Nikuradse + Prandtl-v.Karman)

[Courtesy of T. Zickler]



Cooling parameters

Velocity and friction factor using $Re(u_{avg}) \rightarrow u_{avg}$ to be solved iteratively:

$$u_{avg} = \sqrt{\frac{2\Delta p}{\delta f} \frac{d}{l}} \quad (19)$$

$$Re = \frac{d}{\nu} \sqrt{\frac{2\Delta p}{\delta f} \frac{d}{l}} \quad (20)$$

Substituting Re in (18) with (20) leads to:

$$u_{avg} = -2 \sqrt{\frac{2\Delta p}{\delta} \frac{d}{l}} \log_{10} \left(\frac{\varepsilon}{3.7d} + \frac{2.51}{\frac{d}{\nu} \sqrt{\frac{2\Delta p}{\delta} \frac{d}{l}}} \right) \quad (21)$$

Simplified approach using water as cooling fluid:

$$u_{avg} \approx 0.3926 \cdot d^{0.714} \left(\frac{\Delta p}{l} \right)^{0.571} \quad (22^*)$$

[Courtesy of T. Zickler]



Cooling parameters

Heat absorbed by coolant medium across a heated surface:

$$P = \dot{m} c_p \Delta T$$

$$\dot{m} = \delta Q$$

- c_p : heat capacity [W s/kg °C] (4.19 kW s/kg °C for water)
- Q : flow rate [liter/s]
- P : power [W]
- ΔT : temperature increase [°C]

Technically, the power P is a function of the ΔT , as the resistance changes with T

energy balance

Flow Q necessary to remove heat P : $Q = \frac{P}{\delta c_p \Delta T}$ $Q_{\text{water}} = 0.2388 \frac{P}{\Delta T}$ (22)

Coolant flow inside a round tube with a bore diameter d : $Q = u_{\text{av}} \frac{\pi d^2}{4} 10^3$ (23)

Temperature increase using water as cooling fluid: $\Delta T = 0.304 \frac{P}{u_{\text{avg}} d^2} \cdot 10^{-6}$ (24)

[Courtesy of T. Zickler]



Cooling parameters

Number of cooling circuits per coil: $\Delta p \propto \frac{1}{K_W^3}$

→ Doubling the number of cooling circuits reduces the pressure drop by a factor of eight for a constant flow

Diameter of cooling channel: $\Delta p \propto \frac{1}{d^5}$

→ Increasing the cooling channel by a small factor can reduce the required pressure drop significantly

[Courtesy of T. Zickler]



Cooling circuit design

Already determined: current density j , power P , current I , # of turns N

1. Select # of layers m and # of turns per layer n
2. Round up N if necessary to get reasonable m and n
3. Define coil height c and coil width b : $A = bc = \frac{NI}{jf_c}$ (Aspect ratio $c : b$ between 1 : 1 and 1 : 1.7 and $0.6 \leq f_c \leq 0.8$)
4. Calculate l_{avg} = pole perimeter + 8 x clearance + 4 x coil width
5. Start with single cooling circuit per coil: $l = \frac{K_c N l_{avg}}{K_w}$ (25)
6. Select ΔT , Δp and calculate cooling hole diameter d : $d = 5.59 \cdot 10^{-3} \left(\frac{P}{\Delta T K_w} \right)^{0.368} \left(\frac{l}{\Delta p} \right)^{0.21} (26^*)$
7. Change Δp or number of cooling circuits, if necessary
8. Determine conductor area a : $a = \frac{I}{j} + \frac{d^2 \pi}{4} + r_{edge} (4 - \pi)$ (27)
9. Select conductor dimensions and insulation thickness
10. Verify if resulting coil dimensions, N , l , V , ΔT are still compatible with the initial requirements (if not, start new iteration)
11. Compute coolant velocity and coolant flow using (21) and (22)
12. Verify if Reynolds number is inside turbulent range ($Re > 4000$) using (17)

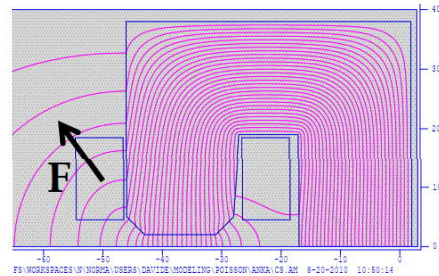
[Courtesy of T. Zickler]



Basic principles : force

On a conductor immersed in magnetic field

$$\mathbf{F} = I \cdot \mathbf{L} \times \mathbf{B}$$



Example for the Anka dipole:

On a the external coil side with $N=40$ turns, $I=700\text{A}$, $L \sim 2.2\text{ m}$
in an average field of $B=0.25\text{ T}$

$$F = 40 \cdot 700 \cdot 2.2 \cdot 0.25 = 15400\text{ N} \sim 1.5\text{ tons}_f$$

[Courtesy of D. Tommasini]

Coil shimming is important also for resistive magnets, especially when cycled.
Forces can be significant in dipoles but also quadrupoles.

Proper shimming of the coils is important – it also called for dedicated campaigns in CERN magnets

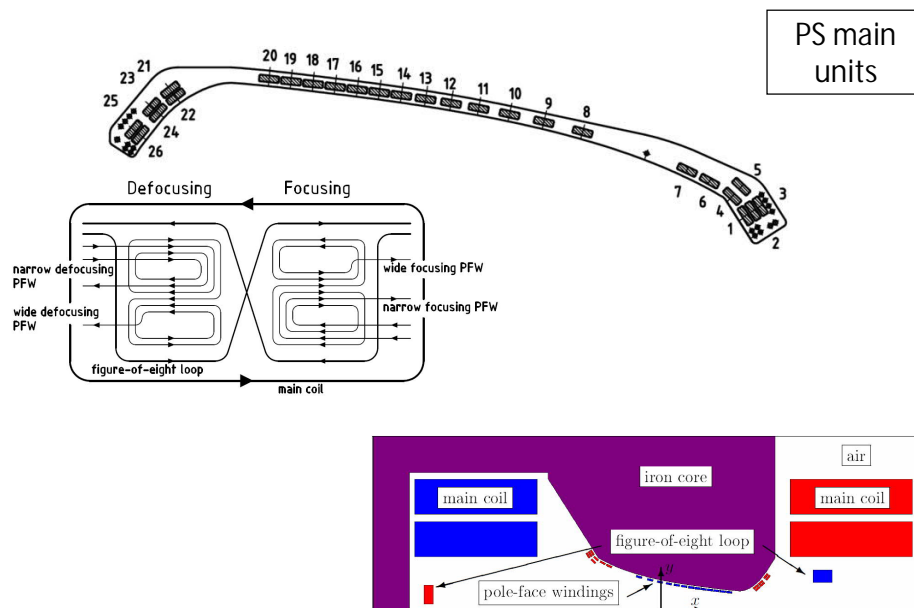


109

First HIE-ISOLDE bending magnet during reception tests

[Courtesy of J. Bauche]

Pole face windings are sometimes (now more rarely) used to correct / shape the magnetic field



110

My personal advice is not to use them, as far as possible... Examples of magnets with pole face windings at CERN are the PS main units, the LEIR main bending, and in the past, the ISR dipoles.

Conclusions (coil design)

Ampere-turns can be computed analytically with very good approximation

Power law scaling with order of the magnet

Several coil geometries are possible

Again, no unique solution

Typically, either copper (in most cases) or aluminum is used

Resistive power, as Joule heating, is dissipated either by forced flow of demineralized water, or by air convection

The main parameter is the current density in the conductor

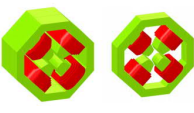
Lorentz forces on the conductor shall be checked

Proper shimming is important, even more for cycled operation

Gallery of cross-sections
see separate file

Fabrication (hints)

In many cases, the fabrication is subcontracted to (specialized) companies – below are examples of technical specifications

<p>ORGANISATION EUROPÉENNE POUR LA RECHERCHE NUCLÉAIRE CERN EUROPEAN ORGANIZATION FOR NUCLEAR RESEARCH</p> <p>CERN EDMS N° 1279694 TE Department / SESAME Project</p> <p>IT-3941/TE/SESAME</p> <p>Invitation to Tender Technical Specification</p> <p>SESAME Storage Ring Combined Function Dipole Magnets</p> <p>This technical specification concerns the supply of 17 combined function dipole electromagnets (including pre-stress) and a set of spare coils for the storage ring of the SESAME synchrotron. The cores of the magnets are laminated steel yokes, the coils are water cooled, wound from hollow copper conductor, and epoxy impregnated. Their mass is approximately 65 tonnes. Delivery shall be completed within 24 months after placement of the contract.</p>  <p>June 2013</p>	<p>ORGANISATION EUROPÉENNE POUR LA RECHERCHE NUCLÉAIRE CERN EUROPEAN ORGANIZATION FOR NUCLEAR RESEARCH</p> <p>CERN EDMS N° 1257262 TE Department / SESAME Project</p> <p>IT-3940/TE/SESAME</p> <p>Invitation to Tender Technical Specification</p> <p>SESAME Storage Ring Quadrupole Magnets</p> <p>This technical specification concerns the supply of 33 focusing and 33 defocusing quadrupole electromagnets (including pre-stress) for the storage ring of the SESAME synchrotron. The cores of the magnets are laminated steel yokes, the coils are water cooled, wound from hollow copper conductor, and epoxy impregnated. Their mass is approximately 650 / 150 kg. Delivery shall be completed within 20 months after placement of the contract.</p>  <p>June 2013</p>	<p>ORGANISATION EUROPÉENNE POUR LA RECHERCHE NUCLÉAIRE CERN EUROPEAN ORGANIZATION FOR NUCLEAR RESEARCH</p> <p>CERN EDMS N° 1279686 TE Department / SESAME Project</p> <p>Price Enquiry Technical Specification</p> <p>Coils for the SESAME Storage Ring Quadrupole Magnets</p> <p>This technical specification concerns the supply of 140 coils for the focusing quadrupole and 140 coils for the defocusing quadrupole electromagnets for the SESAME storage ring. These coils are water cooled, wound from hollow copper conductor and epoxy impregnated under vacuum. Their mass is approximately 18 / 6 kg. Delivery shall be completed within 14 months after signing the contract.</p>  <p>June 2013</p>
EDMS 1279694	EDMS 1257262	EDMS 1279686

114

These are three examples from SESAME magnets – which are representative of what is typically requested at CERN in technical specifications of resistive magnets.

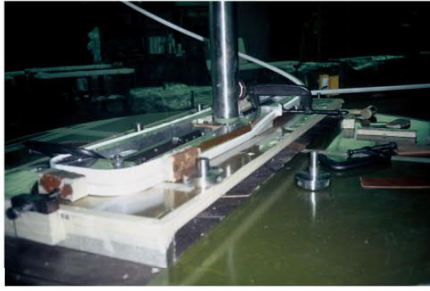
For the combined function bending magnets, the contract covered the whole production. For the quadrupoles, there were two separate contracts, one for the coils and one for the magnets (with coils provided as a component by CERN).

There are other examples of procurement of only yokes – like when we went from solid to laminated constructions for the East Area renovation. And it also happens to purchase separately the electrical steel, then the stamped laminations, etc.

Warning: brazing needs a particular attention!



Manufacture : coils



Introduction to accelerator physics

Varna, 19 September, 1 October 2010

Davide Tommasini : Magnets (warm)

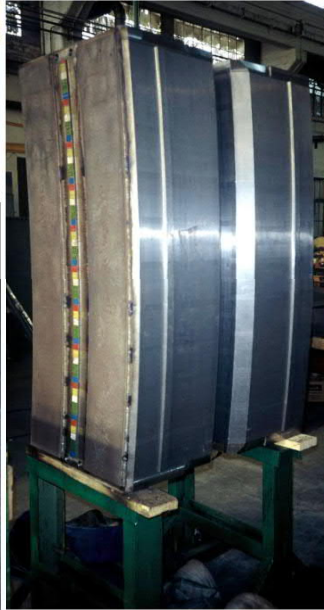
[Courtesy of D. Tommasini]



Manufacture : yoke



Introduction to accelerator physics



Varna, 19 September, 1 October 2010

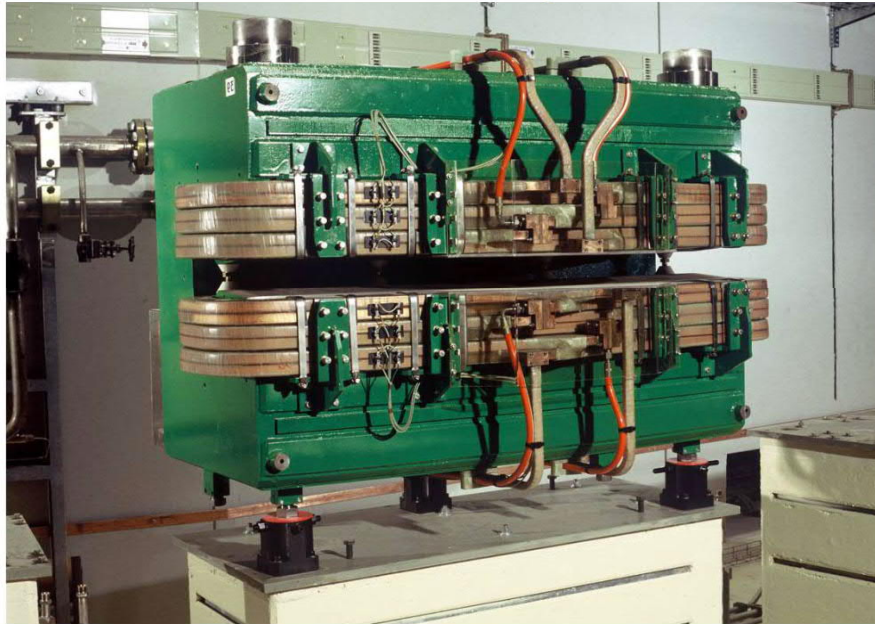


Davide Tommasini : Magnets (warm)

[Courtesy of D. Tommasini]



Manufacture : yoke



[Introduction to accelerator physics](#)

[Varna, 19 September, 1 October 2010](#)

[Davide Tommasini : Magnets \(warm\)](#)

117

[Courtesy of D. Tommasini]

This is a picture of the ELETTRA main bending magnets, which are combined function dipole + quadrupole magnets, built in the 1990s.



Corrector dipole North Experimental area

Magnet with solid yoke parts assembled with bolts.



Main parameters	
Name	MDX
Type	Vertical correcting dipole
Installation	SPS experimental area
Nominal peak field [T]	1.33
I_{peak} [A]	240
Résistance [Ω]	0.305
Inductance [H]	0.221
Yoke length [mm]	400
Gap [mm]	80
Total weight [kg]	1000

Introduction to accelerator physics

Varin, 19 September, 1 October 2010

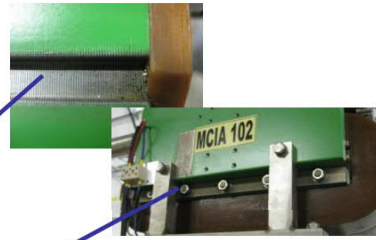
Davide Tommasini : Magnets (warm)

[Courtesy of D. Tommasini]



Corrector dipole in TI2 and TI8 LHC injection lines

Magnet with glued laminated yokes assembled with bolts.



Main parameters	
Name	MCIA V
Type	Vertical correcting dipole
Nominal peak field [T]	0.26
I_{max} [A]	3.5
N. Of turns	1014
Résistance [Ω]	13.9
Yoke lenght [mm]	450
Gap [mm]	32.5
Total weight [kg]	300

[Courtesy of D. Tommasini]



Corrector dipole for E-Cloud experiment in SPS

Magnet with laminations welded in a steel envelope
half-yokes assembled with bolts.




Main parameters	
Name	MDVW
Type	Vertical correcting dipole
Nominal peak field [T]	0.266
I_{max} [A]	55
N. Of turns	2 x 50
Résistance [Ω]	1.76
Inductance [H]	1.12
Yoke lenght [mm]	429
Gap [mm]	200
Total weight [kg]	1100

[Courtesy of D. Tommasini]

Acceptance tests

Acceptance tests: ex. from CERN standard template



**Water Cooled Magnet
Certification Report**
Template EDMS Document: 1103493

EDMS Document number
To be filled by the QA

MTF identifier	
Another identifier	
Manufacturer	
Construction year	
Requested by	

Previous certification?
☐ No
☐ Yes

EDMS Document
To be filled by the magnet responsible

FINAL RESULT
☐ Certified Good
☐ Certified Fair
☐ To be Refurbished
☐ Discontinued

Non-conformities?
☐ No
☐ Yes

EDMS Document
To be filled by the QA

If yes, provide nonconforming report

	Name	Date
Operator		
Workshop / certifications responsible		
Technical responsible		
QA responsible		

Page 1 of 8

1 – GENERAL INFORMATION

Yokes identifiers	Coils identifiers

To be filled in order accordingly to the Polarity convention for normal conducting magnets (EDMS 1105981)

Presence of a vacuum chamber
☐ No
☐ Yes, picture:

Interlock circuit
☐ WIC
☐ Other

Number of channels:

Interlock circuit details

Box picture:
Connector picture:

Electrical power connection

Picture:
Dimensions of holes or terminal block:

Hydraulic circuit

Connector type:
Connector picture:
Circuit grounded? ☐ Yes ☐ No

IP2X protective covers

☐ Yes, picture:
☐ No

Magnet weight


Page 2 of 8

Acceptance tests: ex. from CERN standard template


2 – VISUAL INSPECTION	
General state (impacts, oxidation presence, etc.) Coils state (insulation, conductor, etc.) Interlock circuit, etc.	
Indicate the name of the pictures if necessary	

3 – HYDRAULIC TESTS	
Static pressure	Test pressure = <div>50 bar</div> bar Duration = minute
No leakage and maintained pressure for the duration of the test <input type="checkbox"/> Ok	


Flow measurement	Nominal pressure ΔP =	bar
	Nominal flow =	l/min
	at $2 \times \Delta P$ or maximum ΔP	ΔP = Flow =
	at nominal ΔP	ΔP = Flow =
	at $\Delta P/2$	ΔP = Flow =

4 – ELECTRICAL TESTS	
	Before starting the electrical tests Make sure the yoke is grounded and that the hydraulic system is properly flushed and bled

Page 3 of 8

Interlock dielectric test	Test voltage =	0.5 kV
	Duration =	1 min
 During the test, connect the magnet coil(s) to the ground		
Interlock circuit details	Insulation resistance R =	Leakage current Ic =
Thermo-switches		

5 kV dc

Coils insulation	Test voltage =	kV
	Duration =	min
 During the test, connect the magnet interlock circuit to ground		
Insulation resistance	R =	
Leakage current	Ic =	

Capacitive discharge		Test voltage(s)
Magnet =	kV	Half-magnet = kV
		Coil(s) = kV
Name of the curves saved in TXT and PNG format		
<input type="checkbox"/> Magnet:		<input type="checkbox"/> Coil 5:
<input type="checkbox"/> Half-magnet 1:		<input type="checkbox"/> Coil 6:
<input type="checkbox"/> Half-magnet 2:		<input type="checkbox"/> Coil 7:
<input type="checkbox"/> Coil 1:		<input type="checkbox"/> Coil 8:
<input type="checkbox"/> Coil 2:		<input type="checkbox"/> Coil 9:
<input type="checkbox"/> Coil 3:		<input type="checkbox"/> Coil 10:
<input type="checkbox"/> Coil 4:		<input type="checkbox"/> Other:

Inductance measurement	Nominal inductance =	Hz
	Nominal frequency =	Hz
at 1Hz =	at 20Hz =	at 100Hz =




Resistance measurement at I = 1 A	Nominal resistance =
$R_{20} = R / (1 + 0.004 \times (T - 20))$	Measured room temperature = °C
Corrected resistance at 20°C: R_{20} =	Measured resistance =

Page 4 of 8

Acceptance tests: ex. from CERN standard template


5 – POWER TESTS			
Thermo-switches trigger test			
Power the magnet at I = A, until the temperature is stabilized, then			
reduce the flow rate until the 1 st trigger Q (l/min) =			
and/or increase the current I (A) =			
Thermo-switch type			
TS	Details	Nominal temperature (°C)	Trigger temperature (°C)
1			
2			
3			
4			
5			
6			
7			
8			
9			
10			
11			
12			
13			
14			
15			
16			
17			
18			
19			
20			
21			
22			
23			
24			
Maximum temperature recorded by the thermal camera, when the last thermos-switch has triggered			°C
All thermo-switches closed after cool down			<input type="checkbox"/> Ok
Interlock circuit continuity test after disconnected			<input type="checkbox"/> Ok

Page 5 of 8

Trigger test of the interlock system	
WITHOUT WATER	
Perform test? <input type="checkbox"/> Yes <input type="checkbox"/> No	
	
<ul style="list-style-type: none">- MANDATORY supervision of a CERN STAFF for the entire duration of the test- Do not exceed 80°C on the coils	
Name of the person supervising the test:	
Stop the water flow, then	
power the magnet at I = A, or A/mm²	
Converter stop	
thermo-switch triggering <input type="checkbox"/> Ok	
Or (Temperature too high without trigger) <input type="checkbox"/> Ok	
Manually	
Maximum temperature reached = °C	
Picture:	
 At the end of the test, let the magnet cool down WITHOUT CIRCULATING WATER	
DC Power test	
	
Before starting the test	
connect the interlock system straight to the converter	
Applied current I = A ΔP = bar	
Coils temperature stabilization at °C	
Water inlet temperature °C	
Water outlet temperature °C	
<input type="checkbox"/> Temperature curve:	
Thermal pictures:	
<ul style="list-style-type: none">- Indicate the magnet orientation with an arrow- Indicate the power connections A and B- Check the polarity accordingly to the convention EDMS 1105981	
<input type="checkbox"/> Ok	

Page 6 of 8

Acceptance tests: ex. from CERN standard template

Pulsed Power test	
 <p>Before starting the test connect the interlock system directly to the converter</p>	
Applied current I =	A
Duration ON =	s
Duration OFF =	s
<div>Valid coils shimming <input type="checkbox"/> Ok</div>	

- At the end of the certification tests, check the **continuity** and the **insulation/ground** at 0.5 kV for 1 min of the interlock circuit.
- Make sure the hydraulic system is properly bled.

Checks performed ☐ Ok

6 – COMMENTS

Page 7 of 8

7 – DOCUMENTS COMPILATION

The documents requested into the first table below must be provided

<input type="checkbox"/>	Picture(s) of the magnet without covers:	
<input type="checkbox"/>	Picture(s) of the magnet opening:	
<input type="checkbox"/>	Picture of the interlock box	
<input type="checkbox"/>	Picture of the interlock connector	
<input type="checkbox"/>	Picture of the power connections	
<input type="checkbox"/>	Picture of the hydraulic connections	
<input type="checkbox"/>	Capacitive discharge files	
<input type="checkbox"/>	Thermal pictures from DC power test	
<input type="checkbox"/>	Thermal pictures from trigger test	
<input type="checkbox"/>	Trigger file and DC power	

<input type="checkbox"/>	Picture of the vacuum chamber
<input type="checkbox"/>	Visual inspection picture(s)
<input type="checkbox"/>	Picture of the magnet with protective covers
<input type="checkbox"/>	Other pictures and files:

Circumstance	Percentage of respondents (%)
(a) self-defense	95
(b) defense of others	85
(c) defense of property	80
(d) defense of a business	75
(e) defense of a country	65

Page 8 of 8

Acceptance tests: ex. mechanical checks (extract)

MQDSE #12

2 – YOKE CONTROL MEASUREMENTS
OPPOSITE QUADRANTS (DIAMETERS)

Nominal value 70.00 mm

[mm]	Distance from hydraulic connection side [mm]				Average
	15	40	60	85	
d ₁₃	70.048	70.042	70.035	70.008	70.033
d ₂₄	70.011	70.04	70.04	70.05	70.035

Hydraulic connections side

Non-connection side

[mm]	measured	target	
max – avg	0.001	≤ 0.05	<input checked="" type="checkbox"/> Ok
avg – min	0.001	≤ 0.05	<input checked="" type="checkbox"/> Ok

Measured with

☐ Vertical measuring column

☐ Mechanical dial gauge

☐ Electronic dial gauge

☐ Measuring arm

☐ Other

page 3 / 8

MQDSE #12

3 – YOKE CONTROL MEASUREMENTS
ADJACENT QUADRANTS

Nominal value 23.568 mm

[mm]	Distance from hydraulic connection side [mm]				Average
	15	40	60	85	
d ₁₂	-0.015	0	+0.02	+0.03	2.3.577
d ₂₃	+0.02	-0.01	+0.01	+0.01	2.3.576
d ₃₄	-0.02	-0.01	0	0	2.3.561
d ₄₁	0	-0.01	-0.04	-0.03	2.3.548

Hydraulic connections side

Non-connection side

[mm]	measured	target	
max – avg	0.012	≤ 0.03	<input checked="" type="checkbox"/> Ok
avg – min	0.017	≤ 0.03	<input checked="" type="checkbox"/> Ok

Measured with

☐ Vertical measuring column

☐ Mechanical dial gauge

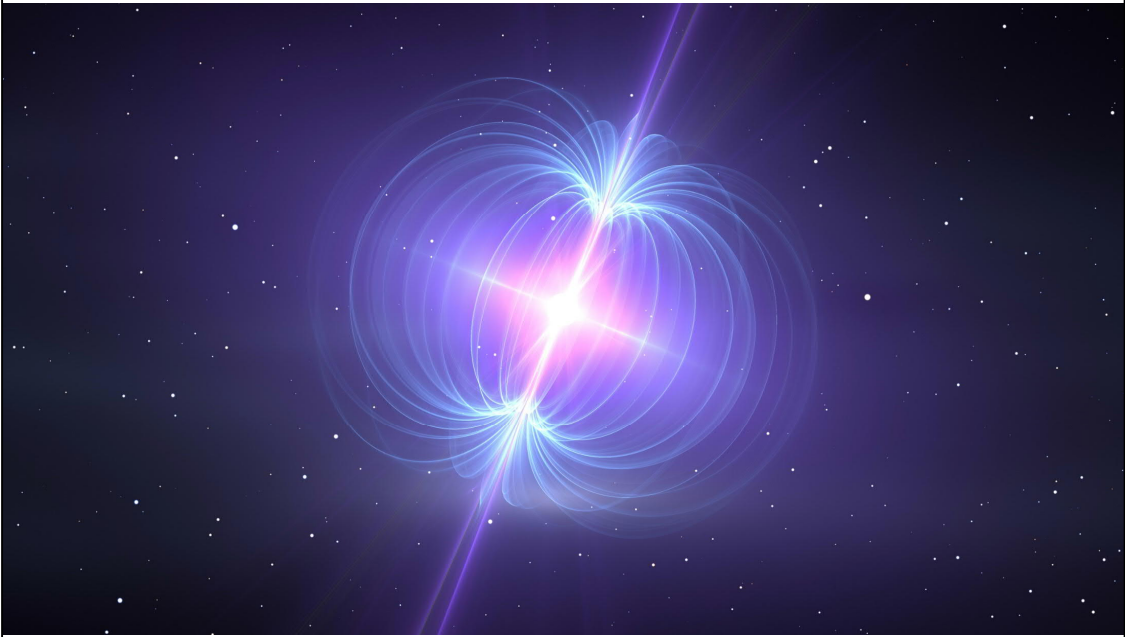
☐ Electronic dial gauge

☐ Measuring arm

☐ Other

page 4 / 8

Thank you



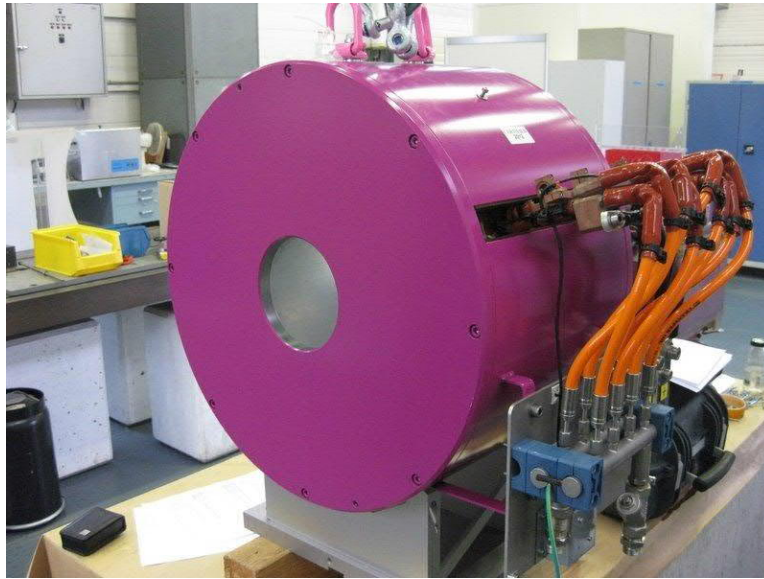
127

An artist's impression of a magnetar — a dead star that generates incredibly high magnetic fields, of the order of 10^9 to 10^{11} T.

[Courtesy of www.quantamagazine.org]

Bonus

LINAC4 solenoids

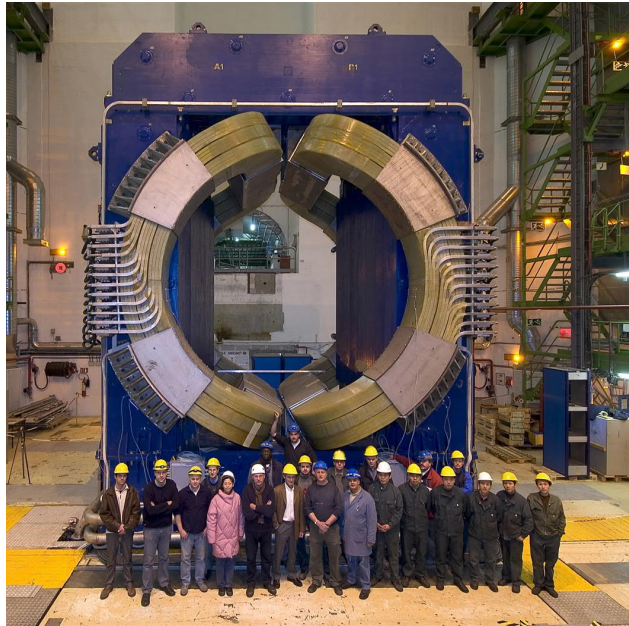


0.26 T, 122 A
aperture diameter 140 mm

129

Resistive solenoids are also a possibility. This is an example of a water cooled unit for the LINAC4 at CERN.

Experimental magnets: ALICE dipole



130

Also ALICE – another experiment in the LHC – has a resistive dipole with aluminum coils. The power is 3.5 MW, for a bending strength of 3 Tm. The average gap is 3.3 m and the maximum field 0.67 T.

Among various references, this presentation provides many details also of the manufacturing:

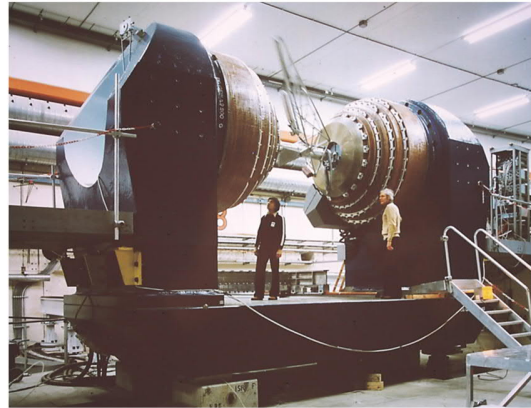
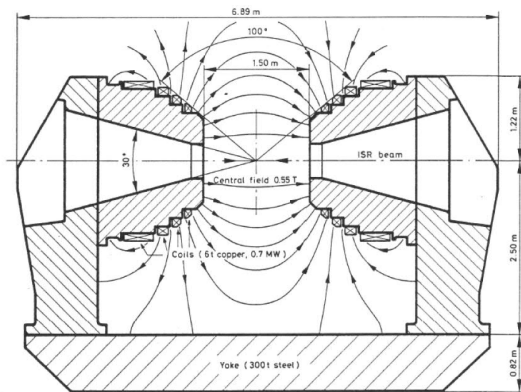
D. Swoboda

The ALICE dipole magnet

<https://indico.cern.ch/event/421493/#1-the-alice-dipole-magnet>

May 2004

Experimental magnets: the Open Axial Field Magnet, ISR



131

Other configurations for resistive magnets in experimental regions are possible: this is an example for the CERN ISR.

More details can be found for ex. in the following reference:

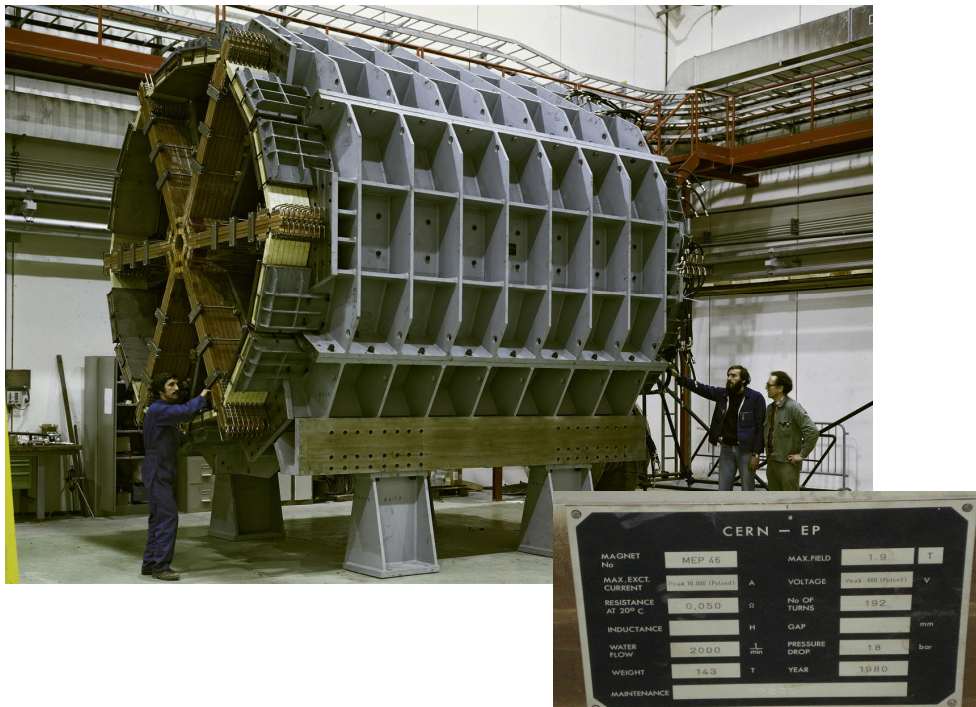
T. Taylor

The Open Axial Field Magnet: Barrier-Free Access

<http://cds.cern.ch/record/2746084>

Oct. 2017

Experimental magnets: toroid for NA10

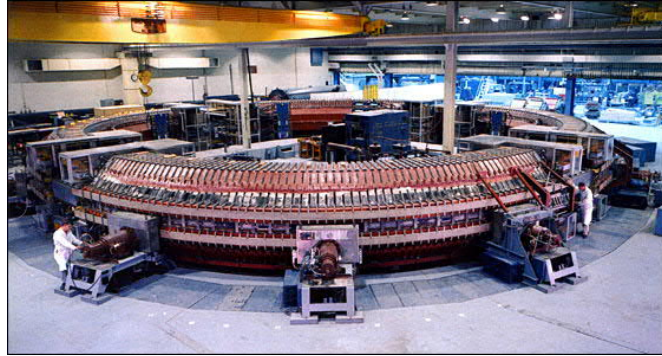


132

Another typical geometry for experimental magnets is also the toroidal configuration – this is an example of a resistive toroid previously installed in the North Area at CERN.

[Pictures courtesy of P. A. Giudici]

Main magnets in synchrotrons before strong focussing: Cosmotron (1953) and SATURNE (1956)



133

Courtesy of

- <https://en.wikipedia.org/wiki/CosmotronWikipedia>
- https://americanhistory.si.edu/collections/search/object/nmah_700258
- <https://cerncourier.com/a/the-sun-sets-on-saturne/>

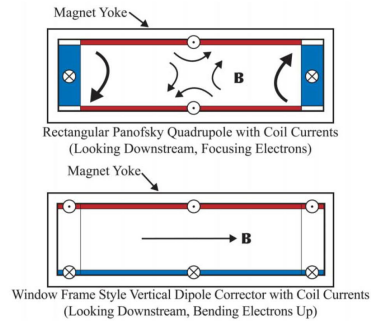
Dipole correctors embedded in quadrupoles (just two examples)

MOPAS074

Proceedings of PAC07, Albuquerque, New Mexico, USA

COMBINED PANOFSKY QUADRUPOLE & CORRECTOR DIPOLE *

George H. Biallas¹, Nathan Belcher, David Douglas, Tommy Hiatt, Kevin Jordan, Jefferson Lab,
Newport News, Virginia, U.S.A.



IPAC2007

International Atomic Energy Agency

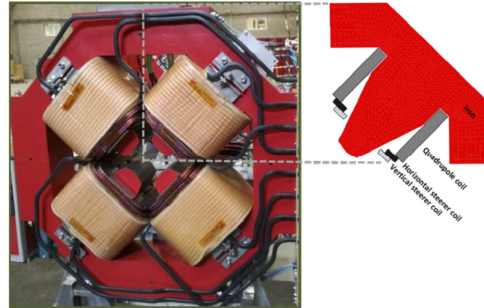
Nuclear Fusion

Nucl. Fusion 42 (2002) 0803A (21pp)

<https://doi.org/10.1088/1741-4265/42/2/020>

Design and manufacturing of the combined quadrupole and corrector magnets for the LIPAc accelerator high energy beam transport line

B. Brañas¹, J. Castellanos¹, C. Oliver², J. Campmany²,
F. Fernández², M. García¹, I. Kirillov¹, J. Marcos¹, V. Massana¹,
P. Mendez¹, J. Mosca¹, F. Toral¹, F. Arranz¹, O. Nomen³ and I. Podadera⁴



Several correctors embedded in an octupole (an example)

IPAC22

APSU Corrector/Octupole

Dipole (H,V) and Skew Quad Corrector

Parameter	Value
Bore radius	15.5 mm
Yoke (laminated) length	84.6mm
DC correction	0.44 mrad
Steering (1 kHz)	4.4 μ rad
Integ. skew gradient	0.73 T

NSLS-II Octupole:

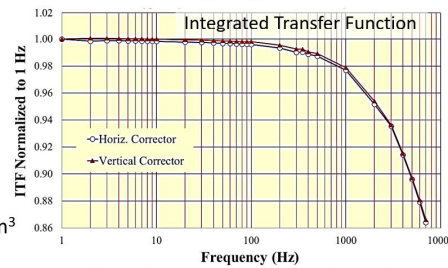
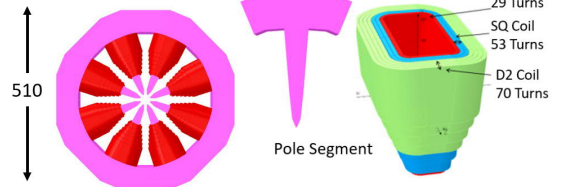
Bore radius: 14 mm

Pole-tip gap: 8 mm

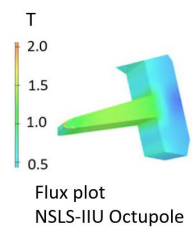
Solid Yoke: 206 mm x 206 mm

Octupole strength ($B'''/6$) = 121,000 T/m³

(Efficiency of 99%)



At 1 kHz. drop in ITF = 2%, phase lag < 4°




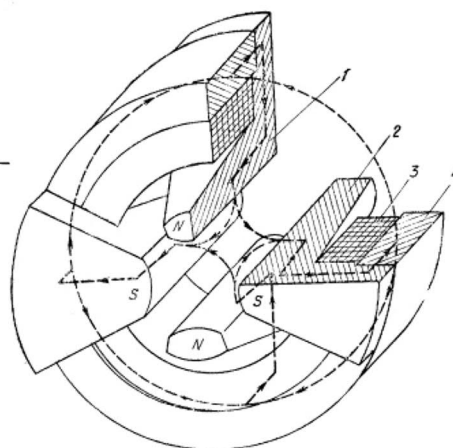
S. Sharma
June 16, 2022

BROOKHAVEN
NATIONAL LABORATORY

Courtesy of S. Sharma, presentation at IPAC22, "Development of Advanced Magnets for Modern and Future Synchrotron Light Sources"

Claw-pole magnet by Malyshev, then revamped by several colleagues, in particular Kashikhin (FNAL) and Volpini (INFN) for superconducting designs

Союз Советских Социалистических Республик  Государственный комитет Совета Министров СССР по делам изобретений, и открытий	О П И С А Н И Е 402171 ИЗОБРЕТЕНИЯ К АВТОРСКОМУ СВИДЕТЕЛЬСТВУ	
	Зависимое от авт. свидетельства № — Заявлено 02.VIII.1971 (№ 1689890/26-25) с присоединением заявки № — Приоритет — Опубликовано 12.X.1973. Бюллетень № 41 Дата опубликования описания 27.II.1974	М. Кл. Н 03h 7/00 Н 01j 3/20 УДК 621.384.6(688.8)
Автор изобретения	И. Ф. Малышев	



The poles can extend past the coils – this is more rare, but it is done – below a couple of examples

TU1RA101

Proceedings of PAC09, Vancouver, BC, Canada

**SPECIAL MAGNET DESIGNS AND REQUIREMENTS
FOR NEXT GENERATION LIGHT SOURCES***

R. Gupta[†] and A. Jain
Brookhaven National Laboratory, Upton, NY 11973, U.S.A.

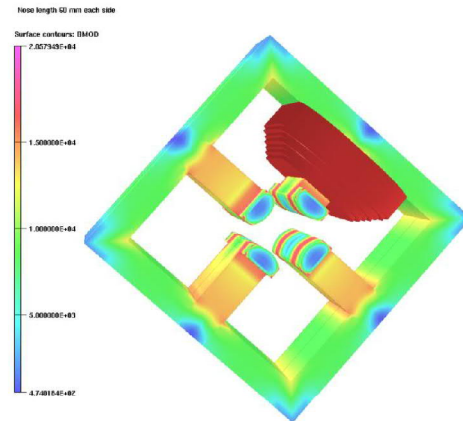


Figure 1: Prototype magnet for NSLS-II with “*extended pole*” or “*nose*”. The dotted line shows the boundary between the nose piece and the main laminations.

DEVELOPMENT OF EXTENDED POLE QUADRUPOLE MAGNET

Kailash Ruwali[‡], Ritesh Malik, Navin Awale, Bhim Singh, Anil Kumar Mishra, B. Srinivasan,
Gautam Sinha and S. N. Singh

Accelerator Magnet Technology Division, Raja Ramanna Centre for Advanced Technology, Indore,
India



The smallest quadrupole?

PHYSICAL REVIEW SPECIAL TOPICS - ACCELERATORS AND BEAMS **18**, 023501 (2015)

High-gradient microelectromechanical system quadrupole electromagnets for particle beam focusing and steering

Jere Harrison,^{*} Yongha Hwang, Omeed Paydar, and Jimmy Wu
Department of Electrical Engineering, University of California, Los Angeles, California 90095, USA

Evan Threlkeld, James Rosenzweig, and Pietro Musumeci[†]
Department of Physics, University of California, Los Angeles, California 90095, USA

Rob Candler[‡]
Department of Electrical Engineering, University of California, Los Angeles, California 90095, USA
and California NanoSystems Institute, Los Angeles, California 90095, USA
(Received 14 August 2014; published 17 February 2015)

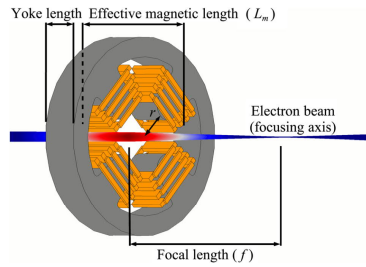


FIG. 1. Particle-tracking illustration of a 0.3 mm electromagnet gap radius, 0.2 mm yoke length MEMS quadrupole acting on an electron beam. The magnitude of the force on the electron beam is illustrated in color (e.g., red = max force). The illustration perspective shows electron beam focusing on-axis of the quadrupole; a perspective from the top would show defocusing of the electron beam.

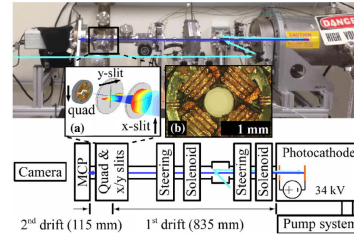
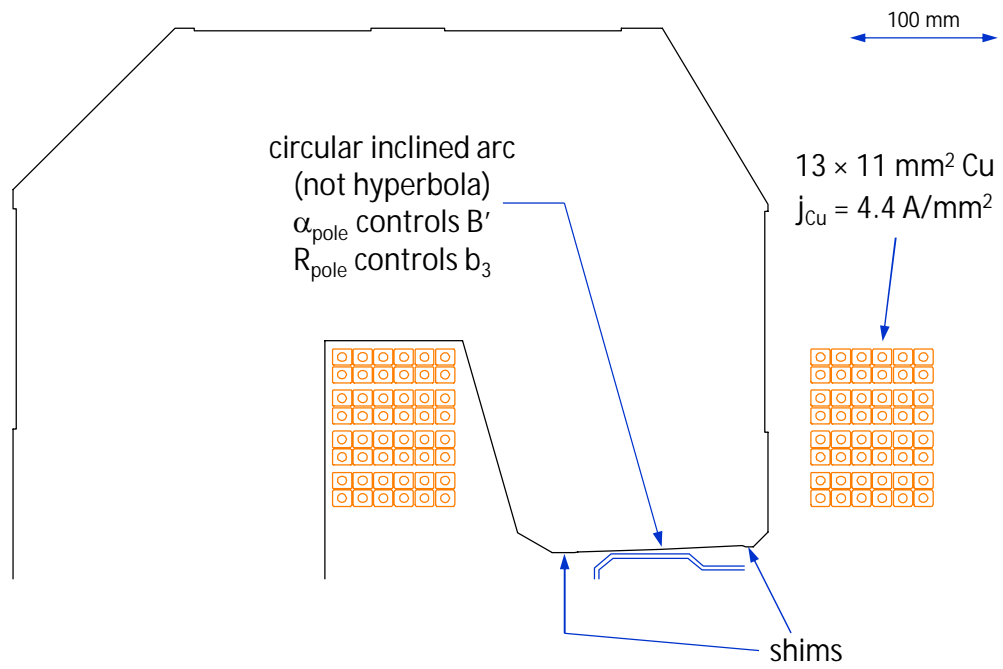


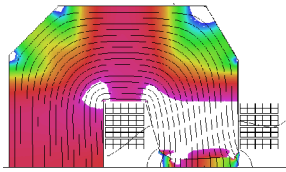
FIG. 9. Photograph and illustration of the electron beam experiment. Inset (a) shows an illustration of the inside of the experiment chamber with an electron beam (colored) entering the chamber from the right, striking a horizontal slit (x-slit) that is inserted into the chamber from below, a vertical slit (y-slit) that is inserted into the chamber from the left, and passing through a MEMS quadrupole (quad) that is inserted into the chamber from above. Inset (b) shows a photograph of a MEMS quadrupole. Cyan arrows illustrate the UV laser path from left to right and blue arrows illustrate the electron beam path from right to left.

SESAME combined function (dipole + quadrupole) magnet: (half of) the cross-section

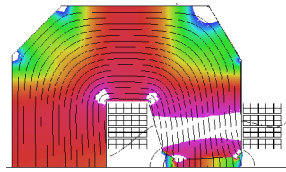


SESAME main bending: the pole is tapered to be gradually filled by flux at 2.5 GeV; at injection energy, the flux lines in the iron are rather different

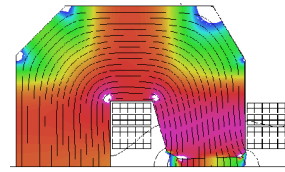
2.5 GeV, $B = 1.45$ T



1.0 T to 1.60 T

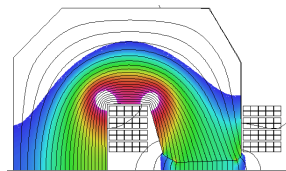


1.0 T to 1.65 T



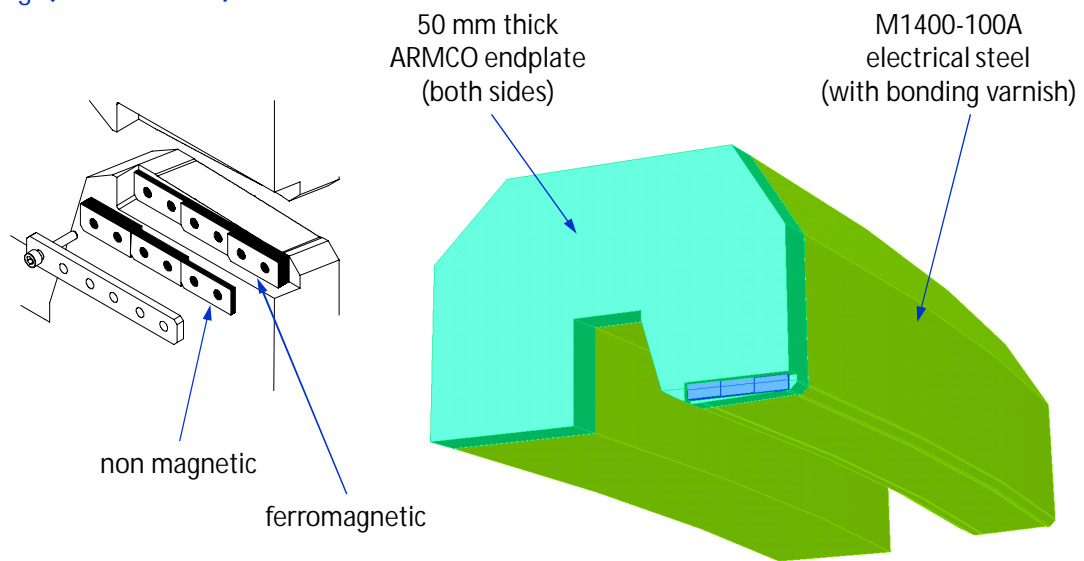
1.0 T to 1.70 T

0.8 GeV, $B = 0.47$ T

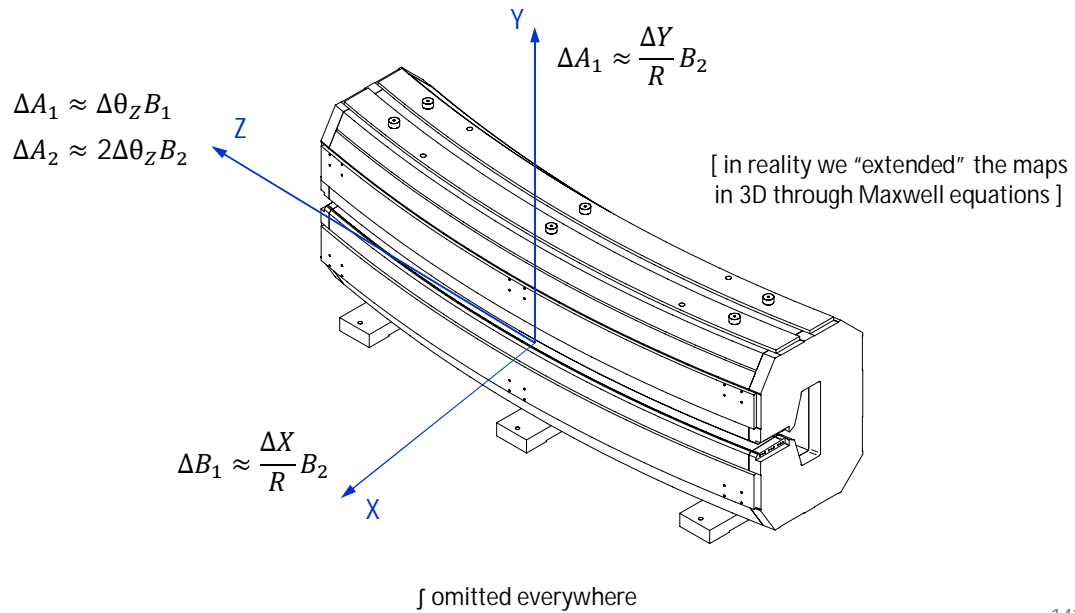


0.25 T to 1.0 T

SESAME main bending: the poles are terminated with three sets of shims, mounted in the endplates, to adjust $\int B$, $\int B'$ and $\int b_3$ (if needed)



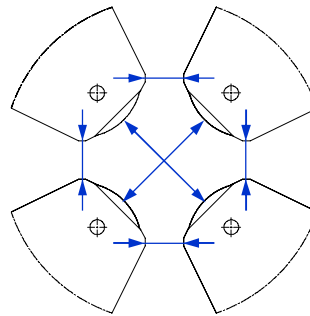
SESAME main bending: the field maps also allowed an optimal alignment, for repeatability of $\int B$, and to cancel skew dipole and quad terms



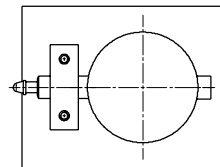
SESAME quadrupoles: as part of the acceptance procedure, we checked on all 66 magnets the key dimensions of the gap

MODSE #05		ELYTT	
[mm]	hydr. connection side	non-connection side	average
d13	70.004	70.022	70.013
d24	70.040	70.018	70.029
max - average		average - min	
0.008		0.008	
[mm]	hydr. connection side	non-connection side	average
d12	23.536	23.588	23.562
d23	23.564	23.571	23.568
d34	23.609	23.596	23.603
d41	23.579	23.586	23.583
max - average		average - min	
0.024		0.017	

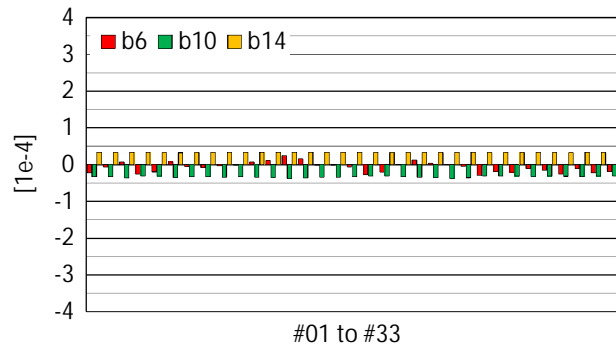
MODSE #05		Carlos / Michel		10/07/2015
[mm]	hydr. connection side	non-connection side	average	
d13	70.030	70.017	70.008	70.005
d24	70.016	70.018	70.022	70.025
max - average		average - min		
0.003		0.003		
[mm]	hydr. connection side	non-connection side	average	
d12	23.643	23.498	23.508	23.568
d23	23.548	23.558	23.568	23.568
d34	23.593	23.588	23.568	23.558
d41	23.578	23.583	23.598	23.598
max - average		average - min		
0.019		0.016		



opposite poles ≤ 0.05 mm
adjacent poles ≤ 0.03 mm



SESAME quadrupoles: the allowed harmonics are well controlled, with b_6 cancelled by the end pole chamfers



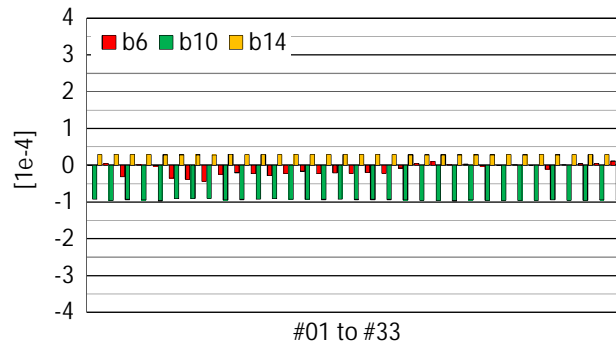
QF (long) @ 250 A

$b_6 = -0.1 \pm 0.1$ rms

$b_{10} = -0.3 \pm 0.0$ rms

$b_{14} = 0.3 \pm 0.0$ rms

harmonics in 10^{-4}
@ 24 mm radius




QD (short) @ 215 A

$b_6 = -0.1 \pm 0.2$ rms

$b_{10} = -0.9 \pm 0.0$ rms

$b_{14} = 0.3 \pm 0.0$ rms

SESAME quadrupoles: the random harmonics are also very satisfactory, witnessing the mechanical symmetry of the assembly

mean \pm rms	QF (long) @ 250 A	QD (short) @ 215 A	solenoidal loop in the connection 
b_3	-0.2 ± 0.8	0.0 ± 1.1	
a_3	-0.1 ± 0.9	0.1 ± 1.2	
b_4	0.3 ± 0.4	0.9 ± 0.9	
a_4	-0.3 ± 0.1	-1.0 ± 0.2	
b_5	0.0 ± 0.1	0.0 ± 0.1	
a_5	0.0 ± 0.1	0.0 ± 0.1	

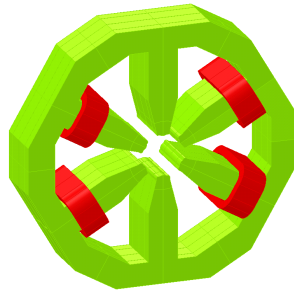
harmonics in 10^{-4} @ 24 mm radius

SESAME sextupoles: the correctors are embedded, using extra (10 A) windings – a popular trick in light sources

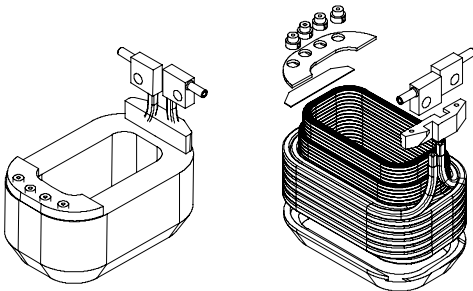
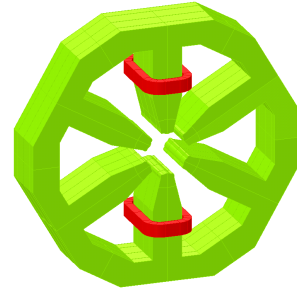
vertical dipole
(0.5 mrad kick @ 2.5 GeV)



horizontal dipole
(0.5 mrad kick @ 2.5 GeV)



skew quadrupole



3 windings per coil package:
main (water cooled) one +
two wound with solid conductor

SESAME sextupoles: the field quality of the sextupoles (with the correctors off) is very good

	mean \pm rms	firm 1 @ 215 A	firm 2 @ 215 A	
	b_4	-0.5 ± 1.5	0.3 ± 1.6	
	a_4	-0.8 ± 1.5	-0.7 ± 1.5	
	b_5	0.8 ± 0.9	0.8 ± 1.1	
	a_5	0.0 ± 0.7	0.3 ± 1.2	
	b_6	0.0 ± 0.5	-0.1 ± 0.8	
	a_6	-0.5 ± 0.2	-0.5 ± 0.1	
"allowed"	b_9	0.4 ± 0.1	0.8 ± 0.1	
	b_{15}	-0.1 ± 0.0	-0.1 ± 0.0	

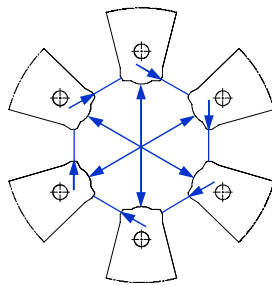
solenoidal loop in the connection

harmonics in 10^{-4} @ 24 mm radius

SESAME sextupoles: also for each of the 66 sextupoles we re-checked at CERN the key dimensions of the gap

MSXSE #002			CNE TECHNOLOGY CENTER		
[mm]	hydr. connection side		non-connection side		average
d14	75.010	75.020	75.040	75.030	75.025
d25	75.020	75.025	75.025	75.025	75.024
d36	75.040	75.030	75.010	75.030	75.028
max - average			average - min		
0.002			0.002		
[mm]	hydr. connection side		non-connection side		average
d12	19.770	19.770	19.770	19.770	19.770
d23	19.760	19.760	19.765	19.760	19.761
d34	19.810	19.810	19.800	19.810	19.808
d45	19.760	19.770	19.780	19.770	19.770
d56	19.780	19.790	19.780	19.785	19.784
d61	19.780	19.770	19.765	19.770	19.771
max - average			average - min		
0.030			0.016		

MSXSE #002			Greg		11/05/2015
[mm]	hydr. connection side		non-connection side		average
d14	74.997	75.013	75.030	75.042	75.021
d25	75.010	75.012	75.015	75.014	75.013
d36	75.046	75.038	75.035	74.998	75.029
max - average			average - min		
0.008			0.008		
[mm]	hydr. connection side		non-connection side		average
d12	19.759	19.771	19.753	19.763	19.762
d23	19.756	19.749	19.758	19.753	19.754
d34	19.772	19.757	19.763	19.750	19.761
d45	19.763	19.773	19.777	19.778	19.773
d56	19.753	19.777	19.774	19.768	19.768
d61	19.745	19.750	19.741	19.740	19.744
max - average			average - min		
0.013			0.016		



opposite poles ≤ 0.05 mm
adjacent poles ≤ 0.03 mm